FAA Finite Element Design Procedure for Rigid Pavements

August 2007

Final Report

This document is available to the public
through the National Technical Information
Service (NTIS), Springfield, Virginia 22161.

U.S. Department of Transportation
Federal Aviation Administration

NOTICE

1. Report No. DOT/FAA/AR-07/33	2. Government Accession No.	3. Recipient's Catalog No.
4. Title and Subtitle FAA FINITE ELEMENT DESIGN PROCEDURE FOR RIGID PAVEMENTS		5. Report Date August 2007
		6. Performing Organization Code
7. Author(s) Edward Guo, Lia Ricalde, and Izydor Kawa		8. Performing Organization Report No.
9. Performing Organization Name and Address SRA International, Inc. 3120 Fire Road Egg Harbor Township, NJ 08234		10. Work Unit No. (TRAIS)
		11. Contract or Grant No. DTFA03-92-D-00035
12. Sponsoring Agency Name and Address U.S. Department of Transportation Federal Aviation Administration Air Traffic Organization Operations Planning Office of Aviation Research and Development Washington, DC 20591		13. Type of Report and Period Covered Final Report
		14. Sponsoring Agency Code AAS-100

15. Supplementary Notes

The federal Aviation Administration Airport and Aircraft Safety R&D Division Technical Monitor was David Brill and the COTR was Satish Agrawal.

16. Abstract
FEDFAA, Finite Element Design—Federal Aviation Administration, is a computer program for both airport rigid and flexible pavement thickness design. NIKE3D (a general-purpose, three-dimensional finite element method (3D-FEM) computer program) is the selected engine for critical stress calculation for airport rigid pavement design. The calculated edge stresses are used in the FEDFAA failure model to determine the slab thickness. Since FEDFAA is a tool for thickness design rather than for analysis, certain program modifications and selection of available elements in NIKE3D have been made during FEDFAA development; it includes (1) selection of the nonconforming eight-node solid element to model all layers of the pavement except the subgrade, (2) introduction of the infinite element to model the infinitely deep subgrade, (3) mesh densities in vertical and horizontal directions, and (4) slab size and width of subbase extension have been determined to fit the needs of the design. A procedure has also been developed to calculate the critical stress of the pavement from the stresses calculated by NIKE3D at the element Gaussian points. Finally, the modified 3D finite element-based program was evaluated by using three criteria: (1) the model must be theoretically correct; (2) the final stress calculation engine with modifications and simplifications provides critical stress close enough to the precise one; and (3) it should be able to complete this computation under aircraft load within a few minutes. This report provides detailed descriptions for model selections, program modifications, and numerical evaluations. The report concludes that the final tool satisfies all three criteria; therefore, it is a reliable and applicable tool for airport rigid pavement design.

17. Key Words Pavement, Stress, Design, Portland cement concrete, NIKE3D, 3D finite element model, Finite element, Infinite element.	18. Distribution Statement This document is available to the U.S. public through the National Technical Information Service (NTIS), Springfield, Virginia 22161.

19. Security Classif. (of this report) Unclassified	20. Security Classif. (of this page) Unclassified	21. No. of Pages 97	22. Price

Form DOT F 1700.7 (8-72)   Reproduction of completed page authorized

TABLE OF CONTENTS

LIST OF FIGURES

LIST OF TABLES

LIST OF SYMBOLS AND ACRONYMS

E	Modulus of Elasticity (Young's Modulus)
k	Modulus of subgrade reaction
σ	Normal stress
δ	Displacement
l_s	Radius of relative stiffness
$σ_r$	Horizontal stress
2D	Two-dimensional
3D	Three-dimensional
AC	Advisory Circular
BISAR	BItumen Structures Analysis in Roads Program
CSG	Concrete strain gages
DLL	Dynamic link library
DOF	Degree of Freedom
FAA	Federal Aviation Administration
FAArfield	FAA Rigid and Flexible Interactive Elastic Design
FE	Finite element
FEDFAA	Finite Element Design-Federal Aviation Administration
3D-FEM	Three-dimensional finite element method
GW	Gross weight
INGRID	INteractive GRID Generator (3D FE Preprocessor Program)
IP	Integration point
JULEA	Jacob Uzan Layered Elastic Analysis
LEA	Layered Elastic Analysis
LEAF	Layered Elastic Analysis Program
LEDFAA	Layered Elastic Design-Federal Aviation Administration
LLNL	Lawrence Livermore National Laboratory
MIM	Modified incompatible modes
NAPTF	National Airport Pavement Test Facility
NIKE3D	A 3D Finite Element Analysis Program developed by LLNL
NIKE3D FAA 1.0	NIKE3D Version 3.3.2 modified by FAA for Rigid Pavement Analysis
PC	Personal computer
PCC	Portland cement concrete
psi	pounds per square inch
RAM	random-access memory
SCI	Structural condition index
SF	Scale factor
SWL	Single wheel load

EXECUTIVE SUMMARY

FEDFAA (Finite Element Design Federal Aviation Administration) is a computer program for both airport rigid and flexible pavement thickness design. It is also the beta version of the Federal Aviation Administration Finite Rigid and Flexible Interactive Elastic Layered Design (FAArfield) program in the Federal Aviation Administration's (FAA) new design procedure for airport pavements.

FEDFAA uses NIKE3D (a general purpose three-dimensional (3D) finite element method computer program) as the engine for critical stress calculation for airport rigid pavement design. The calculated edge stresses are used in the FEDFAA failure model to determine the slab thickness. Since FEDFAA is a tool for thickness design rather than for analysis, certain program modifications and selection of available elements in NIKE3D have been made during FEDFAA development:

- selection of the nonconforming eight-node solid element to model all layers of the pavement except the subgrade;

- introduction of the infinite element to model the infinitely deep subgrade;

- mesh densities in vertical and horizontal directions, and

- slab size and width of subbase extension have been determined to fit the needs of design. A procedure has also been developed to calculate the critical stress of the pavement from the stresses calculated by NIKE3D at the element Gaussian points.

The modified 3D finite element-based program was evaluated by using the following criteria:

- the model must be theoretically correct;

- the final stress calculation engine should provide critical stress close to the precise one; and

- the model should be able to complete this computation under aircraft load within a few minutes.

This report concludes that the final tool satisfies the three criteria; therefore, it is a reliable and applicable tool for airport rigid pavement design.

In more than a half century of development of airport Portland cement concrete (PCC) pavement design procedures, the critical stress in the PCC pavement under aircraft loading has been defined as a damage indicator, which is closely correlated to the most frequently observed distress in PCC pavements, namely cracks. The maximum edge strain, that is proportional to the stress, was found to be larger than any maximum interior strains in past full-scale tests [USACE (1), (2), and (3)]. These findings have been repeatedly verified by many other full-scale tests. The latest verification was obtained from the recently completed tests at the Federal Aviation Administration (FAA) National Airport Pavement Test Facility (NAPTF) (Guo, Hayhoe, and Brill 2002). Also, finding a crack initialized from the interior rather than from the edge is rare in field experience. Therefore, the calculation of critical edge stress became a necessary step in developing the new rigid pavement failure model in the Finite Element Design-Federal Aviation Administration program (FEDFAA).

FEDFAA is a computer software program for airport pavement thickness design. The FEDFAA program was developed based on the current FAA design procedure, LEDFAA, which stands for Layered Elastic Design-Federal Aviation Administration [FAA (1) and (2)]. LEDFAA calculates the maximum rigid pavement interior stress using the Layered Elastic Analysis (LEA) method and then converts it into an equivalent critical edge stress. LEA cannot calculate the critical edge stress directly. In FEDFAA, the PCC stress computation model has been replaced by the three-dimensional finite element method (3D-FEM) because 3D-FEM can directly calculate the maximum edge stress at a joint. NIKE3D, a general purpose 3D-FEM computer program used by the FAA under a software sharing agreement with Lawrence Livermore National Laboratory (LLNL), has been adapted by the FAA to calculate slab stresses. To better meet the requirements of FEDFAA, a graphical Microsoft® Windows®-based program, AUTOMESH, was written to make execution of the NIKE3D program easier and user friendly. The related work can be found in Brill (1998) and Brill (2000).

The program suite originally developed by LLNL includes NIKE3D (a finite element processor) and INGRID (a mesh generator and preprocessor). NIKE3D, version 3.3.2, was modified by the FAA to suit the needs of rigid pavement analysis. The modified program is referred to in this report as NIKE3D FAA 1.0. NIKE3D is a general-purpose computer program for analyzing both static and dynamic responses of an inelastic solid. NIKE3D FAA 1.0 is a special-purpose program used to predict critical stresses in a PCC slab and overlay under a given aircraft loading. Many subroutines used in the original NIKE3D are not needed in FEDFAA and have been deleted. As a result, the number of files in NIKE3D FAA 1.0 has been reduced to 350 files from the original 1045.

As a computational tool for airport pavement design, FEDFAA determines the thickness of a pavement structure that will provide satisfactory performance under an expected aircraft traffic mix. The prediction of the pavement damage indicator, critical stress under a given load, is only one step needed to achieve this goal. FEDFAA requires many special capabilities other than calculating a critical stress, for example:

- FEDFAA should be able to calculate slab thickness for pavements under traffic mixes that include new large aircraft such as the Boeing 777 and the new Airbus 380.

- The slab thickness design should be completed in a reasonable time.

- The selected model must be able to treat two or more sliding interfaces simultaneously for PCC overlay design.

A finite element (FE) model, such as the one produced by NIKE3D FAA 1.0, replaces the continuous domain of the pavement structure with a domain consisting of discrete elements. The stresses returned by NIKE3D FAA 1.0 are located at the integration point (IP) of each element, not necessarily at the critical points. Therefore, FEDFAA needs to include a systematic method for estimating the critical stress for design based on the NIKE3D-calculated stresses. As discussed in this report, FEDFAA includes procedures for both interpolating and extrapolating computed stresses to the critical locations.

FEDFAA is the first pavement design procedure to directly incorporate 3D-FE computation of critical edge stresses for PCC pavement. The FEM has had about a 35-year history since the first book was published [Zienkiewicz and Chen, 1967]. By 1995, 380 books, 4,000 conference proceedings, and 56,000 papers had been published, and 310 general-purpose FE programs had been developed [Mackerle, 1995]. However, none of the achievements and progress in FE development can guarantee that a given computer program will be reliable and able to satisfy the needs of a specific application. Therefore, the FAA decided to evaluate NIKE3D FAA 1.0 to minimize potential problems. Three criteria were used in the evaluation.

- The model must be theoretically correct.

- The procedure must adequately satisfy the major needs for airport pavement design.

- Since calculating the slab's critical stress dominates the total time needed for pavement design, it should be able to complete this computation for typical aircraft loads within a reasonable period of time.

Detailed descriptions of the FAA modifications to NIKE3D are presented in this report, as are the evaluation procedures used and the results. Following is a brief explanation of some key considerations in this project.

1.1 SELECTION OF THE NONCONFORMING FE.

The FAA began using 3D-FEM to model rigid airport pavement responses in the mid 1990s [Brill, 1998]. Since these initial modeling efforts using NIKE3D, the most important change introduced is that an eight-node brick element with an incompatible modes formulation replaces the four-node shell element in modeling the PCC layer. This incompatible modes element is also referred to as a nonconforming element for reasons explained in section 2.3. The same nonconforming element has also been used to replace the normal eight-node element previously used for modeling the pavement supporting structure. There are significant advantages to using nonconforming brick elements over either normal brick or two-dimensional (2D) shell elements.

First, two independent sliding interfaces, one between the overlay and the existing PCC slab and the other between the existing slab and the stabilized or granular subbase, can now be successfully modeled. The critical stresses at the overlay and existing pavement slab can be calculated simultaneously. Both stresses are necessary for developing a model for overlay design that can consider the interaction between the new overlay and the existing PCC layer.

Second, the incompatible solid element can simulate both bending and tensile-compressive behavior. Zienkiewicz and Taylor (2000) showed that the incompatible element accurately simulates the pure bending behavior of a thin plate. Bending dominates the rigid pavement responses near the wheel load center. Since the normal (i.e., fully compatible) eight-node solid element cannot correctly simulate the bending behavior of a plate, several layers of elements must be used to model the PCC layer. In the current model, incorporating incompatible elements, the number of elements through the thickness of the PCC layer has been reduced to one. This not only improves the accuracy of the calculation, but also reduces the computation time needed to complete a pavement design.

Third, it has been verified that the incompatible modes element is not only suitable for modeling the PCC slab, but also excellent for modeling all the structural layers of the pavement. Numerical comparisons, performed by the FAA, indicate that the critical stress error using NIKE3D FAA 1.0 in calculating the Boussinesq solution [Boussinesq, 1885 or Huang, 1993] is less than 1 percent.

1.2 SLIDING INTERFACE MODEL IN NIKE3D FAA 1.0.

A general penalty-based interface model incorporating frictional sliding with gaps between contact surfaces was selected [Brill, 1998] to model the fully unbonded interface condition between the PCC slab and the subbase layer. In NIKE3D, this model is designated type 3– frictional sliding with gaps. A scale factor (SF) is applied to the penalty stiffness to control the depth of interpenetration. The default value of the SF is 1.0, but after a large number of numerical tests, SF = 10.0 was found to give the best results. Some numerical comparisons between the results predicted by NIKE3D FAA 1.0 and known theoretical results are presented, where it is verified that type 3 is the model most appropriate for pavement design. It predicts interior maximum stress very close to the theoretical value. The value of SF = 10.0 is found to work well for all numerical cases.

1.3 COMPARISON TO KNOWN THEORETICAL SOLUTIONS.

As mentioned previously, the basic requirement of software selected for airport pavement design is that it must be theoretically correct in calculating the desired critical response. The correctness of the computed responses has been verified by three types of analysis.

- The basic formulas for FE analysis, from the element stiffness matrix, to the assembly of these elements, to the global stiffness matrix, have been reviewed. The functioning of these formulas in the source code has been verified.

- If the assumed shape functions used for the elements cover the solution of a simple problem, such as simple tension or compression and/or pure bending, the results

calculated by the program should have minimal error when compared to the theoretical solution. Some simple problems have been selected to compare the computed and the theoretical solutions to verify the theoretical correctness of NIKE3D FAA 1.0.

- The accuracy of the NIKE3D FAA 1.0 results were checked against reliable theoretical or numerical solutions for pavement-type structures, where such solutions are available. Convergence of the NIKE3D FAA 1.0 solution was also verified. FE solutions are always approximations of the theoretical (continuum) solution. Convergence to the continuum solution is expected as the model is further refined.

1.4 MEETING THE FUNCTIONAL REQUIREMENTS OF FEDFAA.

The critical stress in a slab under a given aircraft load is needed in pavement design. Verifying the following requirements is sufficient to ensure that NIKE3D FAA 1.0 can satisfy the requirements of FEDFAA.

a.   Where an overlay exists, NIKE3D has the capability to calculate the critical stress in the overlay and in the existing slab, simultaneously.

b.   Both the maximum edge stress and the location of stress sign change (i.e., the distance between the load center and the point where the edge stress changes sign) are well correlated to those calculated by the procedures in existing FAA design standards, Advisory Circular (AC) 150.5320-6D.

c.   The critical stresses under a multiple-tire gear are well correlated to those calculated by the method used in AC 150.5320-6D. Requirements a. and b. will help ensure that the new design procedure is a continuous development of the design procedure the FAA has been refining for more than a half century.

d.   The critical stress can be obtained in a few minutes on a personal computer (PC), leading to a new PCC pavement design being completed within a reasonable period of time. A rule of thumb is that 5 minutes for a traffic mix containing 10 aircraft, for a new rigid pavement design, is reasonable for an office application.

Based on the above criteria, a single slab supported by a multiple elastic layer system has been selected as the physical model to predict the critical stress of the PCC slab. The single slab (no joints) model avoids consideration of the large variation in the joint load transfer during the 20-year service time, reduces the computation time, and keeps the results well correlated to the critical free-edge stress used as the damage indicator by AC 150.5320-6D.

1.5 DETERMINATION OF STANDARD ELEMENT MESH AND ESTIMATION OF CRITICAL STRESS.

For a design program, opposed to an analysis program, it is less important to be able to compute a specific response under a specific load with a high degree of accuracy than to accurately capture the variation of the critical response under a changing load configuration. This is because the design thickness is related to the computed critical stress through the failure model, which

can be appropriately calibrated. The following have been considered to satisfy the three criteria listed in section 1.

- The finer the mesh that is used, the more accurate the calculated critical stress will be. Based on the objective of gaining speed, appropriate mesh sizes need to be determined for design. Numerical comparisons using different meshes show that the selected mesh can minimize the computation time while retaining the needed accuracy.

- The model of a slab on a multiple layer foundation is different from the model of a slab on a Winkler foundation, as used in AC 150.5320-6D. The critical stress calculated using the new model depends on the foundation type. The most conservative model (i.e., yielding the highest computed critical stresses) is one in which the vertical edges of the slab and the foundation layers coincide (cliff-type model). A more realistic model extends a portion of the foundation layers beyond the free edge of the slab (step-type model). Considerable effort has been dedicated to determining the appropriate step width.

- The infinite element, which has been successfully used in engineering practice [Zienkiewicz and Taylor, 2000], is an approximate approach for simulating a deep subgrade layer. It can reduce the total number of elements in the computation, leading to a reduction in the computation time, and can provide reliable approximate results. Numerical comparisons are presented in this report to show the benefit of using infinite elements.

- The 3D-FE analysis returns stresses at points in the interior of the elements that do not in general coincide with the maximum stress needed for design. The critical stress location for a large slab under aircraft gear loading usually occurs on the bottom surface of the slab, midway along the loaded edge. None of the calculated stresses at the Gauss points is a critical stress. Therefore, different interpolation and extrapolation techniques have been tested to estimate the critical stress at the slab bottom surface, based on the stress states computed at interior points.

2. BASIC THEORY OF NONCONFORMING EIGHT-NODE SOLID ELEMENT.

Basic equations for calculating the pavement stresses by the 3D-FE procedure are presented in this section. A detailed treatment of this subject can be found in many textbooks on FE methods, such as Zienkiewicz and Taylor (2000) or Cook, Malkus, Plesha, and Witt (2002). The basic equations include assumed shape functions for the different types of elements being used, the relationship between strain and displacements as defined by the assumed shape functions and the nodal displacements, the relationship between stresses and strains and derivations of the governing equations to solve for the nodal displacements, and derivation of the global and element stiffness matrices. Accuracy and precision criteria are also briefly discussed.

Theoretical analyses are given to show why the eight-node incompatible mode element was selected. The formula for infinite elements and their general concepts are also presented. The flow diagram of NIKE3D FAA 1.0 and numerical tests are given to verify that the program

NIKE3D FAA 1.0 follows the correct formulation for 3D-FE methods and provides accurate and reliable critical stresses for pavement design.

To simplify the analysis and to concentrate on the reasons for the selection of the nonconforming element, the critical stress is assumed to be the load-induced stress in a linear elastic system with zero initial stress and strain. Complicating factors such as sliding interfaces are not considered in this section.

2.1 GENERAL PROCEDURE FOR OBTAINING PAVEMENT CRITICAL STRESS.

A simplified numerical model of a slab resting on multiple elastic layers is shown in figure 1. There are many available approaches in FE analysis; however, the most popular is the displacement approach, in which the nodal displacements in x, y, z directions (figure 1) are defined as essential unknowns in the analysis. Under assumptions of geometric and material linearity and isotropy, the desired critical stress can be obtained by following the procedure in figure 2. Detailed descriptions are presented in the following sections.
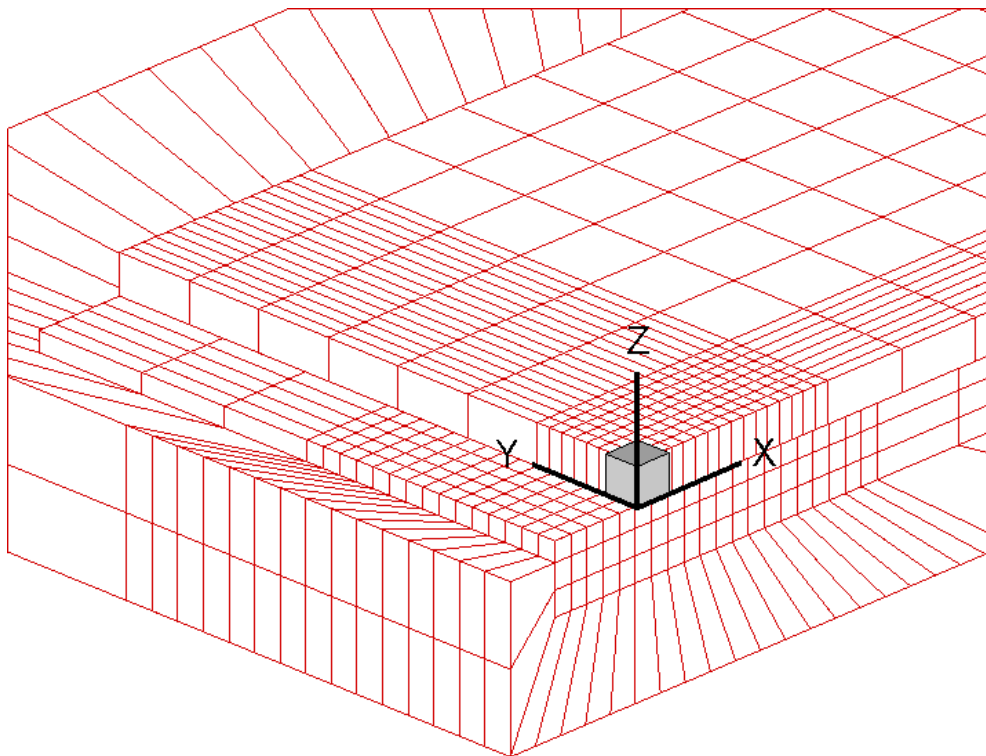
Figure 1. The 3D-FE Pavement Model

$$[K]\{a\}_G = \{F\}$$

1. The global nodal displacements $\{a\}_G$ are obtained by solving the governing equations. $[K]$ is the global stiffness matrix. $\{F\}$ is the global nodal force vector.

$$[U] = [N]\{a\}_L$$

2. The local displacement vector $\{a\}_L$ for an element can be selected from $\{a\}_G$. The displacements at any point in the element can be determined by the assumed shape functions $[N]$ after $\{a\}_L$ is obtained.

$$\begin{aligned}[\varepsilon] &= [S]\{U\} \\ &= [S][N]\{a\} \\ &= [B]\{a\}\end{aligned}$$

3. Strains are calculated by the linear geometrical equations in the theory of elasticity. $[B]$ is the strain-displacement matrix.

$$[\sigma] = [D]\{\varepsilon\}$$

4. Stresses are calculated by Hooke's Law. $[D]$ is the stress-strain matrix.

$\sigma_{critical}$ = The maximum stress obtained by searching over all stresses for all elements.

Figure 2. Procedure for Calculating Critical Stress for Pavement Design

2.2 SHAPE FUNCTIONS FOR TRILINEAR HEXAHEDRAL ELEMENT.

Figure 3 shows an eight-node hexahedral solid element and its local coordinate system. A pavement structure is divided into many such elements (figure 1), each being defined by eight nodes, numbered 1 to 8 in the order shown (figure 3).

In figure 3, x, y, and z are local coordinates with the origin at the element center; u, v, and w show the positive directions of displacements for the coordinates x, y, and z; and X, Y, and Z show the positive directions of the nodal forces. At each node, from 1 to 8, three degrees of freedom (DOF) correspond to the three displacements u, v, and w.
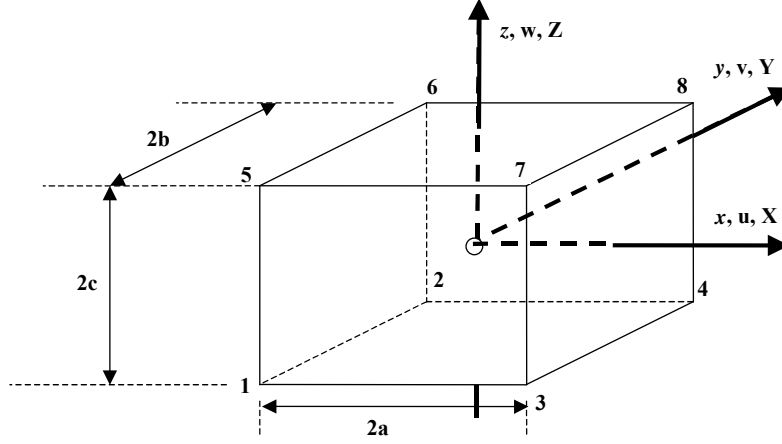
Figure 3. Eight-Node Hexahedral Solid Element

Shape functions, shown in equation 1, are assumed to express the variation of the displacements within an element.

$$N_1 = \frac{1}{8}(1-\xi)(1-\eta)(1+\zeta)$$

$$N_2 = \frac{1}{8}(1-\xi)(1-\eta)(1-\zeta)$$

$$N_3 = \frac{1}{8}(1-\xi)(1+\eta)(1-\zeta)$$

$$N_4 = \frac{1}{8}(1-\xi)(1+\eta)(1+\zeta)$$

$$N_5 = \frac{1}{8}(1+\xi)(1-\eta)(1+\zeta)$$

$$N_6 = \frac{1}{8}(1+\xi)(1-\eta)(1-\zeta)$$

$$N_7 = \frac{1}{8}(1+\xi)(1+\eta)(1-\zeta)$$

$$N_8 = \frac{1}{8}(1+\xi)(1+\eta)(1+\zeta)$$

(1)

where

$$\xi = \frac{x}{a}; \eta = \frac{y}{b}; \zeta = \frac{z}{c}$$

(2)

are the natural coordinates that range [-1, 1] for the element.

If $u(x, y, z)$, $v(x, y, z)$, and $w(x, y, z)$ are displacements at any point defined by the coordinates x, y, and z, and $\{a\}^e$ is a vector whose elements are the 24-nodal DOF for the element in figure 3, then

8

$$u(x,y,z) = \sum_{i=1}^{8} N_i(x,y,z) a_{1+(i-1)\times 3}^e$$

$$v(x,y,z) = \sum_{i=1}^{8} N_i(x,y,z) a_{2+(i-1)\times 3}^e \qquad (3)$$

$$w(x,y,z) = \sum_{i=1}^{8} N_i(x,y,z) a_{3+(i-1)\times 3}^e$$

The shape functions determine the characteristics of the responses to be obtained. The shape function in equation 1 only provides continuity of displacements at interfaces between the adjacent elements, so that it is defined as $C0$ continuity [Zienkiewicz and Taylor, 2000].

In matrix form, equation 3 becomes

$$\{U\}_{3\times 1} = [N]_{3\times 24} \{a\}_{24\times 1}^e \qquad (4)$$

where
$$\{U\}_{3\times 1} = [uvw]_{3\times 1}^T \qquad (5)$$

$$\{a\}_{24\times 1} = [a_1 a_2 a_3 a_4 ... a_{24}]_{24\times 1}^T \qquad (6)$$

$$[N]_{3\times 24} = \begin{bmatrix} N_1 & 0 & 0 & N_2 & 0 & 0 & ... & N_8 & 0 & 0 \\ 0 & N_1 & 0 & 0 & N_2 & 0 & ... & 0 & N_8 & 0 \\ 0 & 0 & N_1 & 0 & 0 & N_2 & ... & 0 & 0 & N_8 \end{bmatrix}_{3\times 24} \qquad (7)$$

2.3 STIFFNESS MATRIX FOR EIGHT-NODE INCOMPATIBLE SOLID ELEMENT.

All formulas in the previous sections were derived for an eight-node solid element in which the shape functions are defined by equation 1. The shape functions in equation 1 are not identical to the true deformations. Hence, the FE solution must always be an approximation. Because the shape functions in equation 1 satisfy the $C0$ continuity conditions on the interface between two elements [Zienkiewicz and Taylor, 2000], the element is called conforming and the deformation models are compatible modes. However, the linear shape functions in equation 1 cannot model the bending deformation very well.

To solve this problem, additional terms are added to equation 1 to simulate the element bending behavior. These additional terms (modes) violate $C0$ continuity, hence, the term incompatible modes. Detailed descriptions can be found in Cook, et al. (2002). Only a brief description is presented here to discuss the concept, derivation, and application of the incompatible element as implemented in NIKE3D by the FAA.

It is well known that the deflection curve of a beam under pure bending is a second order polynomial function, as shown in figure 4(a). However, the assumed shape function in equation 1 is only a first order polynomial function in each direction. Therefore, the best that can be done

by using equation 1 is to use a trapezoid, as shown in figure 4(b), to approximate the deformed shape, as shown in figure 4(a).

(a) True Deformation   (b) Assumed Deformation by Equation 1
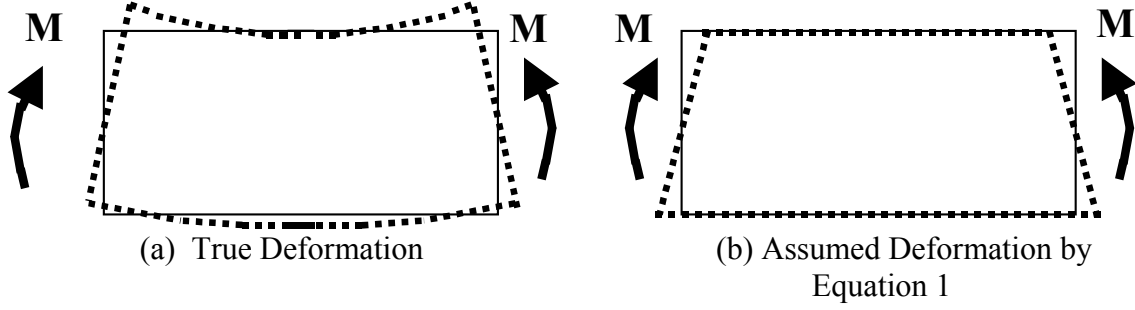
Figure 4. Discrepancy Between True and Assumed Deformed Shape for Compatible Element Formulation

Significant error is introduced by using the conforming element in PCC pavement analysis since the bending deformation dominates the critical stress in a PCC slab. Figure 4 shows that shear deformation, though it does not exist in the pure bending case, is artificially generated and absorbs a significant amount of energy converted from the work done by the traffic load. Theoretically, this error leads to the calculated deflection due to bending being much smaller than it should be, a phenomenon known as shear locking.

To solve the problem, Wilson, et al. (1973) and Taylor, Beresford, and Wilson (1976) suggested adding second order terms into the shape functions, as shown below.

$$u = \sum_{i=1}^{8} N_i a_{1+(i-1)\times 3} + \left(1-\xi^2\right)b_1 + \left(1-\eta^2\right)b_4 + \left(1-\zeta^2\right)b_7$$

$$v = \sum_{i=1}^{8} N_i a_{2+(i-1)\times 3} + \left(1-\xi^2\right)b_2 + \left(1-\eta^2\right)b_5 + \left(1-\zeta^2\right)b_8 \qquad (8)$$

$$w = \sum_{i=1}^{8} N_i a_{3+(i-1)\times 3} + \left(1-\xi^2\right)b_3 + \left(1-\eta^2\right)b_6 + \left(1-\zeta^2\right)b_9$$

In matrix form

$$\{U\} = [N]_{3x24} \{a\}^e_{24x1} + [N_C]_{3x9} \{b\}^e_{9x1} \qquad (9)$$

where $[N]$ is the same as in equation 7 and $\{a\}$ is the same as in equation 6.

$$[N_C] = \begin{bmatrix} N_{C1} & 0 & 0 & N_{C2} & 0 & 0 & N_{C3} & 0 & 0 \\ 0 & N_{C1} & 0 & 0 & N_{C2} & 0 & 0 & N_{C3} & 0 \\ 0 & 0 & N_{C1} & 0 & 0 & N_{C2} & 0 & 0 & N_{C3} \end{bmatrix} \qquad (10)$$

$$N_{C1} = 1 - \xi^2$$
$$N_{C2} = 1 - \eta^2 \qquad (11)$$
$$N_{C3} = 1 - \zeta^2$$

$$\{b\} = \left[b_1 b_2 b_3 b_4 b_5 b_6 b_7 b_8 b_9 \right]^T \qquad (12)$$

Equations 8 and 9 show that three partial spherical functions with second order polynomials are added into the assumed element shape function. Therefore, for an element deformation dominated by bending, equation 9 will provide more accurate results when compared to equation 4. However, because the shape functions of equation 9 break $C0$ continuity, an overlap or gap may develop at the interface between the adjacent elements.

The following new definition may be introduced to simplify the derivation of the stress and strain calculations for the incompatible element.

$$\{a_i\}_{33x1} = \left[\{a\}^T \{b\}^T \right]^T \qquad (13)$$

$$[N_i]_{3x33} = \left[[N][N_C] \right] \qquad (14)$$

Without any constraint, the displacement vector for an incompatible element has 33 unknowns, while a compatible element has only 24 unknowns. If these nine unknowns are calculated by solving the first equation in figure 2, the total number of unknowns from using incompatible elements would be much more than from using compatible elements. Therefore, those additional unknowns are treated as internal unknowns, and static condensation [Wilson, 1974] is used to reduce the total unknowns of each element from 33 to 24.

The static condensation technique is implemented in NIKE3D. Accuracy and reliability of the incompatible nodes element in NIKE3D have been verified by a patch test and are presented in section 2.6.

2.4 CONCEPT AND APPLICATION OF INFINITE ELEMENT.

The structural model for PCC pavement analysis contains a semi-infinite domain. An infinitely deep subgrade can be approximated in the numerical model by a deep layer with zero displacement at the bottom of the layer. If the discretized domain above the fixed boundary consists of normal eight-node hexahedral elements, many layers are needed, which would, in turn, require a relatively long time to complete a pavement response analysis. Therefore, the infinite element has been introduced to represent the deep subgrade. Zienkiewicz and Taylor (2000) provide an example to show that the use of infinite elements in a Boussinesq problem significantly improves the displacement response compared to the same problem done with standard linear elements.

The infinite element capability was not available in the original NIKE3D program. In a project sponsored by the FAA [Brill and Parsons, 2000], the infinite element was installed into NIKE3D

FAA 1.0. The use of infinite elements obviates the issue of selecting the position and boundary conditions for a truncated analysis domain. It also saves storage space and computation time since the total number of elements is much smaller than required for conventional FEs. With an infinite element foundation, the total number of DOFs is approximately the same as for a dense liquid model, but the solution is more realistic since it obeys a solid elastic material model based on Young's modulus E and Poison's ratio μ, rather than the dense liquid model based on the modulus of subgrade reaction k.

Equation 1 shows the shape function for an eight-node solid element. For simulating the infinitely deep subgrade, the shape functions have to be modified. The following equation is used for mapping in the infinite direction x, while the mappings in finite directions y and z are still defined by equation 2.

$$x = -\frac{\xi}{1-\xi}x_o + \left(\frac{1}{1-\xi}\right)x_q \tag{15}$$

One can directly observe that

$$\xi = -1 \Rightarrow x = \frac{x_o + x_q}{2} = x_p$$
$$\xi = 0 \Rightarrow x = x_q \tag{16}$$
$$\xi = 1 \Rightarrow x = \infty$$

The following condition has been used in the derivation of equation 16 (figure 5):

$$x_q - x_p = x_p - x_o = a \tag{17}$$

where a is the characteristic length of the infinite element and point o is the decay origin that can be defined as a pole for the mapping [Cook, et al., 2002]. Since equation 17 is used in the formula derivation, similar conditions should be used in the application of the infinite element for pavement analysis. The pavement surface under a load is analogous to the decay origin so that the characteristic length of the infinite element is recommended to be the same as the distance between the top of the subgrade and the pavement surface.

A similar mapping equation may be obtained by using x_p instead of x_o

$$x = -\frac{2\xi}{1-\xi}x_p + \left(\frac{1+\xi}{1-\xi}\right)x_q = N_p x_p + N_q x_q \tag{18}$$
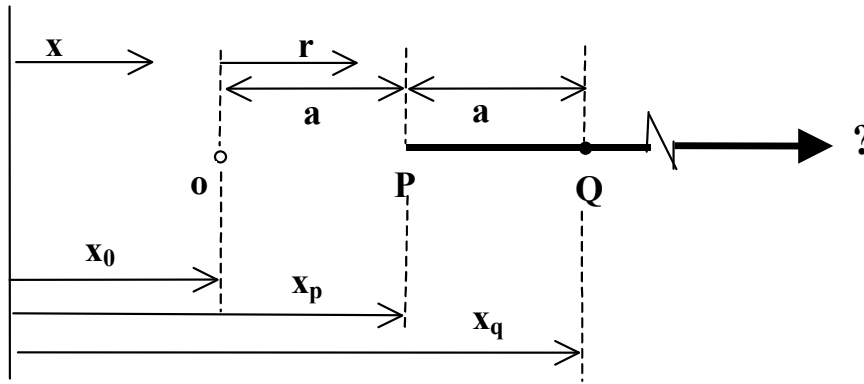
Figure 5. Mapping Function From Finite Length to Infinite Length [Cook, et al., 2002]

The variation range of ξ is from -1 to 1. When $\xi = -1$, $N_p = 1$, and $N_q = 0$, this leads to $x = x_p$. When $\xi = 0$, $N_p = 0$, and $N_q = 1$, this leads to $x = x_q$; and when $\xi = 1$ and $N_p = N_q = \infty$, this leads to $x = \infty$. The use of these mapping functions produces an approximate decay for displacements in the infinite element.

The above brief derivation shows how an infinitely deep domain can be approximated by FEs with standard shape functions using appropriate mapping functions. The infinite elements are treated in NIKE3D as a material type that can be assigned to a particular element under either ordinary or incompatible modes options. In the current model, the bottom layer of elements is composed of infinite elements with an incompatible modes formulation. More detailed descriptions and derivations can be found in Brill and Parsons (2000); Cook, et al. (2002); and Zienkiewicz and Taylor (2000).

2.5 NUMERICAL VERIFICATION—SINGLE-ELEMENT STUDY.

The main objective of this section is to evaluate the performance of an incompatible modes element through single-element numerical examples. Based on the characteristics of the incompatible modes element, the procedure for determining the critical stress in pavement design is described.

A single element is used to check the performance of the shape functions in the incompatible modes elements. The nodal and load positions are given in figure 6. The bottom nodes of the element are fixed (nodes 1, 2, 3, and 4) and the top nodes of the element are free (nodes 5, 6, 7, and 8). Three load conditions are used to test the performance of the element under three common deformation modes: simple compression, pure bending, and a combination of bending and shear. Loads and other input data are presented and separated for each case. Results are listed in table 1. Table 1 compares the theoretical result from simple mechanics to the numerical result obtained from NIKE3D FAA 1.0.

13

P8

P5

P6

P7

8(0, 10, 30)

7(10, 10, 30)

5(0, 0, 30)

6(10, 0, 30)

n_z

H

$P_5 \bullet n_z = P_{5Z}$

z

y

x

4(0, 10, 0)

3(10, 10, 0)

B

1(0, 0, 0)

2(10, 0, 0)

B
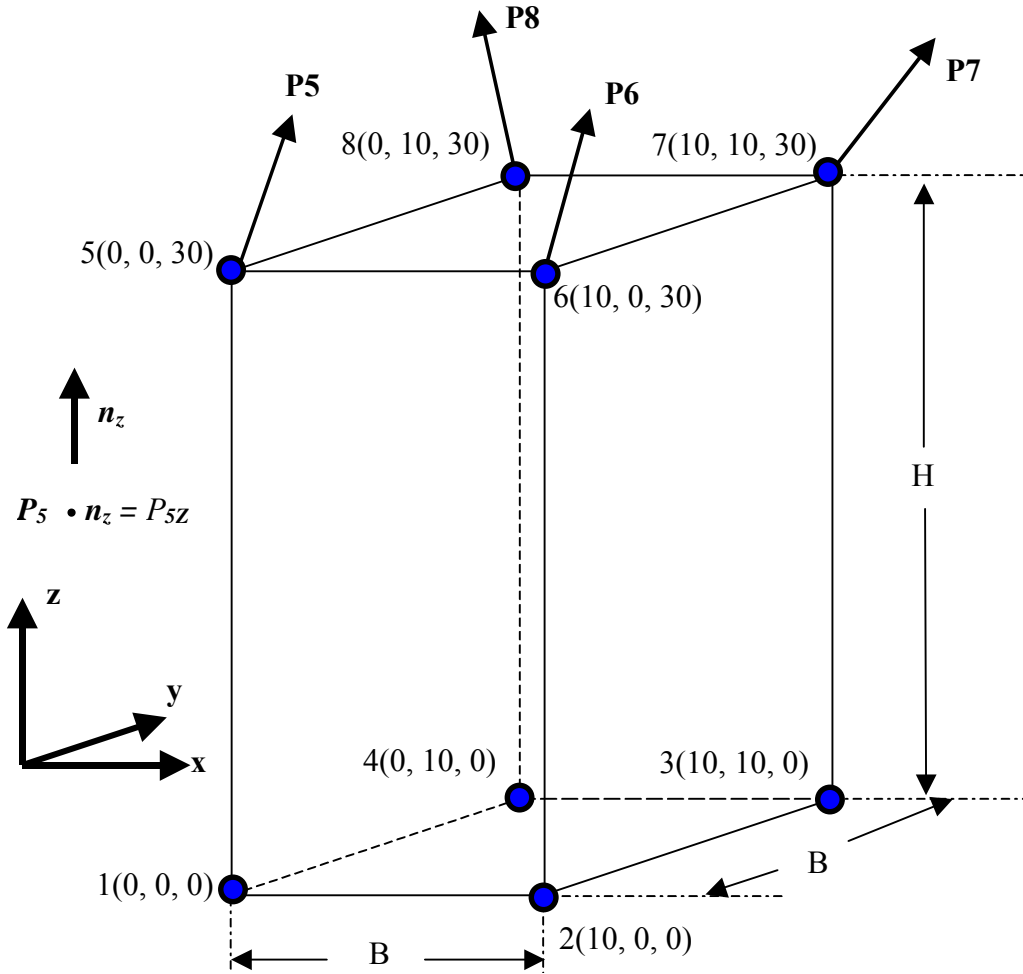
Figure 6. Model for Single-Element Study

Table 1. Performance of Elements

Case	Variable	Incompatible Modes Element	Theoretical Solution
1	σ_z	-100	-100
	δ_z	-0.3	-0.3
2	σ_z	173.2	173.205
		173.2	173.205
		-173.2	-173.205
		-173.2	-173.205
		173.2	173.205
		173.2	173.205
		-173.2	-173.205
		-173.2	-173.205
	δ_x	2.69570 / 2.69571 Average = 2.69571	2.7 / 2.7 Average = 2.7
	δ_z	0.898743 / -0.898798 $\lvert$Average$\rvert$ = 0.898771	0.9 / -0.9 $\lvert$Average$\rvert$ = 0.9
3	σ_z	519.2	219.615
		-520.2	-219.615
		-520.2	-219.615
		519.2 $\lvert$Average$\rvert$ = 519.7	219.615 $\lvert$Average$\rvert$ = 519.615
		519.2	819.615
		-520.2	-819.615
		-520.2	-819.615
		519.2	819.615
	τ_{zx}	60.78	100.0
		141.9	100.0
		141.9	100.0
		60.78 Average = 100.2	100.0 Average = 100
		139.1	100.0
		59.03	100.0
		59.03	100.0
		139.1	100.0
	δ_x	8.59297 / 8.54073 Average = 8.56685	10.8 / 10.8 Average = 10.8
	δ_z	2.74942 / -2.59245 $\lvert$Average$\rvert$ = 2.671	2.7 / -2.7 $\lvert$Average$\rvert$ = 2.7

σ_z in psi, δ_z and δ_x in inches

2.5.1 Case 1: Pure Compression.

Stresses are uniform throughout the element and displacements are uniform over the cross section. Nontrivial responses are given by

$$\sigma_z = \frac{\sum_{i=5}^{8} P_i x n_z}{B^2} \qquad (19a)$$

$$\delta_z = \sigma_z x \frac{H}{E} \qquad (19b)$$

where P_i is the load vector at node i, $P_i = [P_{ix} * i + P_{iy} * j + P_{iz} * k]^T$, n_z is the unit vector in the z direction, E is the Young's modulus, and dimensions B and H are defined in figure 6. Substituting in equation 19a the input values $B = 10$ in., $H = 30$ in., $E = 10,000$ psi, $P5_z = P6_z = P7_z = P8_z = -2500$ lb., and all other components of applied nodal loads are zero, yields $\sigma_z = -100$ psi and $\delta_z = 0.3$ in.

2.5.2 Case 2: Pure Bending.

Stresses are computed at eight Gauss IPs, located at $[\pm \eta = 0.57735, \pm \xi = 0.57735, \pm \zeta = 0.57735]$. A couple is introduced by specifying that $P5_z = -P6_z$ and $P7_z = -P8_z$. In this case, the theoretical stress value at the IP is given by

$$\sigma_z = \pm \frac{2P_{5(z)}}{\dfrac{B^3}{12}} x \frac{0.57735B}{2} \qquad (20a)$$

and the lateral displacement δ_x of a point at the top center of the element is given by

$$\delta_x = \frac{P_{5(z)}}{E\left(\dfrac{B^3}{12}\right)} x H^2 \qquad (20b)$$

For the same input values as in case 1, except that $P5_z = -P6_z = 2500$ lb and $P7_z = -P8_z = 2500$ lb, equations 20a and 20b yield $\sigma_z = \pm 173.205$ psi and $\delta_x = 2.7$ in.

2.5.3 Case 3: Combined Shear and Bending.

Input data: $E = 10,000$ psi, $B = 10$ in., $H = 30$ in.
$P5_x = P6_x = P7_x = P8_x = -2500$ lb; $P5_y = P6_y = P7_y = P8_y = P5_z = P6_z = P7_z = P8_z = 0$. $\mu = 0$.

Bending stresses at upper four IPs:

$$\sigma_z = \pm \frac{4xP_{5x}x\dfrac{(1-0.57735)xH}{2}}{\dfrac{BxB^3}{12}} x \frac{0.57735xB}{2} = \pm 219.615\,psi \qquad (21)$$

Bending stresses at lower four IPs:

$$\sigma_z = \pm \frac{4xP_{5x}x\dfrac{(1-0.57735)xH}{2}}{\dfrac{BxB^3}{12}} x \frac{0.57735xB}{2} = \pm 819.615\,psi \qquad (22)$$

Shear stresses at upper and lower IPs:

$$\tau_{xz} = \frac{3x4xP_{5x}}{2xBxB} x\left[1-0.57735^2\right] = 100\,psi \qquad (23)$$

Displacement (δ_x) at the top center of the element:

$$\delta_x = \frac{4xP_{5x}}{3xEx\dfrac{BxB^3}{12}} xH^3 = \frac{4x2500}{3x10000x\dfrac{10x10^3}{12}} x30^3 = 10.8\,psi \qquad (24)$$

As discussed previously, the FE solutions are always an approximation to the exact solutions. The stress result at the IP is more accurate than at other points. Therefore, the comparisons are made for stresses computed at IPs. Findings from the comparisons in table 1 are summarized below.

- For case 1, both displacements and stresses calculated by using the incompatible modes element are identical to the analytical results. The stresses at each IP are the same as in the analytical results.

- For case 2, the errors in the displacements when using the incompatible element are less than 0.16 percent, and the stresses at the IPs are identical to the analytical results. This indicates that the additional shape functions defined by equation 9 simulate the pure bending very well, so the incompatible mode of the eight-node solid element is a satisfactory selection for pavement analysis. The critical stress in a loaded pavement is dominated by slab bending.

- For case 3, the numerical errors are much larger than in the previous two cases. The calculated transverse displacements at the top of the cantilever beam are 20 percent less than the analytical results.

Also, the calculated bending stresses at all IPs are almost the same, a situation that is significantly different from the analytical results. The magnitudes of stresses by theory at the four top IPs are much lower than at the four lower IPs. However, the average stresses at the tension side and the compression sides are very close to the corresponding average stresses obtained in the theoretical analysis. This observation confirms a general rule: the average stress at the four IPs for an incompatible mode element is superior to the stress value at a particular IP and should be used for design.

Furthermore, the calculated shear stresses at the eight IPs are different, but the theoretical ones are the same. The average shear stress is still very close to the shear stress from theoretical analysis. This finding also supports the recommendation of using average stress instead of stress at each individual IP for pavement design.

2.6 NUMERICAL VERIFICATION—PATCH TEST FOR NONCONFORMING ELEMENT.

The numerical analysis in section 2.5 shows that the application of the incompatible modes element can provide accurate stress responses at the single-element level if the element is under pure compressive or pure bending deformations. The application can also provide accurate average stresses for an element under a combination of bending and shear deformations. A pavement must be represented by many elements. Therefore, it still remains to investigate whether the pavement response converges to a correct value as the element size decreases and the number of elements increases.

Since the nonconforming eight-node element is used in FEDFAA, it is necessary to test if the continuity is achieved for any mesh configuration. The necessary and sufficient conditions for convergence are a patch test, as discussed in Zienkiewicz and Taylor (2000). A nonconforming element is said to pass the patch test if an arbitrary patch of elements subjected to nodal displacements corresponding to a state of constant strain produces constant stress. A patch test is presented in this section to demonstrate that the nonconforming element in NIKE3D satisfies the necessary convergence condition.

Taylor, Beresford, and Wilson (1976) pointed out that the incompatible element "can pass the patch test only when it is a parallelogram. This implies that the element will produce a convergent sequence of solutions only if the mesh subdivisions form a pattern of parallelograms." For pavement analysis, irregularly shaped elements are usually used to minimize the computation time. To overcome this limitation, a repairing method, applicable for irregular elements, was presented in Taylor, Beresford, and Wilson (1976). A variation of this method, known as modified incompatible modes (MIM) was implemented in the original NIKE3D package [Maker, 1995]. The patch test presented in this section confirms that the MIM element has been accurately implemented in NIKE3D FAA 1.0 to ensure convergence when using irregularly shaped elements.

An eight-element parallelepiped hexahedron with fixed bottom boundary conditions was selected to conduct the patch test, as shown in figure 7. The height, length, and width of the system are 30, 10, and 10 inches, respectively. The coordinates of x, y, and z for the 27 nodes are shown in figure 7. The top of the system is under a uniformly distributed load with a pressure of 100 pounds per square inch (psi). The equivalent nodal loads are given in figure 7. Other input data

include the system elastic modulus E = 10,000 psi and Poisson's ratio μ = 0. The theoretical solution of displacement at the top is 0.3 inch and the vertical stress is -100 psi at any point.
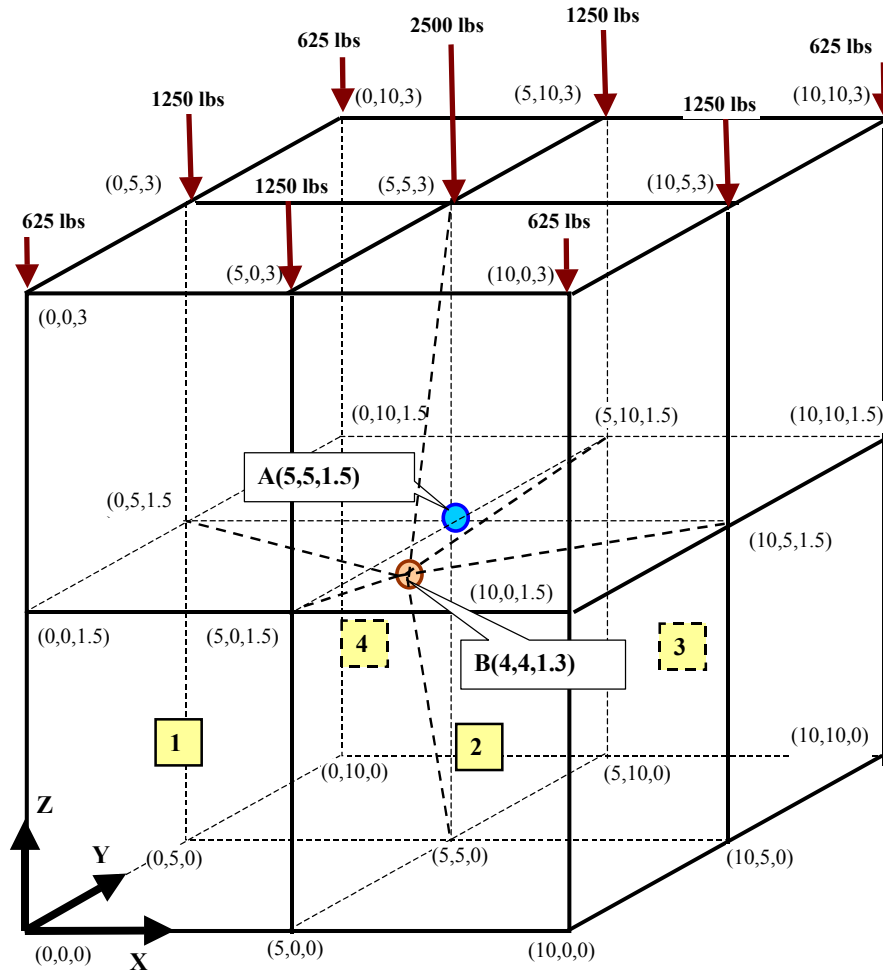
Figure 7. An Eight-Element System for Patch Test

Two cases have been analyzed. Case 1 uses equal elements by setting the coordinates of point A to (5, 5, 15). Case 2 uses unequal and irregular elements by setting the coordinates of point B to (4, 4, 13). All other input data are the same for the two cases. The displacements at all 27 nodes and stresses at the eight IPs for the lower four elements in figure 7 are presented in appendix A, tables A-1 and A-2, respectively. A shift of point A to B at any other location leads to the element shape changing from a parallelepiped to an irregular hexahedron. If the calculated results are independent of the shift, the patch test is passed and the convergence condition is satisfied. The results in tables A-1 and A-2 show that the vertical displacements and compressive stresses are independent of the new location of point B. The same results (δ_z and σ_z) are obtained for point B at any point nearby point A. Therefore, the patch test is satisfied.

3. INTERIOR RESPONSES COMPARED WITH KNOWN SOLUTIONS.

3.1 BOUSSINESQ SOLUTION.

The solution of an elastic semispace under a uniformly distributed circular load was obtained by Boussinesq in 1885. The Boussinesq equations for stress

$$\sigma_z = q\left[1 - \frac{z^3}{\left(a^2 + z^2\right)^{1.5}}\right] \tag{25}$$

$$\sigma_r = \frac{q}{2}x\left[1 + 2\mu - \frac{2(1+\mu)z}{\left(a^2 + z^2\right)^{0.5}} + \frac{z^3}{\left(a^2 + z^2\right)^{1.5}}\right] \tag{26}$$

and deflection under the load center

$$w = \frac{(1+\mu)qa}{E} \times \left\{\frac{a}{\left(a^2 + z^2\right)^{0.5}} + \frac{(1-2\mu)}{a} \times \left[\left(a^2 + z^2\right)^{0.5} - z\right]\right\} \tag{27}$$

are given by Huang (1993). In equations 25 to 27:

$\quad q =$ distributed vertical load
$\quad a =$ radius of load patch
$\quad (r,z) =$ cylindrical coordinates
$\quad E =$ Young's modulus
$\quad \mu =$ Poisson's ratio

The Boussinesq expression for stress along the r axis ($z = 0$) is

$$\begin{aligned} \sigma_r &= -\frac{1+2\mu}{2}xq\cdots(r < a) \\ \sigma_r &= -\mu xq\cdots(r = a) \\ \sigma_r &= -\frac{1-2\mu}{2}xqx\frac{a^2}{r^2}\cdots(r > a) \end{aligned} \tag{28}$$

The mesh shown in figure 8 was used to compare the output of the 3D-FEM model with an infinite element foundation to Boussinesq's problem. For this comparison, the following input data are used: $E = 10,000$ psi and $\mu = 0.40$.

In the Boussinesq's example, it is assumed that the load patch is a circle with radius $a = 9.403$ in., so an assumed uniform contact pressure of $q = 180$ psi gives a total load of 50,000 lb. For the FE problem, the same load and contact pressure are assumed, but the load patch is a square with sides equal to 16.67 in. As shown in figures 8 and 9, it is only necessary to model one-quarter of the total FE domain due to symmetry.
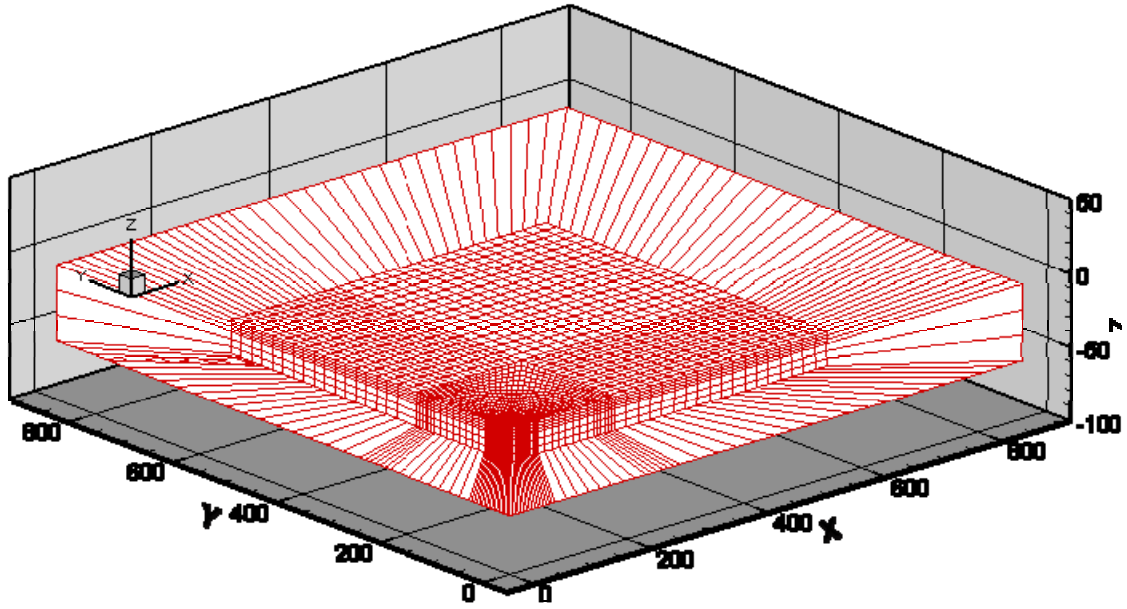
Figure 8. Mesh for Comparison to Boussinesq's Solution
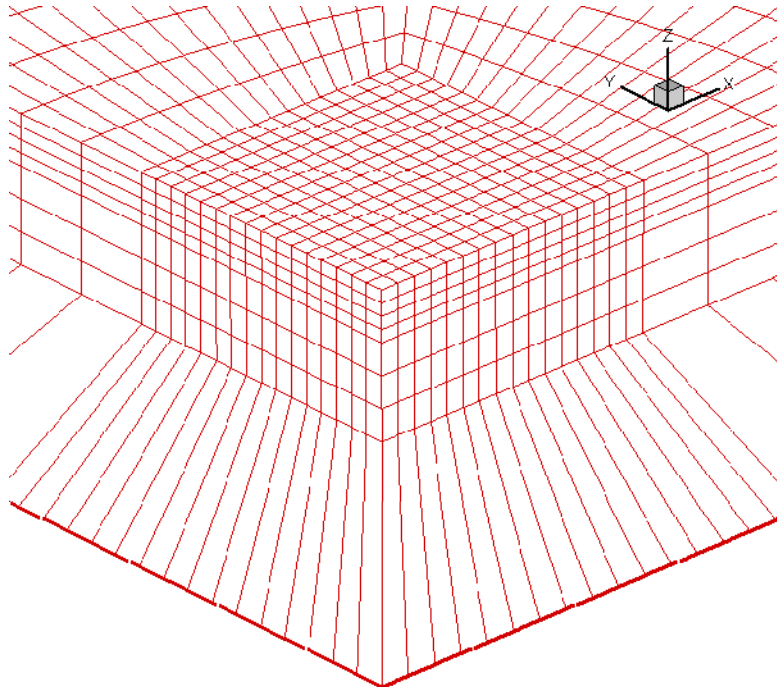
Figure 9. Detail of Mesh for Comparison to Boussinesq's Solution

Figure 10 compares the computed deflection basin from NIKE3D to the maximum surface deflection from equation 27 with $z = 0$. The surface deflection profile using a layered elastic analysis program (LEAF) is also shown. Figure 11 compares horizontal stress σ_r as computed by equation 28 with the equivalent stresses computed by NIKE3D and LEAF. (In figure 11, the FE stresses are computed at IPs and linearly extrapolated to the surface.) Figure 12 plots horizontal stresses σ_r with depth z below the surface, comparing the NIKE3D solution to Boussinesq.
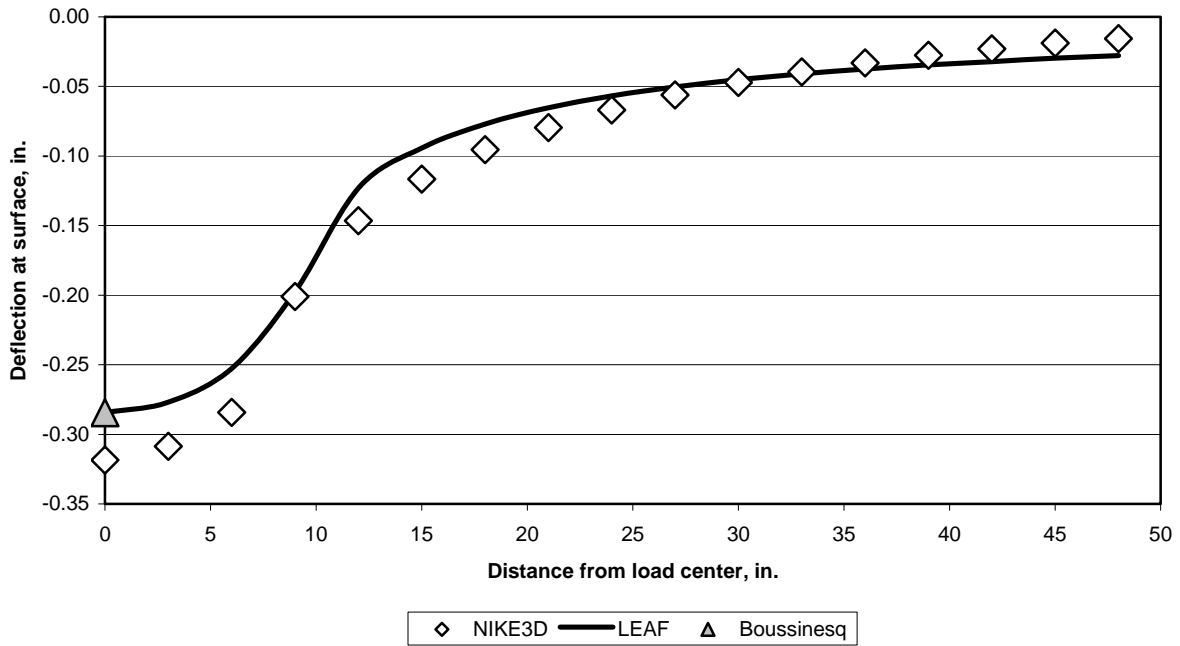
Figure 10. Surface Deflection as Function of Distance From Load Center for Boussinesq Problem
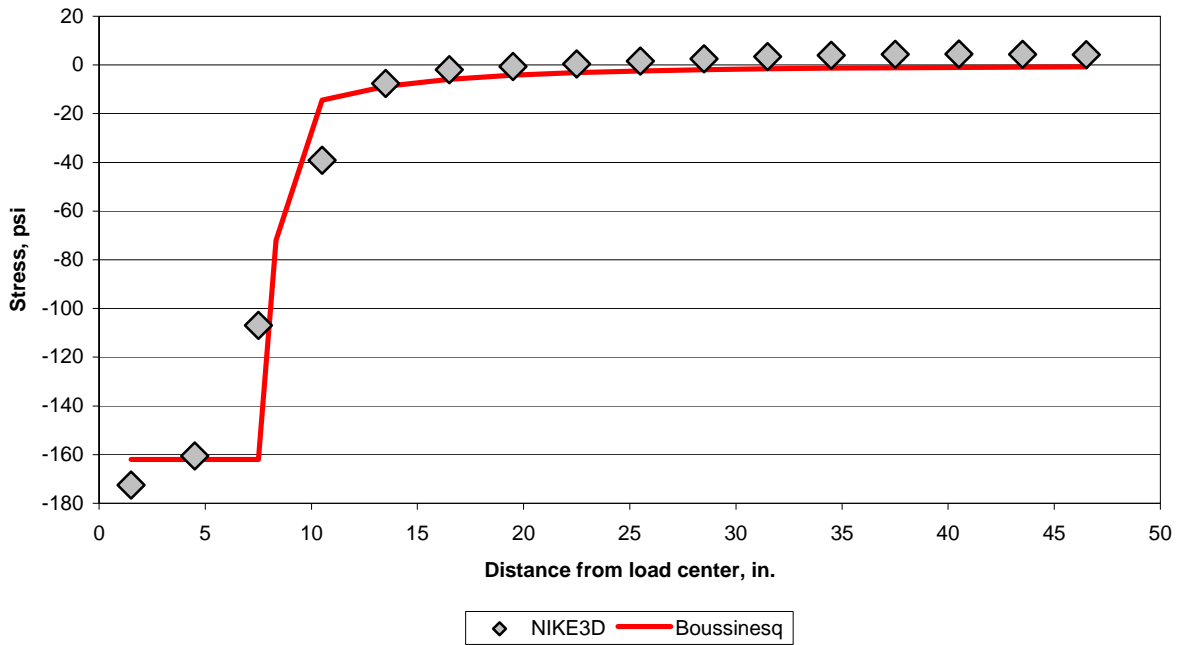
Figure 11. Horizontal Stress σ_r at the Surface as Function of Distance From Load Center for Boussinesq Problem
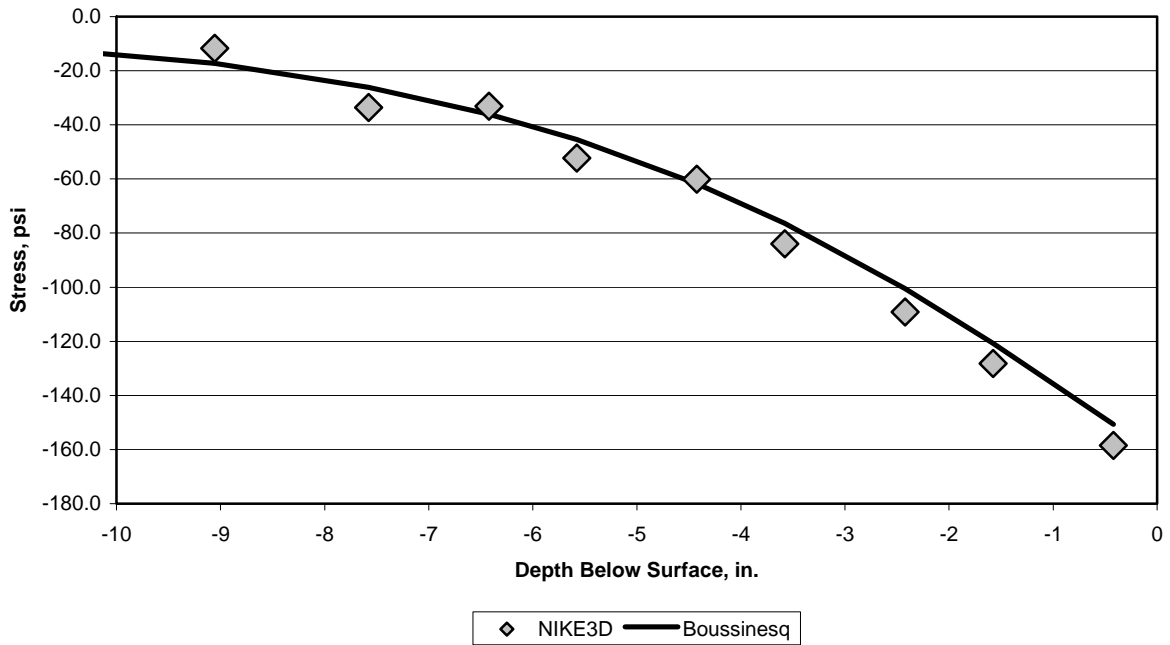
Figure 12. Horizontal Stress σ_r Beneath the Load Center as Function of Depth for Boussinesq Problem

23

3.2 COMPARISON BETWEEN LEAF AND BISAR.

The BItumen Structures Analysis in Roads (BISAR) [Koninklijke/Shell, 1978] program is based on layered elastic theory and is used by the U.S. Army and the U.S. Air Force to calculate interior stresses for rigid airfield pavements. The LEAF program, developed by the FAA, is also based on layered elastic theory and is used by the FAA to calculate interior stresses for rigid pavements. The interior stress is then converted into edge stress in the current FAA LEDFAA design procedure program. The new FEDFAA program retains LEAF for flexible pavement design and for the first approximation on rigid pavement design. The FE response will determine the pavement final thickness based on edge stress. BISAR- and LEAF-calculated stresses are compared in this section for different interface conditions. Comparisons were limited to slab structures on infinitely deep foundations. Two different subgrades were assumed, high ($E = 100,000$ psi) and low ($E = 4,500$ psi) modulus of elasticity.

3.2.1 Bonded Interface.

The first case considers a fully bonded interface between the PCC slab and the layer beneath the slab. Interior stresses were computed for two pavement structures, both with an 18-inch PCC slab ($E_C = 4,000,000$ psi and $\mu = 0.15$). The subgrade modulus (E_{SG}) is 4,500 psi in the first structure and 100,000 psi in the second. A 50,000-pound single wheel load (SWL) with 180 psi tire pressure is applied to both structures.

Figure 13 shows very good agreement between BISAR and LEAF through the slab thickness for both pavement structures. The structure with the lower subgrade strength (4,500 psi) shows higher interior stresses than the structure with high subgrade strength, as expected.
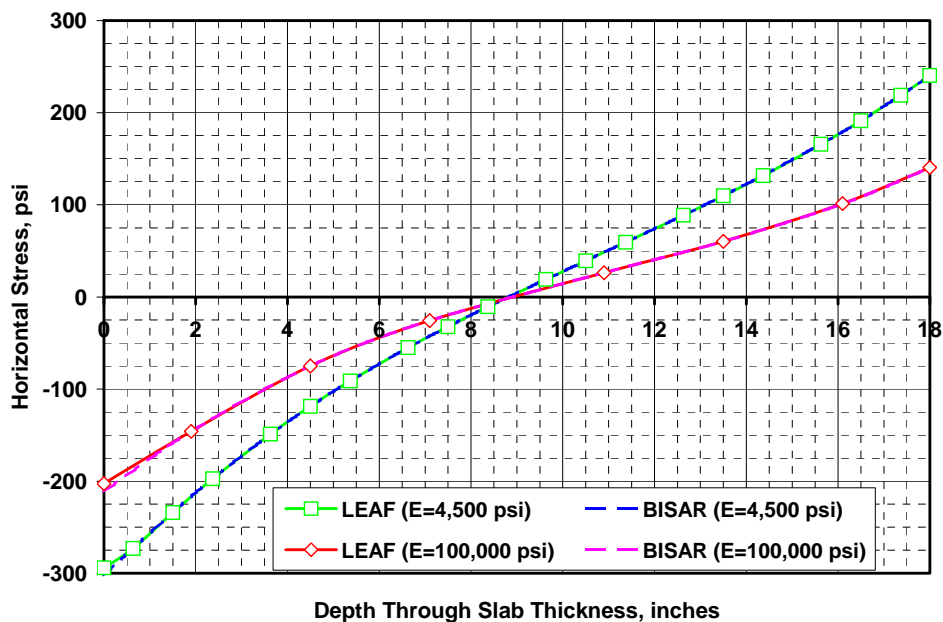
Figure 13. Interior Stress Through Slab Thickness With Fully Bonded Interface

3.2.2 Unbonded Interface.

The second case considers an unbonded interface. The structure is identical to structure 2 from section 3.2.1, (E_{SG} = 100,000 psi), except that the interface condition is changed from fully bonded (fixed) to fully unbonded (sliding). BISAR- and LEAF-calculated stresses again have very good agreement, as shown in figure 14.
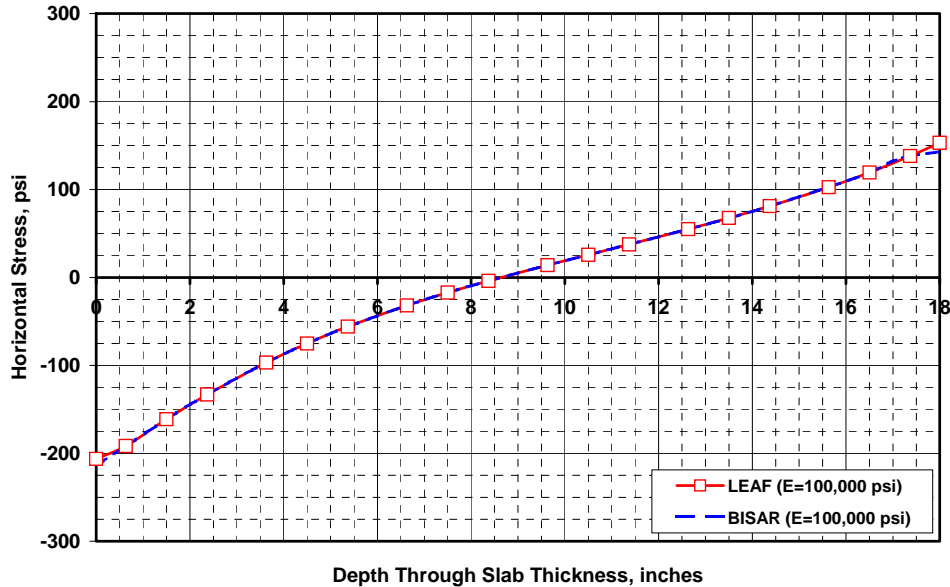
Figure 14. Interior Stress Through Slab Thickness With Fully Unbonded Interface

3.2.3 Portland Cement Concrete Overlay With Unbonded Interface.

The examples in this section used three pavement structures (A, B, and C) with similar structural properties but have varying subgrade strengths. The structures were originally designed to support 6,000 passes of the B747-200 (gross weight (GW) = 833,000 pounds and 200 psi tire pressure) as calculated by AC 150.5320-6D. Structural properties are described in table 2.

Table 2. Pavement Structures for PCC Overlay Comparison

Pavement Structure	Pavement Thickness, h (inches)			E (ksi)			μ
	Pav A	Pav B	Pav C	Pav A	Pav B	Pav C	
PCC slab	16.17	13.46	12.60	4,000	4,000	4,000	0.15
CTB	4.00	4.00	6.00	500	500	500	0.20
Subbase	4.00	6.00	6.00	30	30	30	0.35
Subgrade				4.5	12.0	22.5	0.40

An 8-inch PCC overlay was added to the pavements in table 2 for interior stress comparison using the LEAF and BISAR programs under the fully unbonded interface condition. A six-wheel main gear of the B777-200B with a 680,000-pound GW and a tire pressure of 215 psi was applied to the structures.

25

The interior stresses calculated by LEAF and BISAR at the bottom of the PCC overlay and the existing PCC slab are presented in appendix A, table A-3 and shown in figures 15 and 16. They compare very well for the different pavement structures used. Pavement A shows the largest calculated stress along the PCC overlay and existing PCC slab.
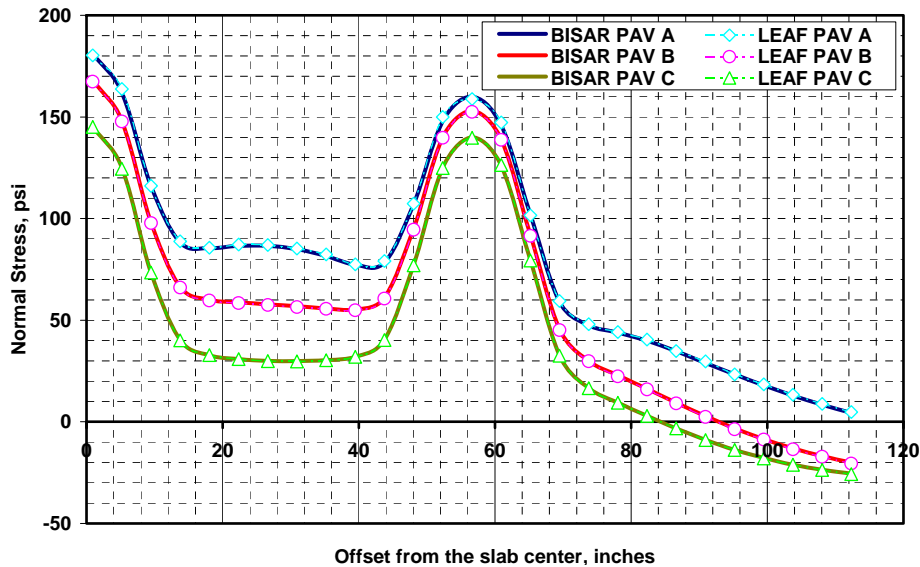
Figure 15. Interior Stress at the Bottom of PCC Overlay
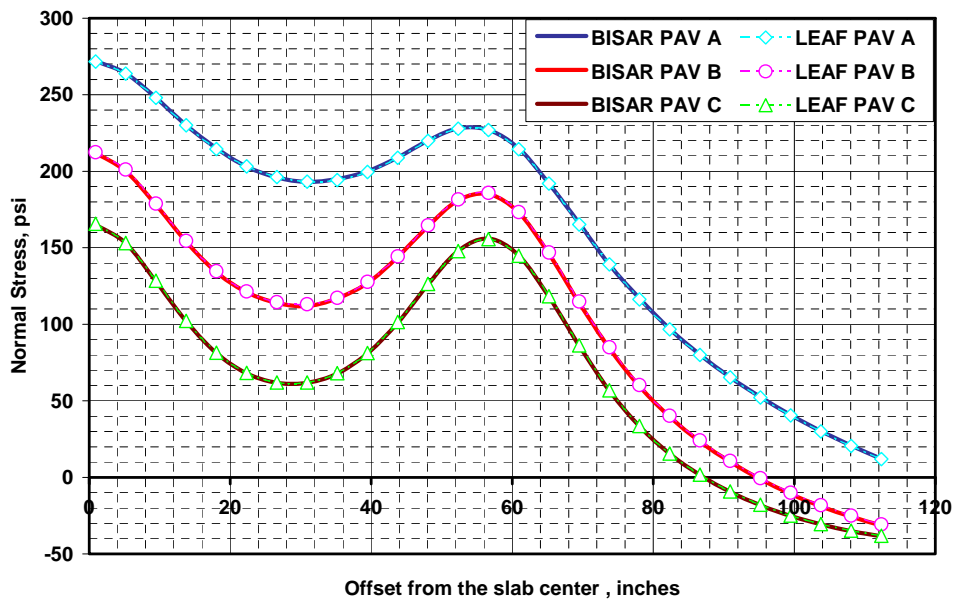
Figure 16. Interior Stress at the Bottom of Base PCC

The maximum stresses at the bottom of the overlay and existing PCC slab are needed in the overlay design. Table 3 shows the calculated maximum interior stresses of the PCC overlay and existing PCC slab for the different pavement structures. The LEAF- and BISAR-calculated stresses compare well for both the overlay and existing PCC slab.

26

Table 3. Interior Stresses Calculated by BISAR and LEAF Through PCC Overlay and Base PCC

| Location | Depth (inches) | | | Interior Stress (psi) | | | | | |
| | | | | BISAR | | | LEAF | | |
	Pav A	Pav B	Pav C	Pav A	Pav B	Pav C	Pav A	Pav B	Pav C
Bottom IP Overlay	7.99	7.99	7.99	324	303	264	324	299	262
Bottom IP Base Slab	24.16	21.45	20.59	487	385	305	487	385	305

To verify the accuracy of LEAF, more numerical comparisons between LEAF computations and Boussinesq analytic solutions for responses under the load center were obtained [Hayhoe, 2002].

3.3 MULTIPLE TIRE EFFECTS.

A comparison of stresses under multiple tire gear loads calculated by NIKE3D FAA 1.0, LEAF, and BISAR is presented in this section.

3.3.1 New PCC Pavement Under Multiple Wheel Gear.

NIKE3D FAA 1.0 is used in this section to calculate interior stresses through the thickness of a new PCC slab at the critical element IPs (table 4). The pavement structures used in the analysis are described in table 2.   The load corresponds to the B777-200B main gear (GW = 680,000 pounds and 215 psi tire pressure). The PCC and all the other pavement layers are modeled by single elements through the thickness to minimize the number of elements in the pavement model.

Table 4. BISAR and NIKE3D FAA 1.0 Interior Stresses at IP Through Slab Thickness for Multiple Wheel Load

| Slab Thickness | Depth at IP (inches) | | | BISAR Stress (psi) | | | NIKE3D Stress (psi) | | |
	Pav A	Pav B	Pav C	Pav A	Pav B	Pav C	Pav A	Pav B	Pav C
Top IP	3.42	2.84	2.66	-322.0	-272.0	-225.0	-315.6	-254.5	-211.4
Middle IP	8.09	6.73	6.30	5.5	1.7	0.3	-8.1	-8.4	-8.6
Bottom IP	12.75	10.62	9.94	304.0	252.0	205.0	299.4	237.7	194.3

Table 4 and figure 17 compare the stresses (through the slab thickness) calculated by NIKE3D FAA 1.0 and BISAR for different pavement structures under multiple wheel load through the slab thickness. The computed stress difference between BISAR and NIKE3D FAA 1.0 ranges from 2 percent (for pavement A) to 5 percent (for pavement C). Both responses compare well through the thickness.
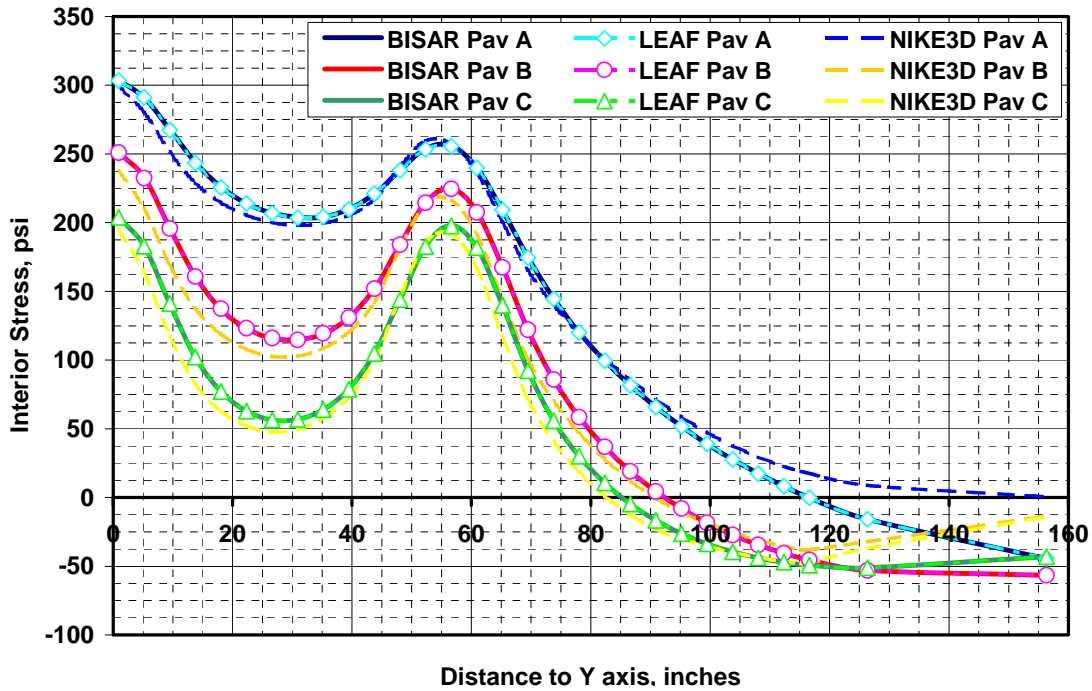
Figure 17. Interior Stress at IP Through Slab Thickness for Different Structures Under Multiple Wheel Load
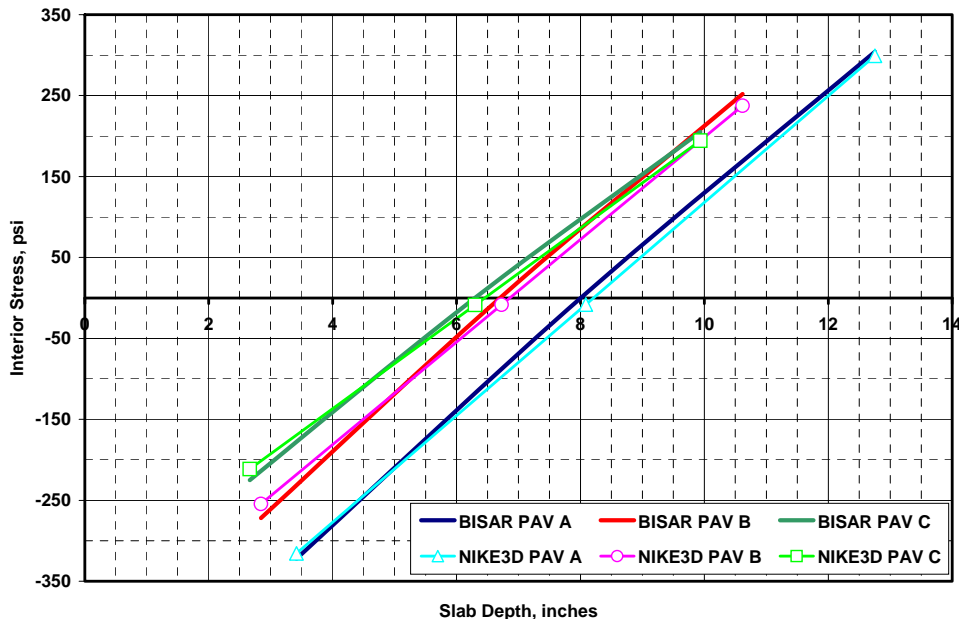
Figure 18. Portland Cement Concrete Slab Centerline Interior Stress for Multiple Wheel Gear

Figure 18 shows the comparison along the PCC slab centerline for the calculated stresses by NIKE3D FAA 1.0, LEAF, and BISAR. The difference in the calculated stresses by NIKE3D and the other two methods is about 5 percent. The stresses show good agreement along the PCC slab centerline.

28

3.3.2 Portland Cement Concrete Overlay Under Multiple Wheel Gear.

To evaluate the overlay capability in NIKE3D, the same pavement structures used previously and described in table 2 are used in this section, with the addition of 8 inches of PCC overlay. The multiple wheel load continues to be the main gear of the B777-200B. A single layer of brick elements is used for both the overlay and the existing slab. The interfaces between the PCC overlay and the existing slab and the subbase are both modeled using the NIKE3D general contact surface option. One fully unbonded sliding surface is defined between the PCC overlay and the top surface of the existing PCC. A second fully unbonded interface is defined between the bottom surface of the existing PCC and the subbase. The calculated stresses are evaluated at the brick element IPs, as described in table 5. The FE overlay pavement model is shown in figure 19.

Table 5. Brick Element IPs Depth for Different Structures

IP Vertical Location	Depth at IP (inches)		
	Pav A	Pav B	Pav C
Top IP PCC Overlay	1.69	1.69	1.69
Bottom IP PCC Overlay	6.31	6.31	6.31
Top IP Base PCC	11.42	10.84	10.66
Bottom IP Base PCC	20.75	18.62	17.94
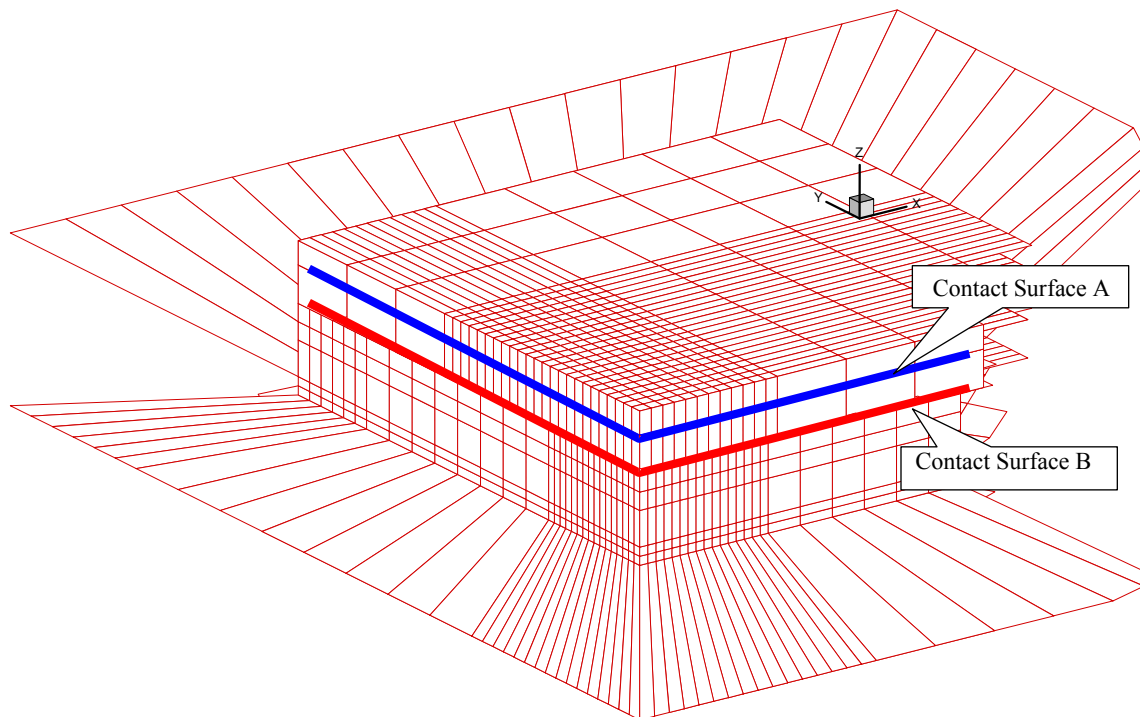
Figure 19. Portland Cement Concrete Overlay Pavement Model

Table 6 presents a comparison of the stresses computed for these structures by the various methods. The stresses listed are the maximum computed stresses at the IP levels.

Table 6. Interior Stress Through Pavement Thickness for Different Pavement Structures—Overlay Case

| Location | Interior Stress (psi) | | | | | | | | |
| | BISAR | | | LEAF | | | NIKE3D | | |
	Pav A	Pav B	Pav C	Pav A	Pav B	Pav C	Pav A	Pav B	Pav C
1	-212.0	-198.0	-175.0	-208.6	-194.9	-171.9	-227.9	-206.0	-183.6
2	181.0	169.0	146.0	180.6	167.9	145.7	203.1	181.5	159.1
3	-282.0	-224.0	-178.0	-282.5	-222.9	-177.6	-272.0	-202.9	-159.3
4	272.0	212.0	166.0	271.9	212.8	166.1	262.0	192.7	148.9

Figures 20 and 21 compare the variation in computed stress through the thickness of the slab for the two models, for the PCC overlay, and the base PCC layer, respectively.

The NIKE3D-calculated stresses compare well with BISAR for the existing PCC slab, especially for the pavement structures that required thicker slabs (low-strength subgrade). By contrast, the maximum NIKE3D stress extrapolated to the bottom of the PCC overlay deviates from the corresponding BISAR stress by 10%. Considering that the stress calculated closer to the center of the element compares consistently well with BISAR, the refinement of the mesh through the thickness might improve the stresses generated by NIKE3D. On the other hand, if the NIKE3D-calculated stresses can be extrapolated from the IPs to the nodes, mesh refinement might be unnecessary.
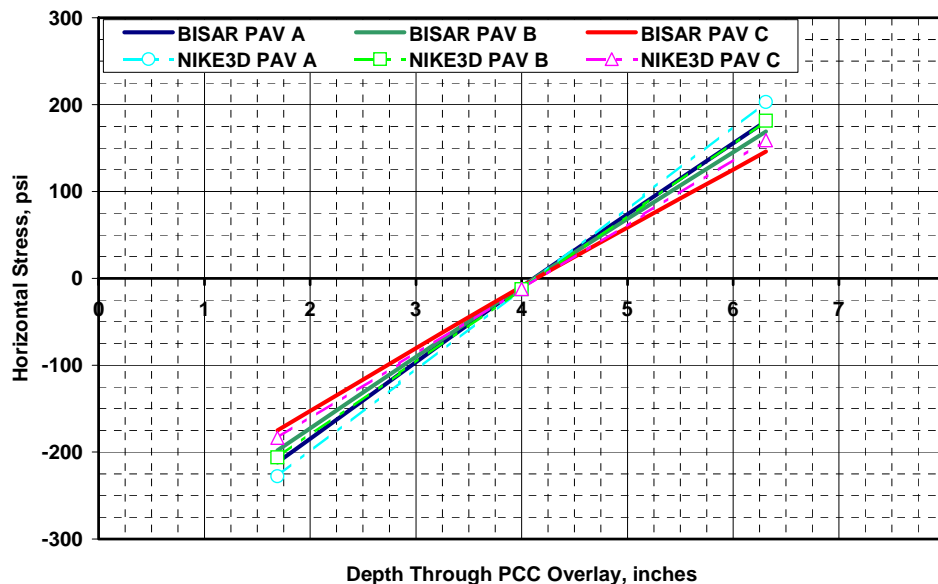
Figure 20. Interior Stress Through Pavement Thickness for PCC Overlay
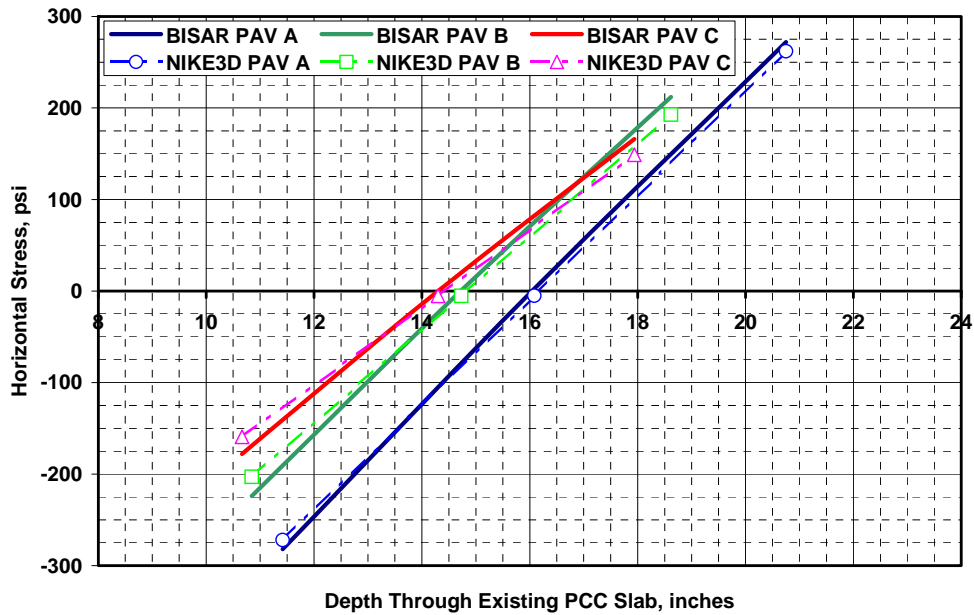
Figure 21. Interior Stress Through Pavement Thickness for Base PCC

Figures 22 and 23 and table A-4 in appendix A compare the stress distribution calculated by NIKE3D and BISAR at the IPs along the slab centerlines for the PCC overlay and the existing PCC slab, respectively.
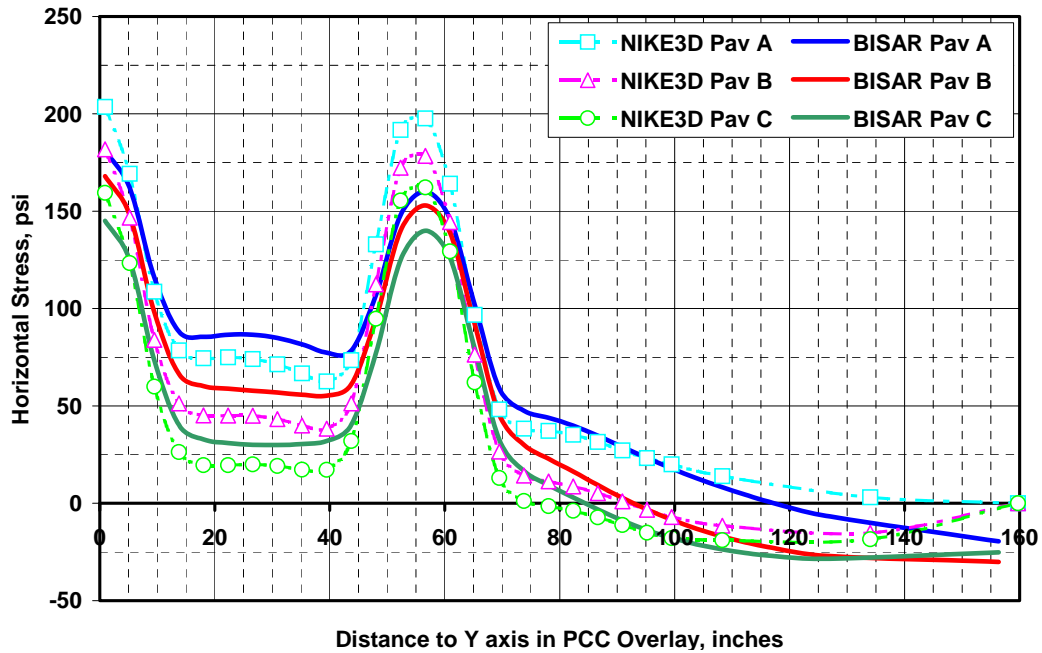
Figure 22. Interior Stress Profiles in PCC Overlay for Multiple Wheel Gear Load

31
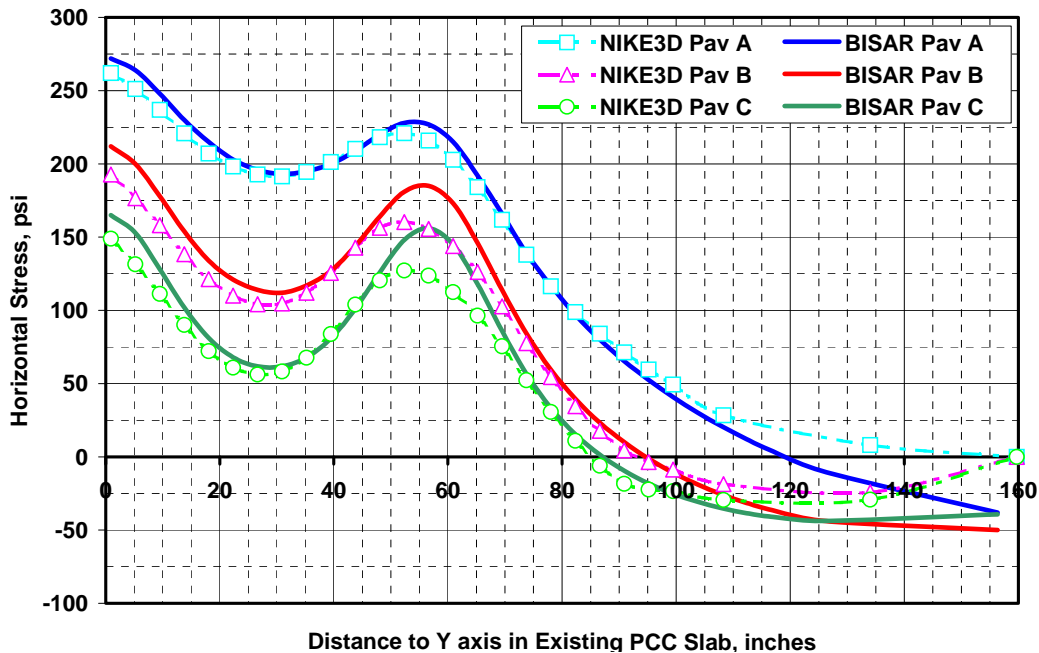
Figure 23. Interior Stress Profiles in Existing PCC Slab (Overlay Case) for Multiple Wheel Gear Load

Again, the stresses calculated by NIKE3D for the existing PCC slab compare better to BISAR than the calculated stresses for the PCC overlay. Although the slab in the pavement model is 30 by 30 ft, in figures 22 and 23 only half the slab is shown due to symmetry (only 160 inches are shown in the figures instead of 180 inches because of the location of the IPs in the elements of the FE pavement model). The stresses calculated by NIKE3D at the IP of the elements for the three pavements go to zero at the slab edge. However, BISAR-calculated stresses converge to zero much more slowly. The differences between the two results are caused by different assumptions and models used in the two programs (as mentioned in section 3.3). In particular, the FE model implies a zero stress condition at the free edge of the slab (x = 180 inches). The layered elastic model cannot replicate this condition.

4. CORRELATION ANALYSIS.

The 3D-FE program NIKE3D calculates the critical edge stress for rigid pavement design using the FAA's new pavement thickness design procedure FAArfield. The existing pavement thickness design procedure using design charts and described in AC 150.5320-6D [FAA (1)] was developed based on the critical edge stress H51 program (slab resting on dense liquid foundation) [Kreger, 1967]. Therefore, the correlation between the stresses calculated by the 3D and H51 models becomes important in the analysis of the differences between the two design procedures. It will also prove helpful in the calibration of the new FE design procedure by matching the calculated thickness to those predicted by the existing FAA design charts for rigid pavements.

32

4.1 EDGE STRESS DISTRIBUTION UNDER A SINGLE TIRE LOAD.

Two FE pavement models were used, referred to in this report as the cliff model and the step model (see figures 24 and 25 respectively). The cliff model has a straight vertical edge that passes through all the layers. In the step model, all the layers below the slab have been extended beyond the slab edge by 24 inches (section 5.4 presents the justification for the selection of the 24-inch extension). In both cases, a single 50,000-pound wheel load with 180-psi tire pressure was applied at the edge of a 30- x 30-foot slab.
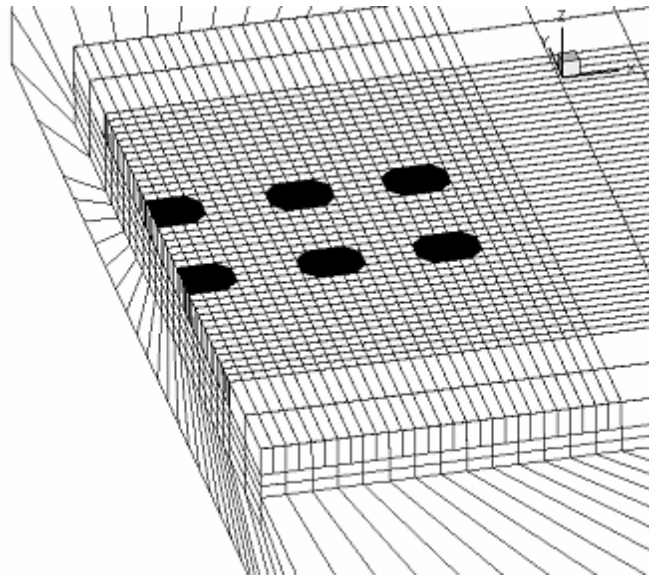
Figure 24. FAA Cliff Pavement Model
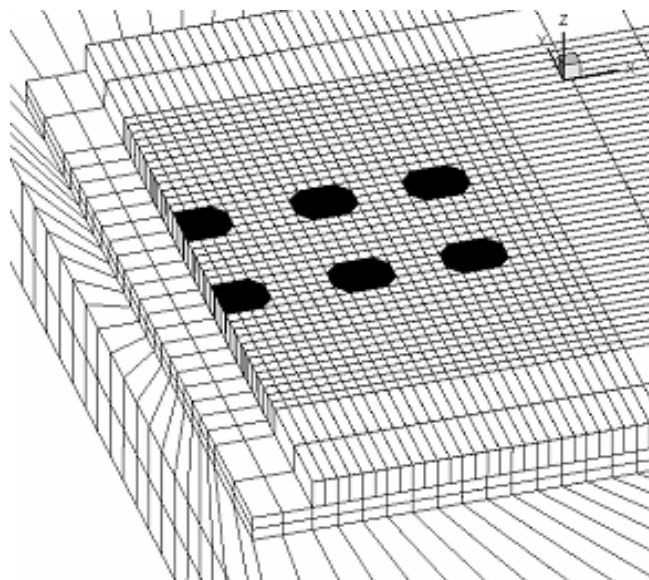
Figure 25. FAA Step Pavement Model

The pavement structures in table 7 were selected to compare responses calculated by the H51 [Kreger, 1967] program, based on the mid-slab resting on dense liquid foundation and NIKE3D. The structures' PCC slabs have the same thickness and material properties. Probably the most important difference between the two structures is the subgrade strength (4,500 psi versus 25,000 psi). Pavement A is a conventional structure on a crushed aggregate (P-209) subbase, while Pavement 37A has a stabilized subbase (P-306, econocrete subbase) over the P-209 subbase. The foundation effective modulus K_{eff}, represents the modulus of subgrade reaction k at the top of the base layer that is directly beneath the P-501 layer. It was computed using the method described in AC 150.5320-6D.

Table 7. Pavement Structures for H51 and NIKE3D Response Comparison

New Pavement A (Low-Strength Subgrade)

Layer	Thickness h (inch)	Elastic Modulus E (psi)	Poisson's Ratio μ	K_{eff} (pci)
P-501 PCC Slab	12	4,000,000	0.15	
P-209 Subbase	6	14,474	0.35	85.2
Subgrade		4,500	0.40	55.4
New Pavement 37A (High-Strength Subgrade)				
P-501 PCC Slab	12	4,000,000	0.15	
P-306 Econocrete	6	700,000	0.20	340.5
P-209 Subbase	6	49,985	0.35	264.0
Subgrade		25,000	0.40	210.0

Figure 26 compares stresses along the slab edge as calculated by NIKE3D (cliff model) and by H51. For Pavement A (low-strength subgrade), the maximum stress at the bottom as computed by NIKE3D agrees to within 99% of the maximum stress computed by H51. Good agreement is achieved, despite the fact that the subgrade models used in the two programs are very different. However, when the pavement has a high-strength foundation (Pavement 37A), the calculated stresses by NIKE3D are reduced from H51 by approximately 8 percent. The shape of the stress distribution along the slab edge as calculated by NIKE3D for both structures is generally consistent with the shape of the stress distribution as calculated by H51.
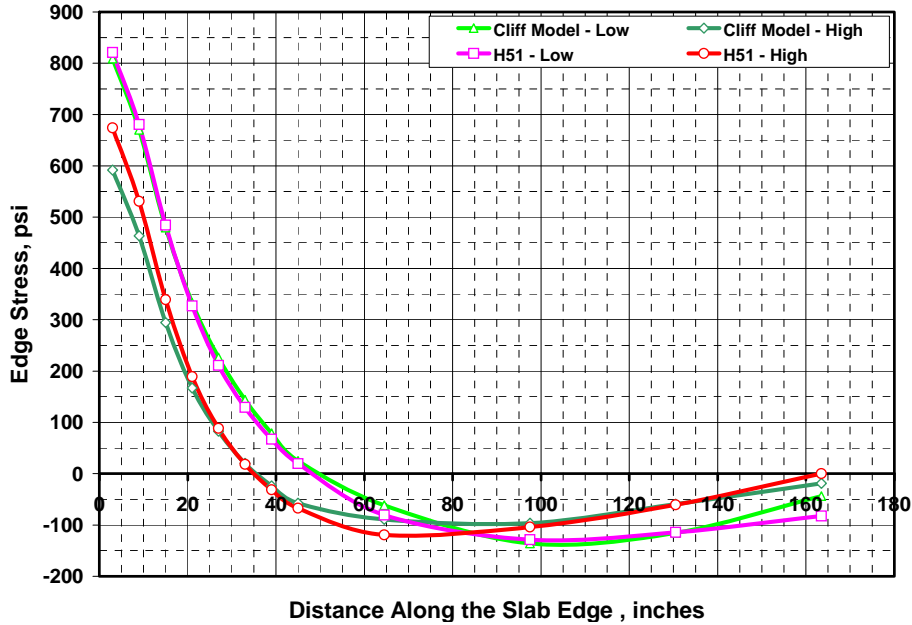
Figure 26. NIKE3D (Cliff Model) Versus H51—SWL

In figure 27, the maximum stresses calculated by H51 are much larger than those predicted by NIKE3D using the step model. For the low-strength foundation, the NIKE3D response drops to 92 percent of the corresponding H51 response, and for the high-strength foundation, the NIKE3D response drops to 70 percent of the H51 response. The NIKE3D edge stress distribution for the low-strength subgrade agrees with the stress distribution calculated by H51. However, for the high-stress subgrade, the NIKE3D stress distribution is only about 50 percent of the H51 distribution.
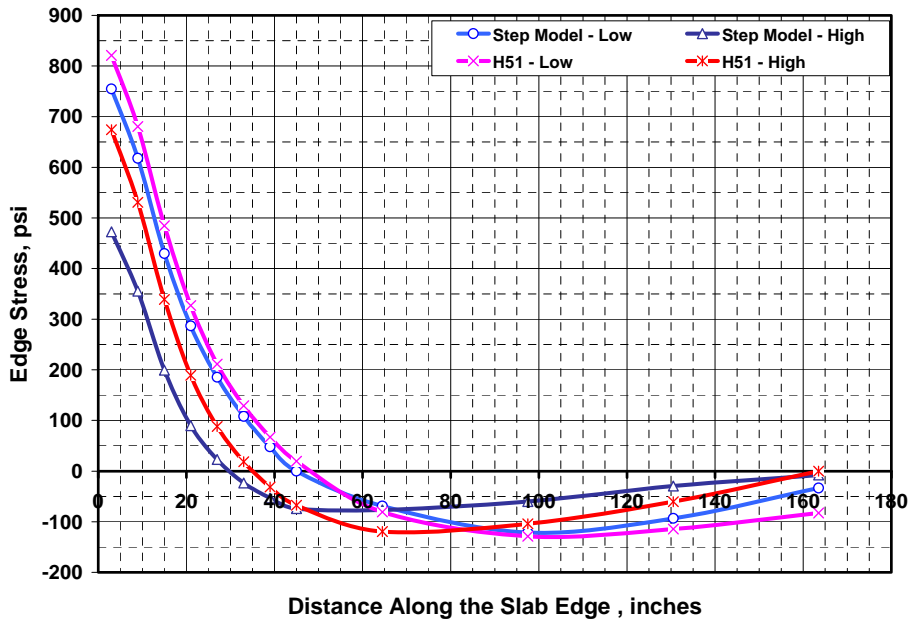
Figure 27. NIKE3D (Step Model) Versus H51—SWL

35

The PCC overlay design on an existing PCC pavement is different from the new PCC pavement design since more factors must be considered. First, the overlay thickness designed for a seriously deteriorated existing PCC pavement should be thicker than a less deteriorated pavement if the predicted traffic and environmental conditions are the same. Therefore, the condition of the existing pavement must be considered as input data in the overlay design. Second, the interaction between the overlay and the existing pavement must be considered in the design procedure. A rational approach is to divide the predicted traffic into several stages, each with equal traffic load and volume. After a PCC overlay is built on an existing PCC pavement, the traffic load in the first stage leads to distresses in the overlay and causes further deterioration in the existing PCC pavement, reducing its supporting capacity. The deterioration of the overlay under the second stage of traffic load is accelerated, even if the load and traffic volume remain the same.

To incorporate the above concept in the design procedure, the critical stresses must be calculated, not only in the overlay, but also in the existing PCC slab. The deteriorated elastic modulus E of the existing PCC pavement can be determined by equation 29, which was proposed by Rollings (1988):

$$E = E_0 x \left[0.02 + 0.0064 x SCI + \left(0.00584 x SCI \right)^2 \right] \tag{29}$$

where the pavement structural condition index (SCI) can be obtained by a distress survey of the existing pavement (AC 150.5380-6A). For a PCC pavement with SCI = 100, the elastic modulus equals the elastic modulus E_0 of the pavement when it is new. For a pavement with SCI < 100, equation 29 is used to determine the reduced elastic modulus for deteriorated pavement.

After the overlay is built on a deteriorated PCC pavement and traffic loads are applied to the overlaid pavement, the SCI of the existing pavement will be continuously decreased based on the calculated critical stress in the existing slabs. The decrease of the SCI will in turn lead to the decrease of elastic modulus of the existing PCC slabs, following equation 29.

LEDFAA calculates interior critical stresses for both overlays and existing slabs. Since the layered elastic response model has been replaced in FEDFAA by NIKE3D, it is necessary to investigate the correlation between critical stresses calculated using these two models.

The correlation analysis was conducted using the pavement structure shown in figure 28, where the overlay thickness h_1 varies from 2 to 16 inches. A 50,000-lb circular load is applied as shown in the layered elastic analysis using the LEAF and BISAR programs. The same load magnitude is applied in calculations using NIKE3D FAA 1.0, but the circular footprint has been replaced by a 16.67- by 16.67-inch-square footprint applied in the center of the free edge of a 30- by 30-ft slab. In the model, the load is uniformly distributed through nodes using the tributary area method. The nodal load is much easier to represent using a square shape instead of a circular shape. The stress returned by NIKE3D for the free edge case is then multiplied by 0.75, based on the assumption that 25 percent of the load is transferred to the unloaded slab. This procedure is used to estimate the critical stress at the joint. All geometric variables, e.g., element

size, mesh, extended foundation width, are the same as for a new PCC pavement thickness design. The default data used in the design is in table 8.
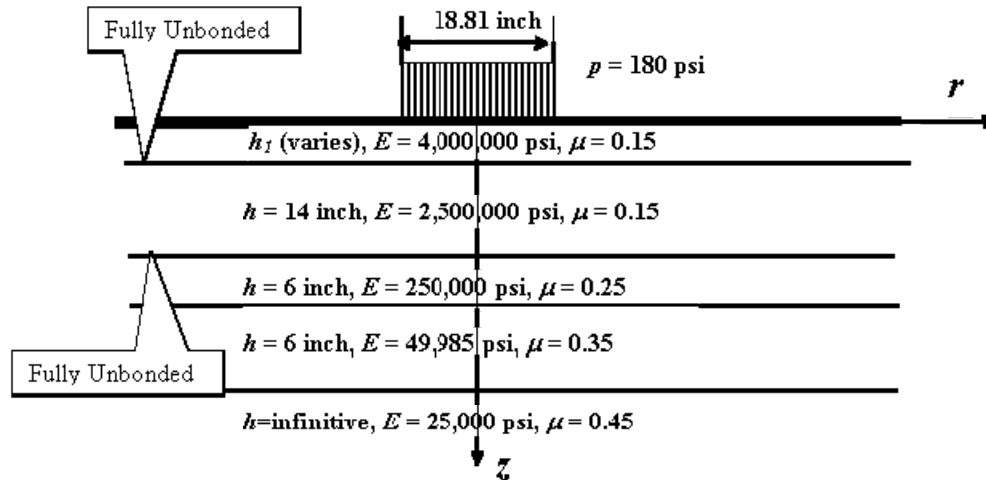
Figure 28. Overlay Structure for Correlation Analysis

Table 8. Portland Cement Concrete Overlay Pavement Structure

Layer	Thickness h (inch)	Elastic Modulus E (psi)	Poisson's Ratio μ
PCC Overlay	10	4,000,000	0.15
Base PCC	14	2,000,000	0.15
Stabilized Base	6	500,000	0.20
Subbase	12	75,000	0.35
Subgrade		4,500	0.40

The curves of maximum tensile stress as a function of overlay thickness are shown in figure 29. Three curves are shown for NIKE3D, LEAF, and BISAR. All three curves show the same tendency: the maximum bending stress on the bottom of the overlay is not proportional to the overlay thickness. Rather, a critical overlay thickness exists that corresponds to the maximum tensile stress in the overlay. For this specific pavement, the critical overlay thickness is approximately 8 inches, as calculated by either LEAF or BISAR, and is about 9 inches when calculated by NIKE3D FAA 1.0.
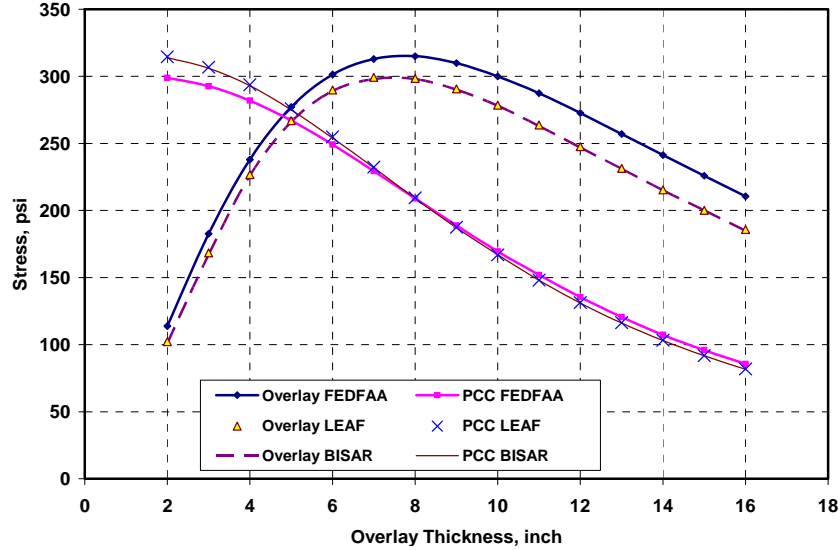
Figure 29. Stress Correlation Calculated by NIKE3D, LEAF, and BISAR

The curves in figure 29 indicate that the maximum tensile stress at the bottom of the existing slab has an inverse relationship to the overlay thickness, i.e., the thicker the overlay, the smaller the maximum tensile stress will be in the existing slab. All curves calculated by NIKE3D FAA 1.0 and LEAF for the overlay and for the existing slab correlate almost perfectly. The comparison shows that the stress magnitudes calculated by NIKE3D FAA 1.0 and LEAF are not the same because they are calculated using different models. However, since the critical stress results are well correlated, the required overlay thickness calculated by NIKE3D FAA 1.0 can be appropriately calibrated and matched to those predicted by the existing design procedure.

4.3 CRITICAL STRESSES FOR PARTIALLY BONDED OVERLAYS.

As originally implemented in NIKE3D, the contact surface had two options: fully bonded (fixed) or fully unbonded (sliding). The fully bonded contact surface is not used in FEDFAA. To implement the partially bonded overlay option, a third interface type (partially bonded) was added. Four subroutines were modified in NIKE3D to make the partially bonded interface available. When the partial bond interface is selected, NIKE3D applies a horizontal spring stiffness at the interface between the rigid overlay and the base PCC. The value of the horizontal stiffness was chosen to agree with the partial bond case as implemented in JULEA (Jacob Uzan Layered Elastic Analysis) and LEDFAA. JULEA defines an interface spring stiffness k as

$$k = \frac{l}{(1-l)} \tag{30}$$

where

$l = 10 \exp{(-m / E_2)}$
$E_2 = E$ of the underlying layer (base PCC)
$m = 700$ for partial bond

38

The stiffness k has units of lb/inch per inch along the radius, per inch along the circumference at radius r (cylindrical coordinate system). In NIKE3D, the equivalent stiffness is obtained as (see subroutine slave2):

$$k = \frac{l}{1-l} xAx \frac{A}{2x\left(\frac{4}{\pi}\right)} \tag{31a}$$

or

$$k = 0.01xk_l xA \tag{31b}$$

The $\pi/4$ factor is a consequence of the transformation from cylindrical to Cartesian coordinates. The additional factor of two is needed because JULEA defines one stiffness that applies to the interface itself. NIKE3D, on the other hand, defines a stiffness for each contact surface, and the interface stiffness is the sum of the horizontal stiffness for the two surfaces. Therefore, it is necessary to divide by two to obtain the equivalent of the original (JULEA) stiffness. The implementation in NIKE3D of the partial bond interface was achieved by modifying the subroutine slave2.

To test the new interface capability, the pavement structure in table 8 was subjected to a B777-200B gear load (680,000-pound GW and 215-psi tire pressure). All three interface types were used, and the responses computed by NIKE3D FAA 1.0 were compared to the corresponding stresses calculated by JULEA. JULEA was selected as the base because it has the capability to consider the effects of the partially bonded interface. The original partial bond case was implemented in JULEA (not LEAF) in LEDFAA 1.2.

Figures 30 and 31 and table A-5 in appendix A show the stress comparison for three different interface conditions for the PCC overlay and existing PCC, respectively. For each case, the stresses and the responses show good agreement through the slab depth.
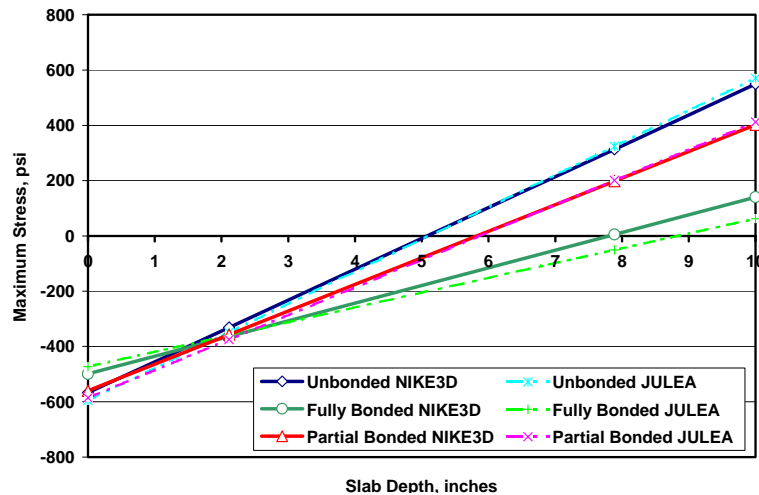
Figure 30. NIKE3D and JULEA Stress Comparison Through PCC Overlay
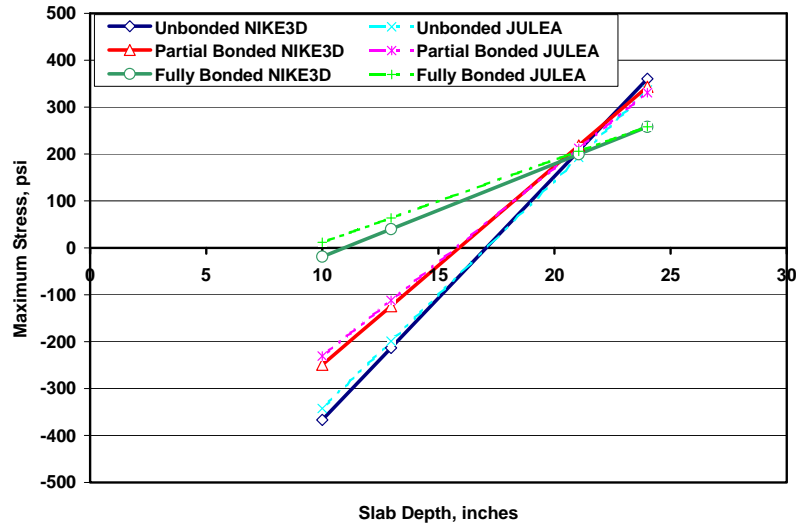
Figure 31. NIKE3D and JULEA Stress Comparison Through Base PCC

5. MODEL PARAMETER SELECTION.

As emphasized at the beginning of this report, the damage indicator for PCC pavement design is the maximum computed stress in the PCC slab. This indicator is used because it is closely related to bottom-up structural cracking.

The pavement service life in the damage model is a function of the maximum stress. The higher the calculated stress, the shorter the pavement service life for the same concrete flexural strength. Because the pavement design is expected to provide satisfactory service for a long period under a wide range of different environmental and traffic conditions, it is difficult to set appropriate quantitative criteria for selecting the model parameters to compute critical stress.

The following qualitative criteria have been considered in this report:

- Model parameters should be chosen to reasonably simulate the actual pavement behavior during its service life.

- To make the design thickness predicted by the new design procedure comparable to existing ones, design thicknesses for typical pavements need to be well correlated to corresponding design thicknesses using the current FAA design procedure (AC 150.5320-6D) for the existing fleet of aircraft.

In some cases, model parameters may be selected to shorten the computation time, provided the results are kept within the range of acceptable accuracy.

40

5.1 HORIZONTAL MESH DENSITY.

To determine the size in plane of the brick element to be used for FEDFAA, a PCC slab of 30 by 30 feet was selected. The objective was to find the best element size, considering computational time and accuracy.

In section 4, the accuracy of NIKE3D-calculated stresses was validated by H51 at the bottom of the slab. Since the NIKE3D-calculated stresses are located at the element IPs, to compare the stresses calculated by NIKE3D FAA 1.0 to the stresses calculated by H51, they have to be extrapolated to the slab bottom. The smaller the element size, the more accurate the extrapolation. The FEDFAA pavement model was tested for the two pavement structures in table 9. The loads used were (a) 50,000-lb SWL with 180-psi tire pressure and (b) 634,500-lb B777-200ER with 215-psi tire pressure.

Table 9. Pavement Structures for Maximum Stress Comparison

Layer	Thickness h (inch)	Poisson's Ratio μ	Low-Strength Subgrade Elastic Modulus E (psi)	High-Strength Subgrade Elastic Modulus E (psi)
PCC Slab	18	0.15	4,000,000	4,000,000
Subbase	6	0.35	14,474	49,985
Subgrade	-	0.40	4,500	25,000

Table A-6 (appendix A) and figure 32 present the calculated maximum stresses for the five models using different element sizes (in plane) for the model horizontal fine mesh under the load of SWL and B777-200ER. In table A-6, the number of equations, iterations, computational time, and accuracy of the calculated stresses for the five models is compared.
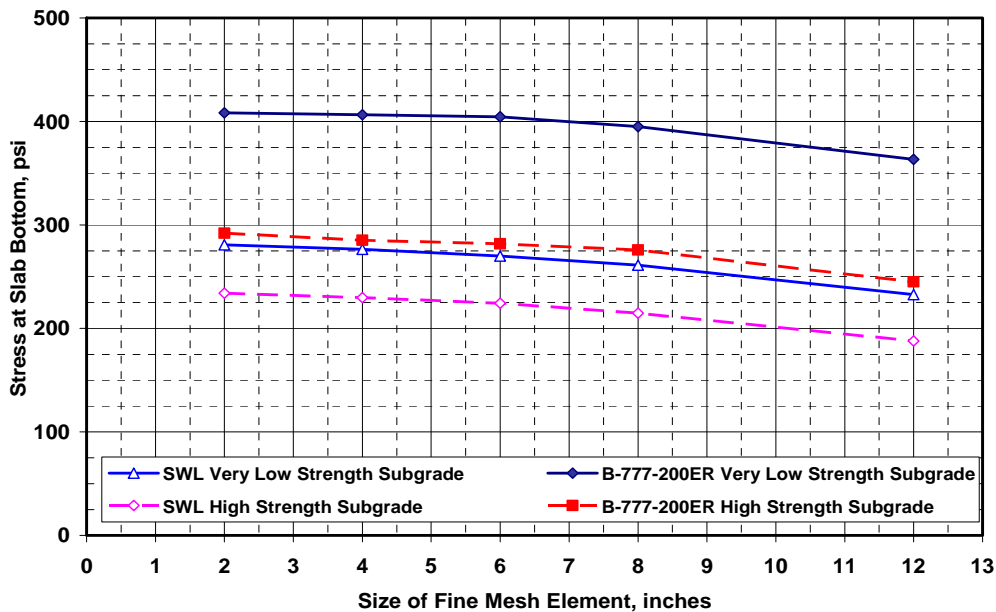
Figure 32. Horizontal Mesh Size Selection

41

Additionally, to evaluate the effect of the element size in the horizontal mesh along the slab edge, the structure presented in table 10 was tested under 50,000-lb SWL with 180-psi tire pressure. Six different element sizes were used: 1.5, 2, 4, 6, and 8 inches. Figure 33 shows the comparison of the stresses along the slab edge (also see table A-7 in appendix A). It can be observed that the stresses along the edge follow the same trend regardless of the particular size of the elements in the mesh.

Table 10. Pavement Structure for Stress Comparison Along Slab Edge

Pavement Layer	Thickness h (inch)	Poisson's Ratio μ	Medium-Strength Subgrade, Elastic Modulus E (psi)
PCC Slab	14	0.15	4,000,000
P-306	6	0.20	700,000
P-209	6	0.35	75,000
Subgrade	-	0.40	15,000
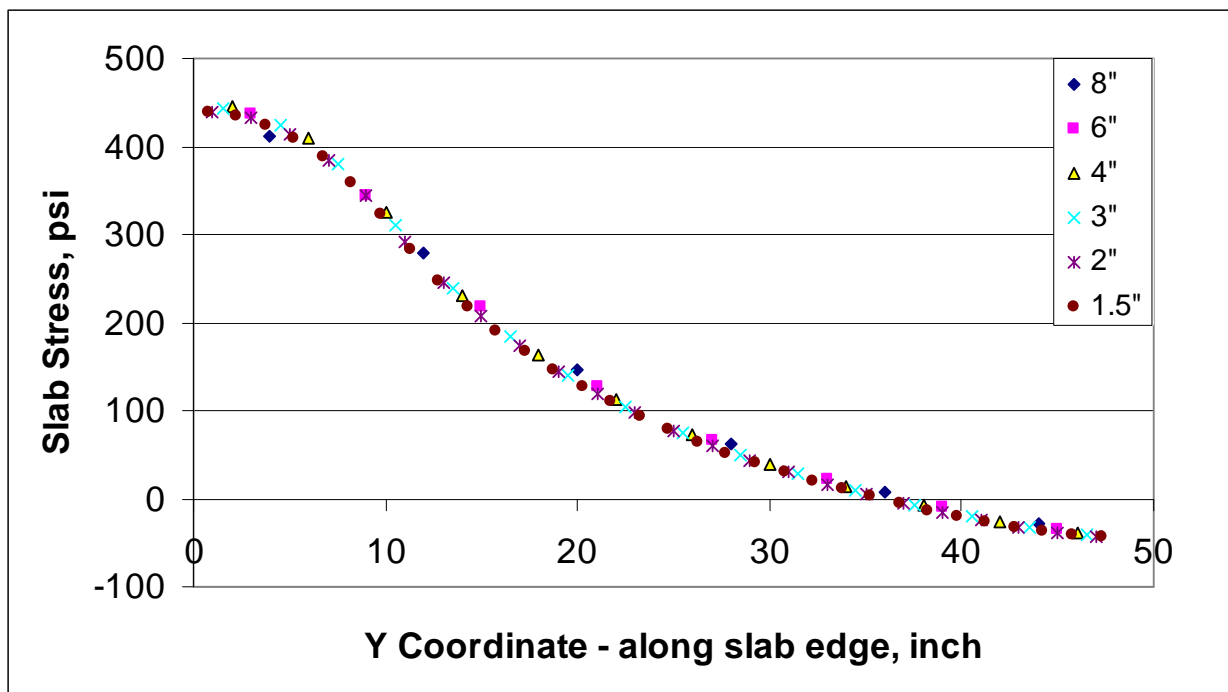
Figure 33. Horizontal Mesh Element Comparison Along Slab Edge

It was determined that the most appropriate element size for the design model is 6 by 6 inches. The reason for this judgment is explained below.

Compared to the 2-inch element size, the response accuracy of the pavement model is slightly higher for the 4-inch than the 6-inch element size model under SWL and multiple tire gear load (from 98% to 100% for the 4-inch element size versus 96% to 99% for the 6-inch element size).

However, the computational time for the 6-inch element pavement model is significantly smaller than for the 2- and 4-inch element sizes. The 6-inch model runs from 20 to 40 percent faster than the 4-inch and 10 times faster than the 2-inch model under SWL and under multiple wheel load runs from 3 to 6 times faster than the 4-inch and 20 to 55 times faster than the 2-inch model.

5.2 VERTICAL MESH DENSITY.

Since the critical stress is located at the bottom of the PCC slab, the vertical mesh of the slab layer will affect the pavement responses calculated by NIKE3D. Two pavement structures under an SWL of 50,000 pounds and 180-psi tire pressure were used to determine the vertical mesh. The pavement structures have a PCC slab thickness of 18 inches over a subgrade with E values of 4,500 and 100,000 psi, respectively.

To check the responses (interior stresses) calculated by NIKE3D, they were extrapolated from the Gaussian IP to the top and bottom of the slab (center of the element in the horizontal mesh) and compared to the stresses calculated by the LEAF program. Three different element sizes were used in the horizontal mesh, 2, 4, and 6 inches, and four different vertical meshes, single-element (18-inch-thick element), two-element (9-inch-thick elements), four-element (4.5-inch-thick elements), and six-element (3-inch-thick elements).

Tables 11 and 12 and figures 34 and 35 compare the NIKE3D linearly extrapolated responses at the bottom and top of the slab to the LEAF responses for low- and high-strength subgrades respectively. In the vertical mesh, for the high- and low-strength subgrade, the model using a single element for the slab thickness (single element) calculates a very similar bottom stress than the model using six elements. For the stress at the top of the slab, the variation between a single element and six elements can be up to 29%; however, since the critical stress is at the bottom of the slab, the choice of using a single element for the pavement model is acceptable.

The effect of element size for the horizontal mesh was discussed in section 5.1; in any case, the difference between the larger and smaller element size in the current example varies from 2% to 7% at the bottom of the slab and 0% to 6% at the top of the slab.

Table 11. Maximum Stress at the Bottom of the Slab

E_{SG} (psi)	Vertical Mesh, Element Number	Horizontal Mesh, Stresses (psi)								
		2-Inch Element			4-Inch Element			6-Inch Element		
		FEDFAA	LEAF	F/L	FEDFAA	LEAF	F/L	FEDFAA	LEAF	F/L
100,000	1	155.8	149.4	1.04	147.7	146.5	1.01	144.7	141.8	1.02
	2	134.7		0.90	12.8.8		0.88	125.6		0.89
	4	151.7		1.02	144.4		0.99	141.8		1.00
	6	153.4		1.03	148.5		1.01	145.8		1.03
4,500	1	204.0	226.5	0.90	199.2	223.4	0.89	195.7	218.4	0.90
	2	186.1		0.82	179.8		0.80	175.9		0.81
	4	200.2		0.88	195.2		0.87	191.8		0.88
	6	206.2		0.91	199.2		0.89	195.7		0.90

Table 12. Maximum Stress at the Top of the Slab

E_{SG} (psi)	Vertical Mesh, Element Number	Horizontal Mesh, Stresses (psi)								
		2-Inch Element			4-Inch Element			6-Inch Element		
		FEDFAA	LEAF	F/L	FEDFAA	LEAF	F/L	FEDFAA	LEAF	F/L
100,000	1	-169.5	-209.7	0.81	-162.0	-211.1	0.77	-158.8	-210.6	0.75
	2	-187.1		0.89	-183.6		0.87	-181.0		0.86
	4	-216.4		1.03	-213.1		1.01	-213.3		1.01
	6	-218.2		1.04	-220.7		1.05	-223.7		1.06
4,500	1	-215.0	-285.4	0.75	-209.8	-286.6	0.73	-206.0	-286.0	0.72
	2	-236.3		0.83	-232.3		0.81	-229.1		0.80
	4	-263.1		0.92	-262.4		0.92	-261.9		0.92
	6	-269.6		0.94	-270.0		0.94	-272.5		0.95

The incorporation of more than a single element in the pavement model vertical mesh greatly increases the number of elements in the model and the computational time without significantly increasing model accuracy. The reason for the lack of sensitivity to the number of elements through the thickness is that nonconforming elements are used in the model. If regular brick elements were used, the response would be strongly dependent on the number of element layers.
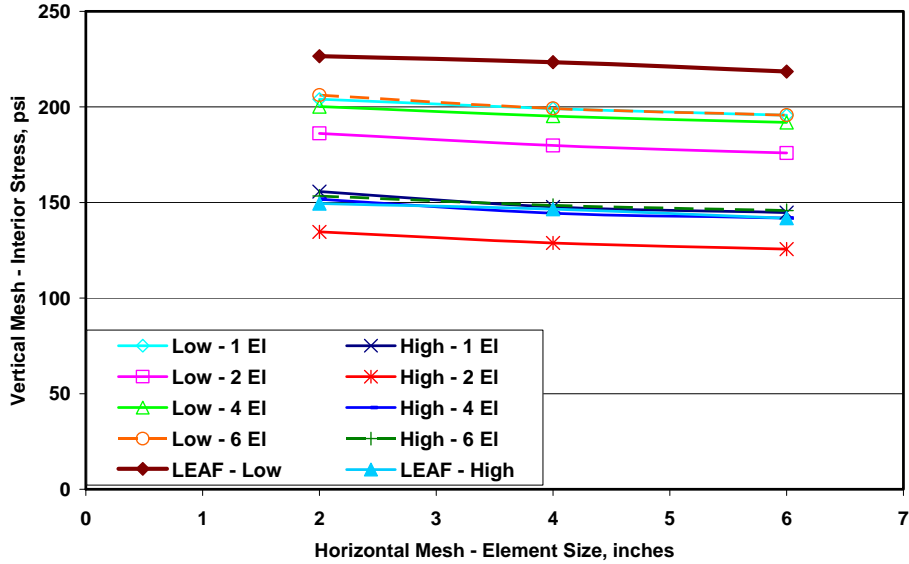
Figure 34. Stress at Slab Bottom for Different Number of Elements in Vertical Mesh
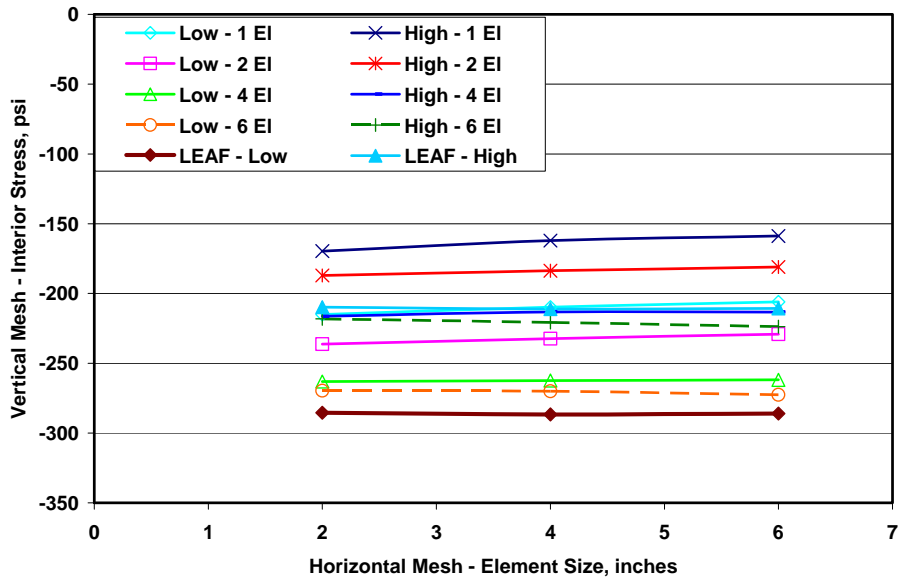
Figure 35. Stress at Slab Top for Different Number of Elements in Vertical Mesh

5.3 SLAB SIZE.

A 30- by 30-foot slab was selected for the FEDFAA design using the single step model. The predicted stresses by FEDFAA for different slab sizes and pavement structures were compared until convergence to the calculated H51 stress was achieved. Table 13 describes the four pavement structures with different subgrade strengths used for the slab size selection.

Table 13. Pavement Structures for FEDFAA Rigid Pavement Model Evaluation

Pavement Structure Layer	Elastic Modulus E (psi)	Poisson's Ratio μ	Modulus of Subgrade Reaction k (psi)
Very Low-Strength Subgrade (A)			
14-inch PCC	4,000,000	0.15	
6-inch P-306	700,000	0.20	183.40
6-inch P-209	14,474	0.35	
Subgrade	4,500	0.40	
Low-Strength Subgrade (23A)			
14-inch PCC	4,000,000	0.15	
6-inch P-306	700,000	0.20	241.37
6-inch P-209	21,404	0.35	
Subgrade	7,500	0.40	
Medium-Strength Subgrade (30A)			
14-inch PCC	4,000,000	0.15	
6-inch P-306	700,000	0.20	304.49
6-inch P-209	35,429	0.35	
Subgrade	15,000	0.40	
High-Strength Subgrade (37A)			
14-inch PCC	4,000,000	0.15	
6-inch P-306	700,000	0.20	340.40
6-inch P-209	49,985	0.35	
Subgrade	25,000	0.40	

Six slab sizes (15, 20, 25, 30, 40, and 50 ft) were tested using the FEDFAA step model under the dual-wheel load of the B727-200 with a GW of 172,000 pounds and tire pressure of 160 psi. Figure 36 and table A-8 in appendix A show the comparison of the maximum stresses calculated by FEDFAA for a 6-inch element size extrapolated to the slab edge and bottom and the stresses calculated by H51 for the same slab sizes and pavement structures.
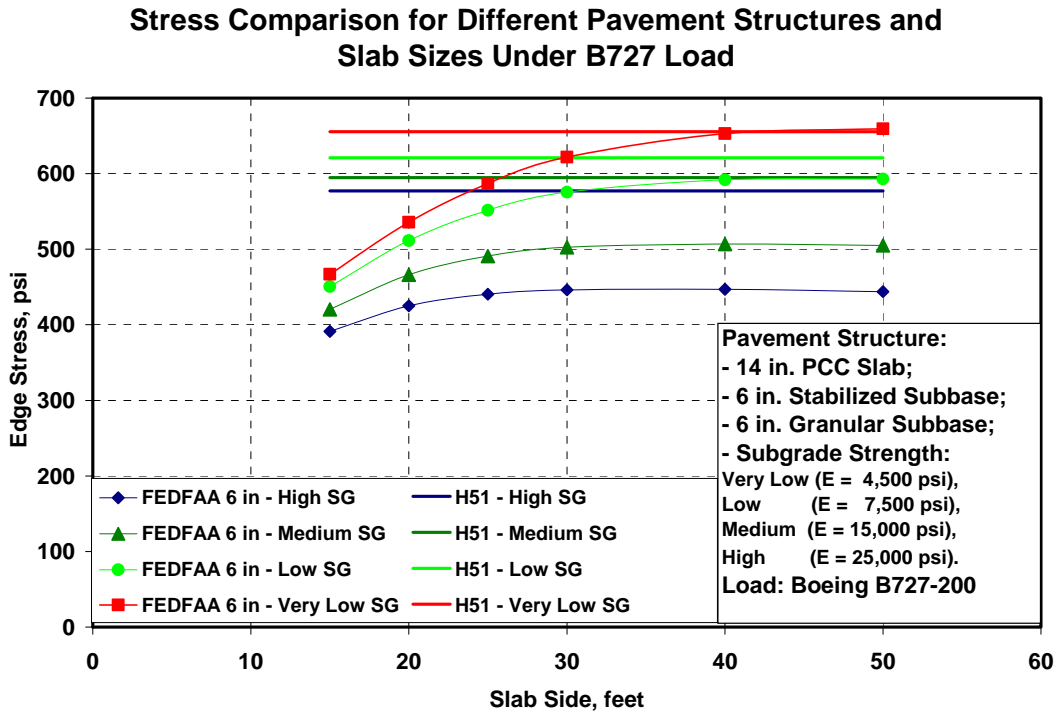
Figure 36. FEDFAA and H51 Stress Comparison

The maximum stress for all the different structures is achieved when the slab size dimensions are 30 by 30 ft. For the very low- and low-subgrade strength, the FEDFAA/H51 ratio has almost no variation when the slab size is larger than 30 ft. However, for the medium- and high-strength subgrade, the ratio slightly decreases when the slab size is larger than 30 ft. Since the maximum stress converges for the different structures when the slab has a 30-ft side, this slab size is chosen with an element size of 6 inches.

5.4 WIDTH OF SUBBASE EXTENSION.

To provide a more realistic model of the edge-loaded slab response, all pavement layers below the slab are extended some distance *d* beyond the edge of the slab. Figure 37 shows the pavement model using different widths of *d* from 0 to 108 inches. The choice of *d* is to some extent a matter of judgment. The determination of an appropriate distance *d* for the model was based on two considerations.

As the value of *d* increases, and all else being equal, the computed stress should converge to a limit value. The selected *d* should be large enough to approximate this limit condition.

The larger the value of *d* selected, the more elements will be required, and the longer the required computation time. The value of *d* should not be chosen so large that it unnecessarily increases computation time.

d=0 inch
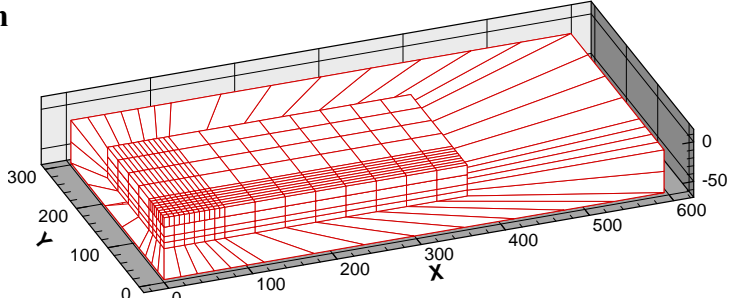
d=24 inches
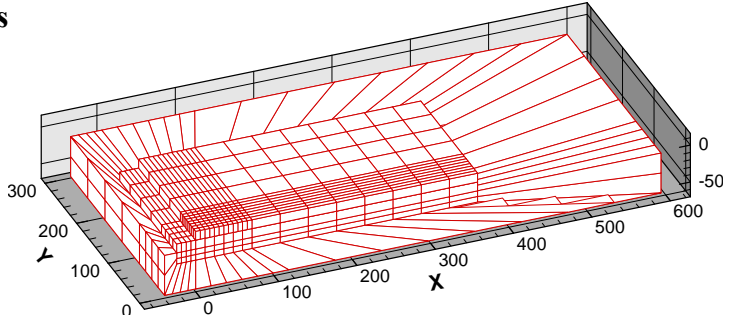
d=72 inches
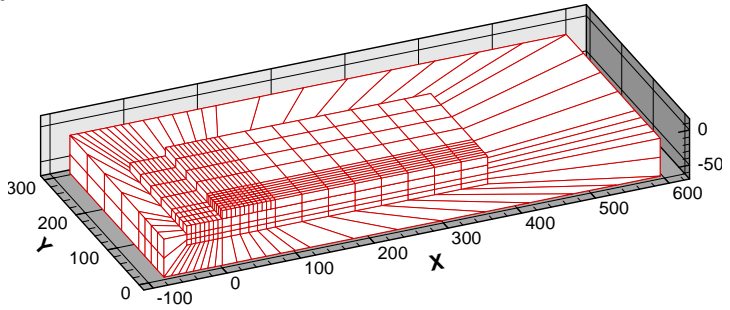
d=108 inches
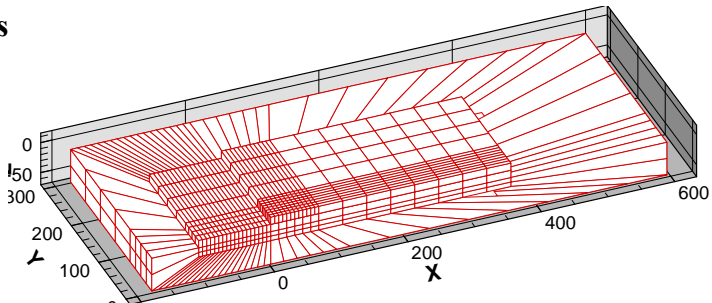
Figure 37. Model With Various Widths of Extended Foundation

48

The analysis was based on two pavement structures, designated as InS5-2 and InS5-6, under an SWL of 50,000 lb and 180-psi tire pressure. The structural properties of these pavements are given in table 14 with a slab thickness of 12 inches. These two pavements can be characterized by the radius of relative stiffness l_s, given in equation 32.

Table 14. Material Properties for Two-Layer Structures With Different Relative Stiffness

ID	Concrete Elastic Modulus E (psi)	Concrete Poisson's Ratio μ	Subgrade Elastic Modulus E_s (psi)	Subgrade Poisson's Ratio M_s	Radius of Relative Stiffness L_s (inch)
InS5-1	6,000,000	0.15	5,000	0.40	66.72
InS5-2	4,000,000	0.15	5,000	0.40	58.28
InS5-3	4,000,000	0.15	10,000	0.40	46.26
InS5-4	4,000,000	0.15	25,000	0.40	34.08
InS5-5	4,000,000	0.15	50,000	0.40	27.05
InS5-6	4,000,000	0.15	75,000	0.40	23.63

$$l_s = \sqrt[3]{\frac{E \times h^3 \times \left(1-\mu_s^2\right)}{6 \times E_s \times \left(1-\mu^2\right)}}$$

(32)

In equation 32, E_s and E represent the elastic moduli of the upper and lower layers, respectively. Similarly, μ_s and μ are the Poisson's ratios of the upper and lower layers, respectively. The range of l_s (23.6 to 66.7 inches) covers the practical range for airport pavements.

The plotted profiles of computed responses along the loaded slab edge for pavements InS5-2 and InS5-6 for various assumed values of d are shown in figures 38 and 39. The plotted deflection is shown in figure 38(a) and (b), while the plotted horizontal bending stress on the bottom plane of the slab is shown in figure 39(a) and (b). Observations from these plots are summarized as follows:

- As expected, the edge deflections and stresses are reduced from the cliff case as the foundation is extended. The greater the width d of the extension, the greater the reduction in both maximum deflection and maximum stress. This is true for both pavement structures.

- Both the deflection and stress curves converge to limit values as the extension d becomes large. The largest value of d considered is 108 inches, but for $d = 108$ in., the responses approximate the infinite case. (Additional increases in d would result in only negligible changes in the computed responses.)

- Though the above observations apply to both pavement structures, there are significant differences between the two structures in the computed deflection response. As expected, the magnitude of deflections is higher for the weaker structure (InS5-2) than

for the stronger structure (InS5-6). However, it is also observed that the shape of the deflection profile is different. For a slab on a strong subgrade (figure 38(a)) there is essentially zero deflection at a finite offset (approximately 120 inches) from the load center, while for a slab on a weak subgrade (figure 38(b)), it appears that the entire slab has been pushed down into the subgrade by the applied load.

- While the extended foundation tends to reduce maximum computed bending stresses for both structures, the reduction is significantly larger on a percentage basis for the strong subgrade.

- It is also found that the width d of the extended foundation tends to affect the location of the point of stress sign reversal. At some offset distance from the load center, the bending stress on the bottom of the slab changes from a tensile (positive) stress to a compressive (negative) stress. In general, as d increases, the location of the stress reversal point shifts toward the load center. This phenomenon is illustrated in figure 39.

The last observation has ramifications for multiple wheel loads. Consider that for any multiple wheel aircraft gear, the spacing between adjacent tires is fixed. The contribution of an additional tire to the critical stress, whether positive or negative, depends on whether that tire is positioned inside or outside the stress reversal point. If, for example, a second tire were to be positioned to the left of the stress reversal point in figure 39(b), then the contribution of that tire to the total critical stress under the first tire would be positive. As the reversal point shifts to the left, the stress contribution of the additional tire likewise shifts from positive to negative (i.e., causes a reduction in critical stress relative to the single tire load). Therefore, it is conceivable that a design based on 3D-FEM structural analysis using the extended step-based model would require a thinner slab for a dual load than for an SWL, whereas the same design using the FAA Westergaard-based [Westergaard, 1926 and 1948], design charts in AC 150.5320-6D [FAA (1)] would require an increase in slab thickness for the additional wheel. This possible discrepancy between the two design models should be considered when comparing designs using the new FEDFAA design procedure to those using conventional FAA (Westergaard-based) design.

Effect of Step Width (d) on Deflection Along the Slab Edge

Ec=4,000 ksi, Es=75 ksi, Ls=23.6 in.
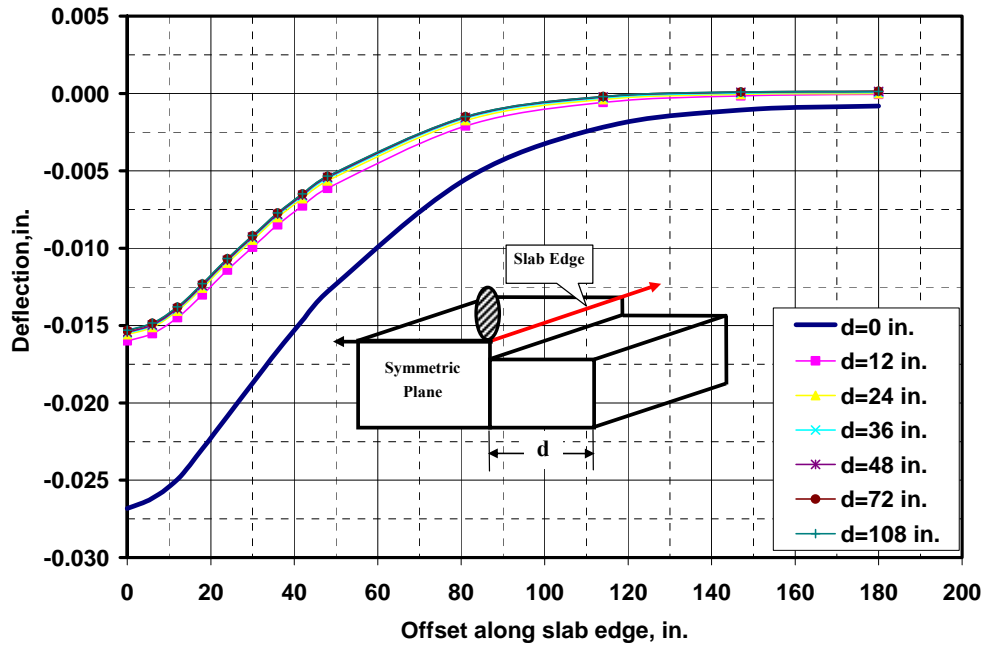
(a) Structure InS5-6, Slab on Strong Subgrade

Effect of Step Width (d) on Deflection Along the Slab Edge

Ec=4,000 ksi, Es=5 ksi, Ls=58.3 in.
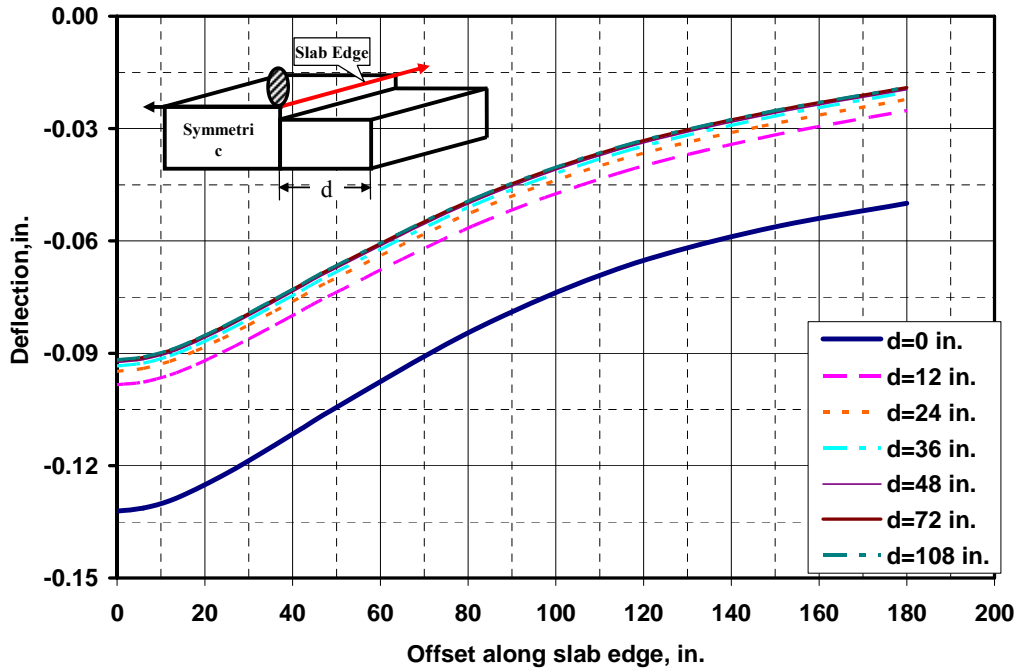
(b) Structure InS5-2, Slab on Weak Subgrade

Figure 38. Effects of Extended Foundation Width on Deflections

51

Effect of Step Width (d) on Stresses at the Slab Bottom

Ec=4,000 ksi, Es=5 ksi, Ls=23.6 in.
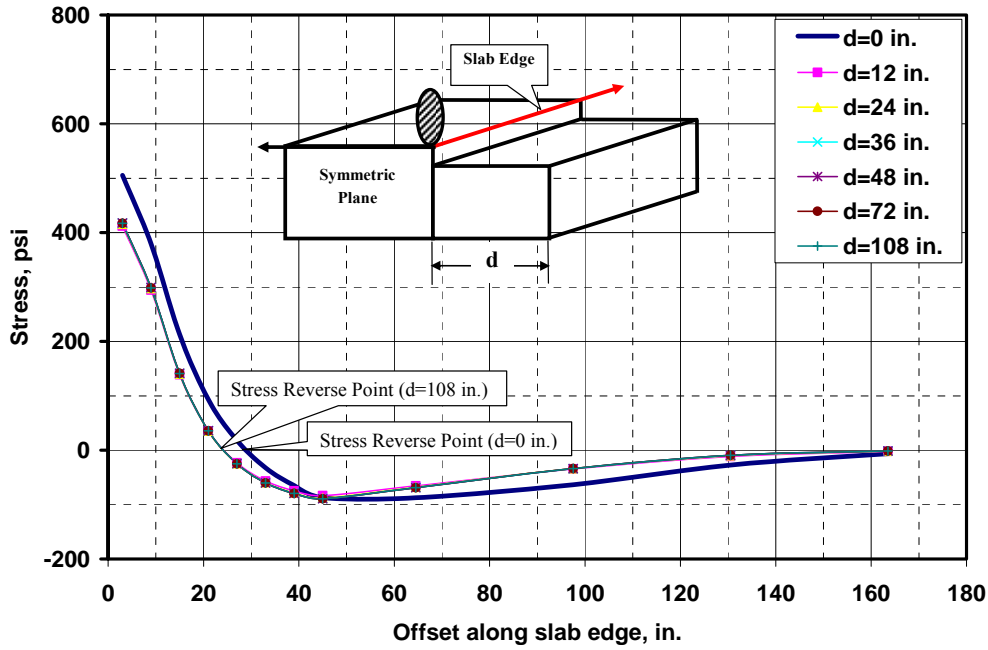
(a) Structure InS5-6, Slab on Strong Subgrade

Effect of Step Width (d) on Stresses at the Slab Bottom

Ec=4,000 ksi, Es=5 ksi, Ls=58.3 in.
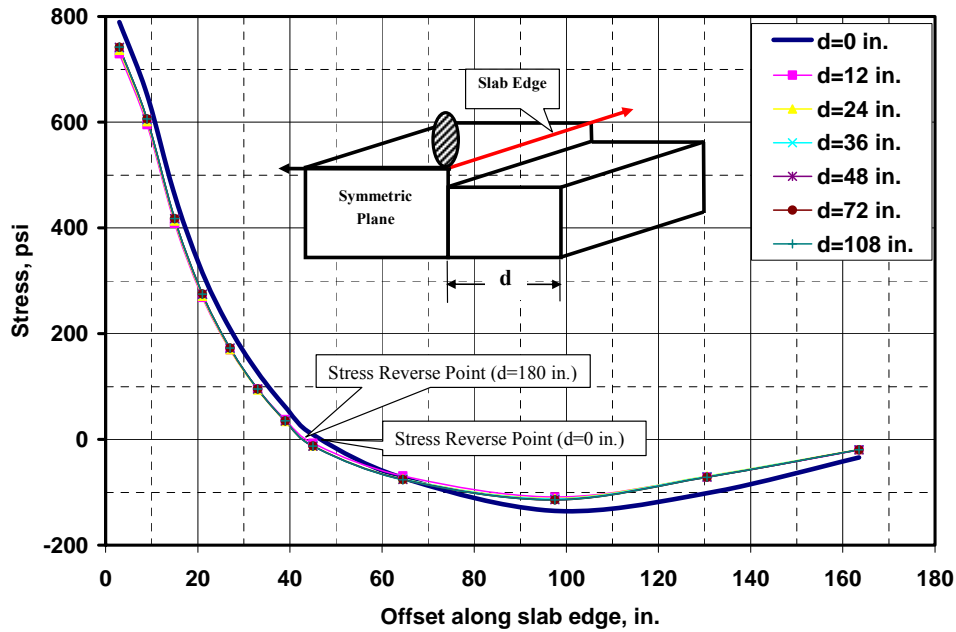
(b) Structure InS5-2, Slab on Weak Subgrade

Figure 39. Effects of Extended Foundation Width on Stresses

52

Based on discussion, the width d of the extended step foundation used in the FEDFAA design procedure is 24 inches. The stress difference using a 24-inch step or a longer step is negligible (table 15).

Table 15. Precision of Using a 24-Inch Extended Foundation

	Step width, d		Diff. in
Responses	d = 24 inches	d = 108 inches	%
Critical Stress at the Bottom, l_s = 58.3 inches (psi)	736.2	741.8	0.8
Critical Stress at the Bottom, l_s = 23.6 inches (psi)	415.6	417.0	0.3
Maximum Deflection, l_s = 58.3 inches (inches)	94.8	91.8	3.2
Maximum Deflection, l_s = 23.6 inches (inches)	15.6	15.3	2.0

5.5 INFINITE ELEMENT MESH FOR SUBGRADE.

The subgrade depth of a pavement varies on different fields. To verify the validity of the infinite elements, a pavement model using FEs was tested. The stresses calculated by NIKE3D FAA 1.0 are the stresses at the element IPs, the results calculated by BISAR are used to verify the accuracy of the deflections and stresses calculated by NIKE3D FAA 1.0. Due to symmetry, only one-quarter of the domain is meshed, as shown in figure 40. The detailed nodal coordinates x, y, and z for NIKE3D FAA 1.0 are given in appendix A.
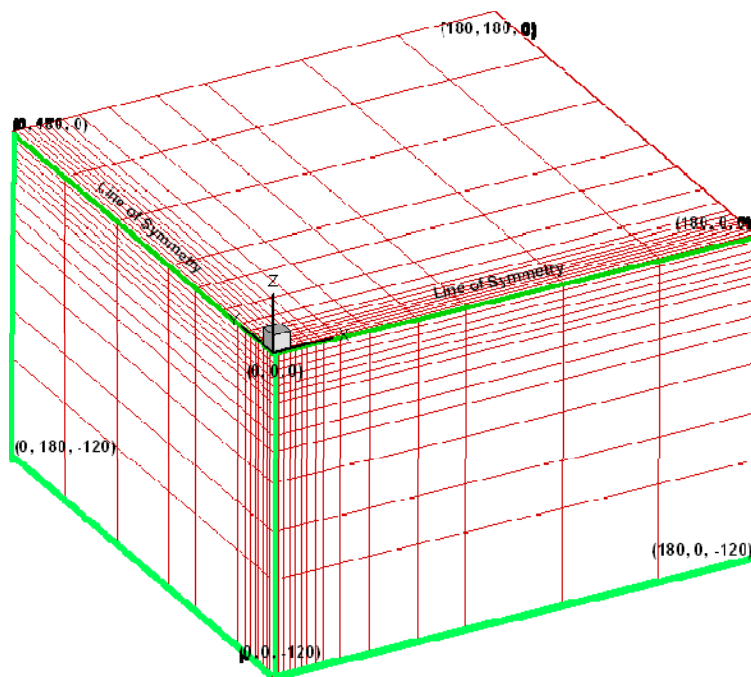
Figure 40. Mesh Used by NIKE3D FAA 1.0 for Comparison With BISAR Results

Figure 41 presents vertical deflections calculated by BISAR and NIKE3D FAA 1.0 along the z axis in figure 8. The boundary condition is fixed (w = 0) at z = 120 inches and free in the z direction (w = 0) at x = 180 inches and y = 180 inches. Figure 41 shows that NIKE3D calculated

vertical deflections are smaller than those calculated by BISAR. Since the boundary condition at z = 120 inches has been fixed, the deflection at that surface is zero by definition. However, the vertical deflection predicted by BISAR at z = 120 inches is 0.0204 inch. If the NIKE3D-computed deflections are adjusted by this value, then the result (figure 41) is almost identical to the curve obtained by BISAR.
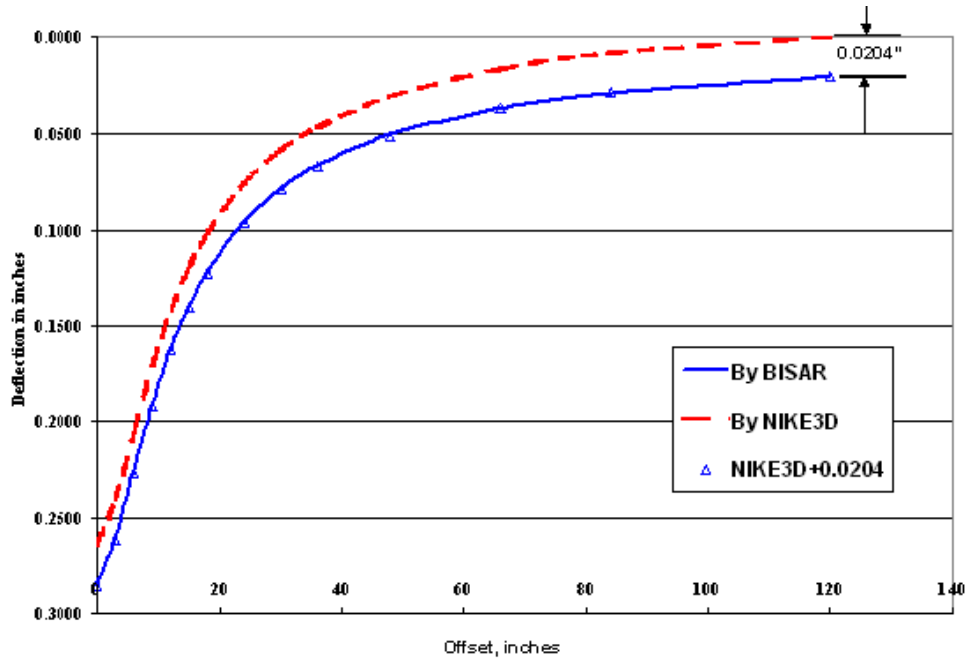
Figure 41. Vertical Deflections Along z Axis by NIKE3D and BISAR

Figure 42 presents the surface deflections calculated by NIKE3D FAA 1.0 and BISAR. The deflections calculated by the two programs also show a difference. The diamond dots in figure 42 show the adjusted surface deflection obtained by adding 0.0204 inch to the deflections calculated by NIKE3D. It can be seen that the adjusted surface deflections are also almost identical to those by BISAR in the area near the loading center, but tend to diverge further away from the loading center. This difference is caused by the nonuniform deflections at z = 120 inches calculated by BISAR.
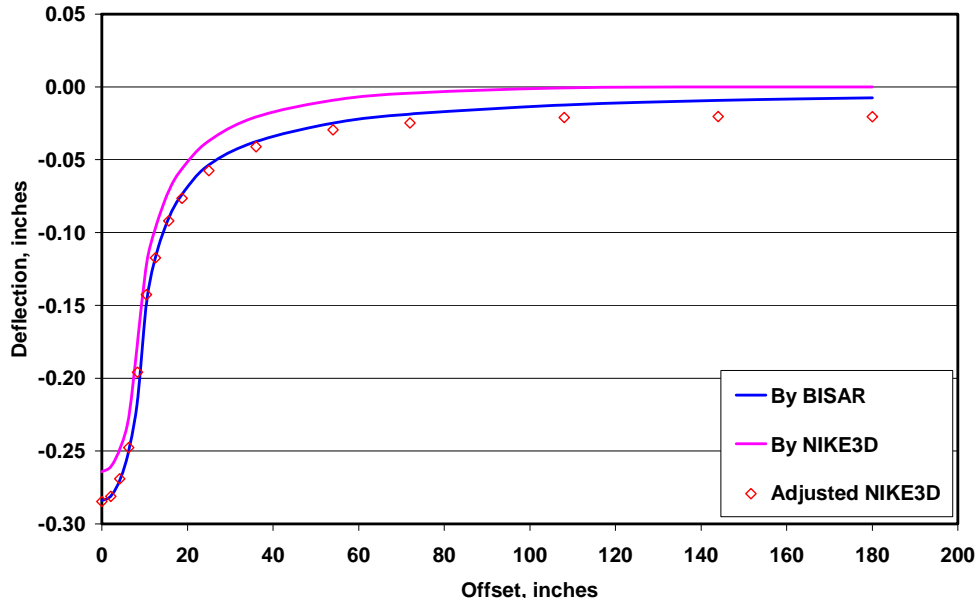
Figure 42. Vertical Deflections Along r Axis by NIKE3D and BISAR

Figure 43 presents the horizontal stress (σ_r) distribution along the z axis. The results by BISAR computed at the IPs yield a smooth curve. The results by NIKE3D at the IPs near the origin fluctuate, but eventually converge to the BISAR curve. The element stresses calculated by the average of the stresses at the Gauss IPs (the diamond dots) also plot along the BISAR curve.
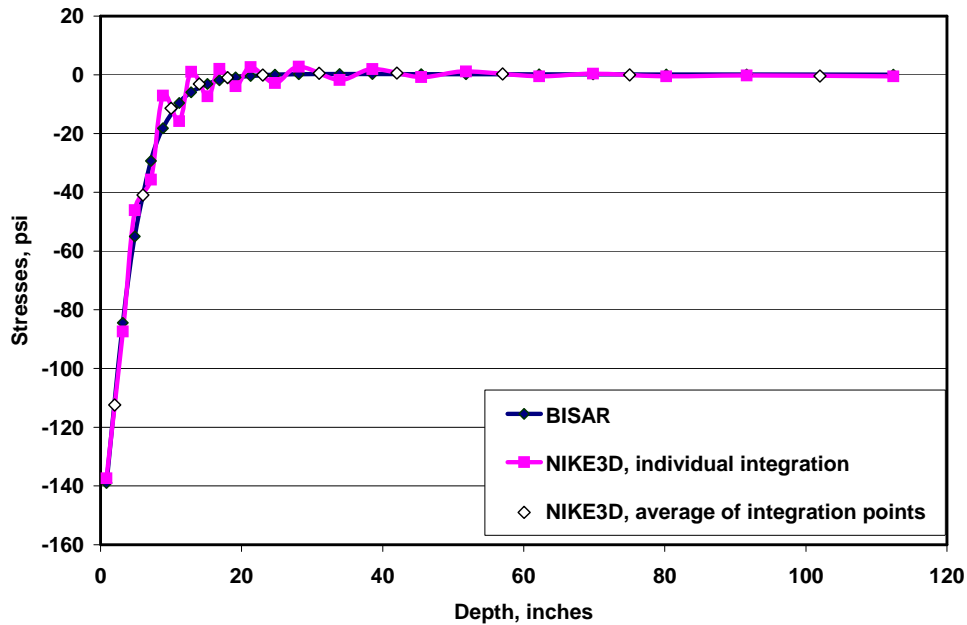
Figure 43. Horizontal Stresses (σ_r) Along z Axis by NIKE3D and BISAR

Figures 44 and 45 show that if a subgrade has a finite depth, the stresses calculated by NIKE3D FAA 1.0 converge to the results calculated by BISAR. For an elastic solid semi-infinite space,

the differences are less than 1 percent if appropriate sizes of elements are used. After a sliding interface is introduced, a pavement can be modeled by a slab resting on an elastic solid foundation with a frictionless interface in between. The numerical comparison for the maximum interior stresses under a single 50,000-pound tire load indicates that the maximum stress differences calculated by NIKE3D FAA 1.0 and BISAR vary from -6 percent to 1 percent for structures with a wide range of subgrade strengths. For a pavement structure with a very deep subgrade, the influence of the subgrade depth must be verified and a realistic procedure for design selected.
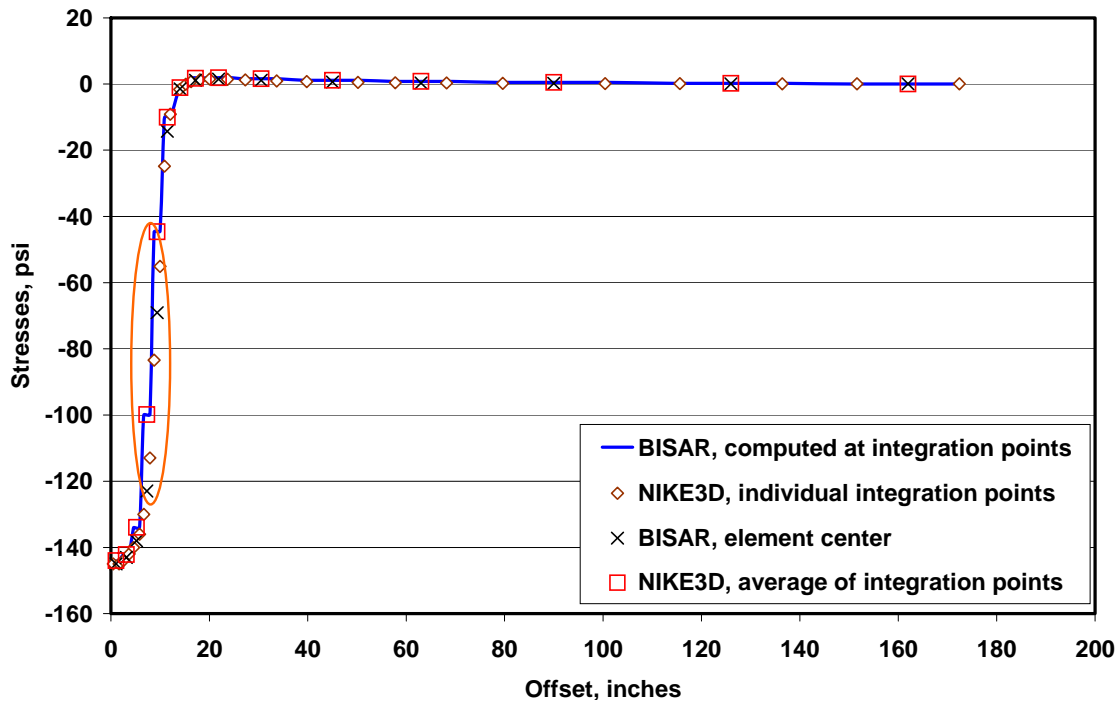
Figure 44. Horizontal Stresses (σ_r) Along r Axis by NIKE3D and BISAR

Figure 45 presents the NIKE3D FAA 1.0 calculated maximum top and bottom stresses by using a total pavement depth varying from 36 to 372 inches. The meshes with a pavement depth of up to 120 inches are shown in figure 40, and the detailed nodal x and y coordinates are given in table A-9 in appendix A. The boundary condition on the bottom of the structure is fixed; deflections in the z direction on the boundary have been set to zero. To evaluate the effects of subgrade depth, $A = 36$ inches is selected as the smallest depth in a numerical analysis. Four 3-inch concrete layers with elastic modulus $E = 6,000,000$ psi and Poisson's Ratio $\mu = 0.15$ rest on five subgrade layers with $E = 5,000$ psi and Poisson's Ratio $\mu = 0.40$. Thicker pavements are obtained by adding one layer under the previous pavement until the total pavement equals 84 inches. A 32-inch layer is added until the total pavement depth equals 372 inches.

56

The Maximum Element Stress at Top and Bottom by NIKE3D
Solid Incompatible Element Approach
An Interior 50,000 lbs Tire Load, p = 180 psi

The top maximum stress = 529 psi calculated by BISAR for the subgrade with infinite depth

The bottom maximum stress = 493 psi calculated by BISAR for the subgrade with infinite depth

Stress in psi (y-axis)

Total Pavement Depth in inches (x-axis)

Legend:
- ◇ Top
- □ Bottom
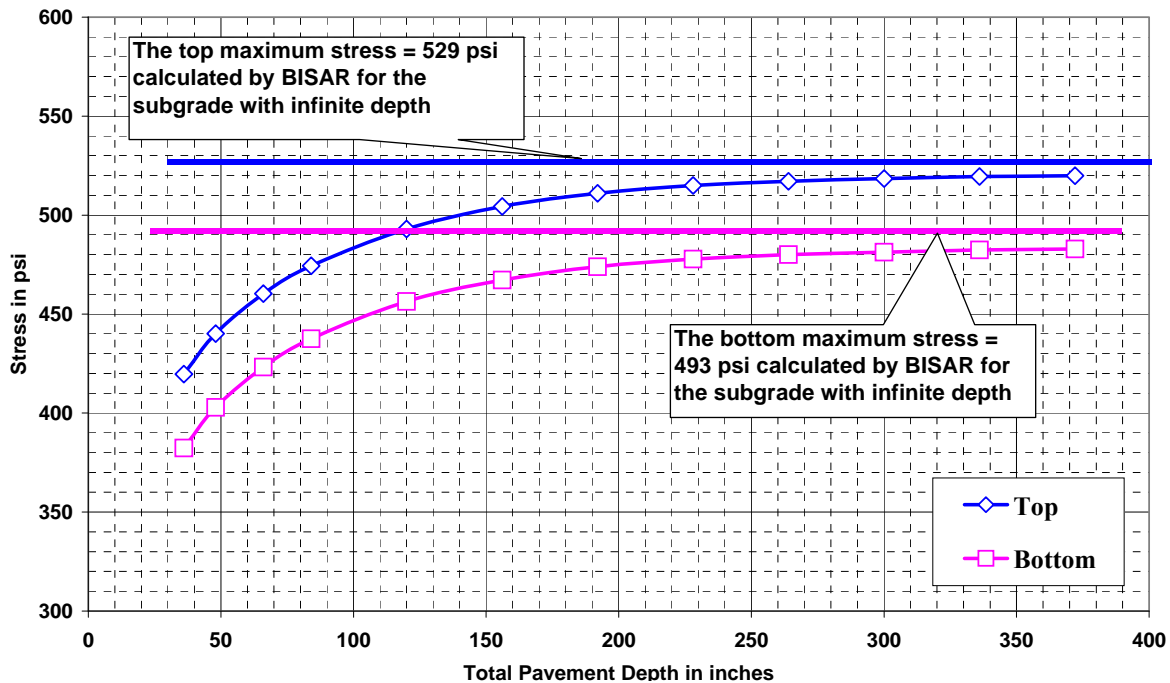
Figure 45. Converging the Maximum Stresses to BISAR Results

The average stresses at the lower and upper IPs are calculated for the elements by the loading center in the first and fourth layers in figure 40. The maximum bottom and top element stresses are calculated using equation 38.   Figure 45 shows that the NIKE3D FAA 1.0-calculated maximum stresses approach the BISAR-calculated maximum stress when the subgrade depth becomes large. However, the total number of nodes and elements have to be significantly increased in the NIKE3D FAA 1.0 computation, which leads to a much longer time in each stress calculation. Therefore, an infinite element technique is selected to model the infinite deep subgrade and obtain reasonable computation time and acceptable precision.

As discussed in section 2.4, the infinite element is a good approach in simulating the subgrade with infinite depth.   The characteristic of the infinite element has an essential difference compared to the FE. The shape functions used for the FEs make the convergence of numerical results possible. When the element size decreases, the numerical results may converge to the true theoretical solution. However, the shape function used in the infinite element (section 2) does not have that feature.   The infinite element procedure can only provide a good approximation. As discussed in section 2.4, the infinite element characteristic length must be selected to conduct the calculation. Since no unique characteristic length can be obtained by theoretical derivation, the distance between the top of the infinite element and the pavement surface is tried and verified by the following numerical analysis:

- Two pavements, InS5-1 and InS5-6 (table 14), were tested, representing slabs built on very weak and very strong subgrade. The nonconforming element size used was 2.08 by

57

2.08 in. to minimize numerical error. Different characteristic depths from 6 to 342 inches were used to calculate the maximum stresses (in magnitude) at the upper and lower IPs. They are then extrapolated to the slab surface and bottom. The maximum stresses at the slab top and bottom for the two pavement structures indicated above are presented in figure 44. The top and bottom maximum stresses calculated by LEAF using infinite depth subgrade are also shown in figure 44.

It can be seen that the NIKE3D-calculated results vary with the selected characteristic depth. However, for a weak subgrade pavement (l_s = 66.7 inches and E_s = 5,000 psi), 25 to 30 inches seems the best choice. For a strong subgrade pavement (l_s = 23.6 inches and E_s = 75,000 psi), 15 to 20 inches seems the best choice. Therefore, the numerical comparisons in figure 45 verify that the distance from the subgrade top to the pavement surface is a reasonable choice in NIKE3D.

6. NEW RECTANGULAR MESH FOR THE LAYERS BELOW THE PCC SLAB.

The original 3D-FE pavement model was built using eight-noded bricks. Due to the poor performance of the regular brick elements under a load, it required several brick sublayers to build a pavement layer. The PCC slab was modeled using shell elements, and several sublayers of brick elements were used to model the layers below the slab. To reduce the number of elements, the sublayers were modeled using a circular geometry. However, since the introduction of the incompatible formulation of the brick element, there is no need to build sublayers. Therefore, the layers under the slab were remodeled following identical formulation to the slab layer. As a result, the model thickness calculation run time has been reduced due to the identical geometry of the different layers.

A 15- by 15-ft PCC test slab was constructed in June 2003 inside the NAPTF on the surface of a cracked slab on medium-strength subgrade (figure 46). The test slab was wet-cured for 28 days. Concrete strain gages (CSG), vertical displacement transducers, and horizontal displacement transducers were installed in the slab to monitor the slab behavior under different testing conditions. Additionally, a feeler gage was used to measure the slab curling and compare the measurements to the sensor readings. The slab was monitored over three distinct periods defined by different conditions:

- Drying for 3 months and 15 days under indoor conditions. At the end of this period, the measured average corner curling reached almost 200 mil. Static load plate tests of up to 40,000 lb, using increments of 5,000 or 10,000 lb, were conducted at the end of this period to measure the displacements and strains of the curled slab.

- Wetting for 2 months, with the slab surface routinely watered. At the end of this period, the measured average corner curling fell to 60 to 80 mil.

- After again drying the surface for 45 days, static plate load tests were conducted. The reason for the static tests was to investigate the slab static response under slab curling conditions. Loads up to 40,000 lb were used. Different plate sizes (diameters of 18, 12, and 6 inches) were used to determine their effects on the critical strains and

displacements. The plate load setup is presented in figure 47 and the sensor location plan in figure 48.

$H_c = 11$ inches, E=6,000,000 psi

$H_{ExistPCC} = 9.75$ inches, cracked slab, E=3,000,000 psi

$H_{Sub1} = 5.875$ inch, E=700,000 psi

$H_{Sub2} = 8.625$ inch, E=24200 psi

Subgrade, CBR = 7 to 8, k=141 pci for EverFe, E=15,000 psi for NIKE3D
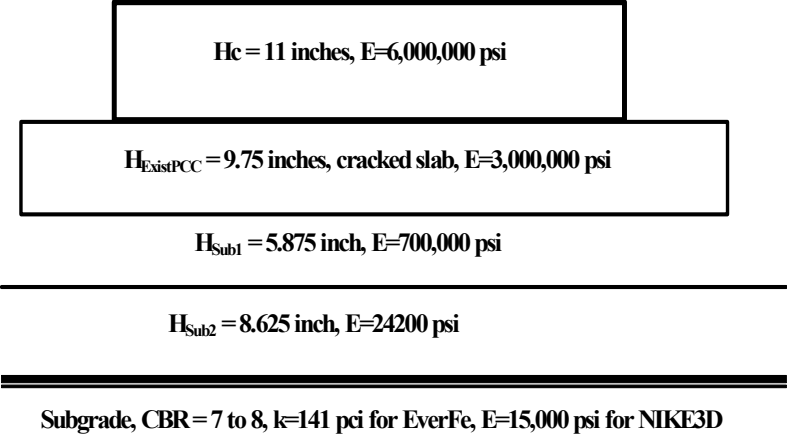
Figure 46. Input Data for 3D-FEM Analysis of the Test Slab

Figure 47. A Single Load is Applied at the Slab
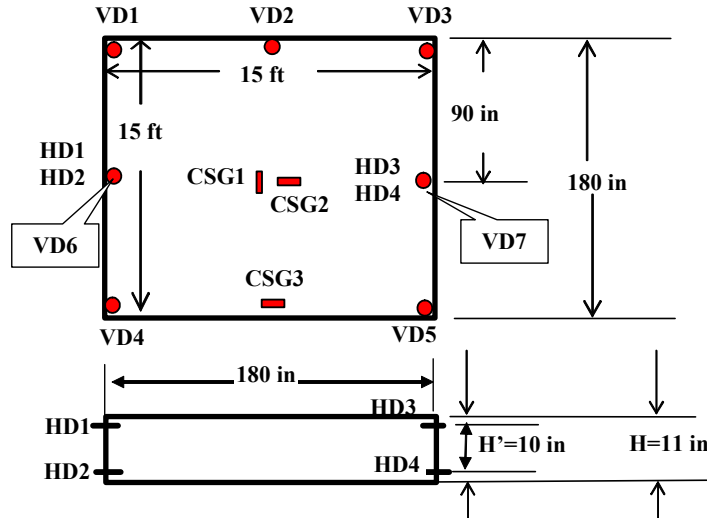
Figure 48. Plane View of the Test Slab and Sensor Location

The measured and predicted strains at strain gage CSG3, for the case where the load is located at the edge directly above the strain gage, are shown in figure 49. The load-induced maximum strain calculated by both the 2D-FE program JSLAB2002 and NIKE3D (cliff model) is much higher than the measured strain. However, when the layers below the slab are extended by 30 inches (step model), the computed strains by NIKE3D match the measured ones. The NIKE3D results suggest that the step model is a more realistic model than the cliff model for predicting the maximum edge stress of a PCC pavement resting on an econocrete subbase layer.
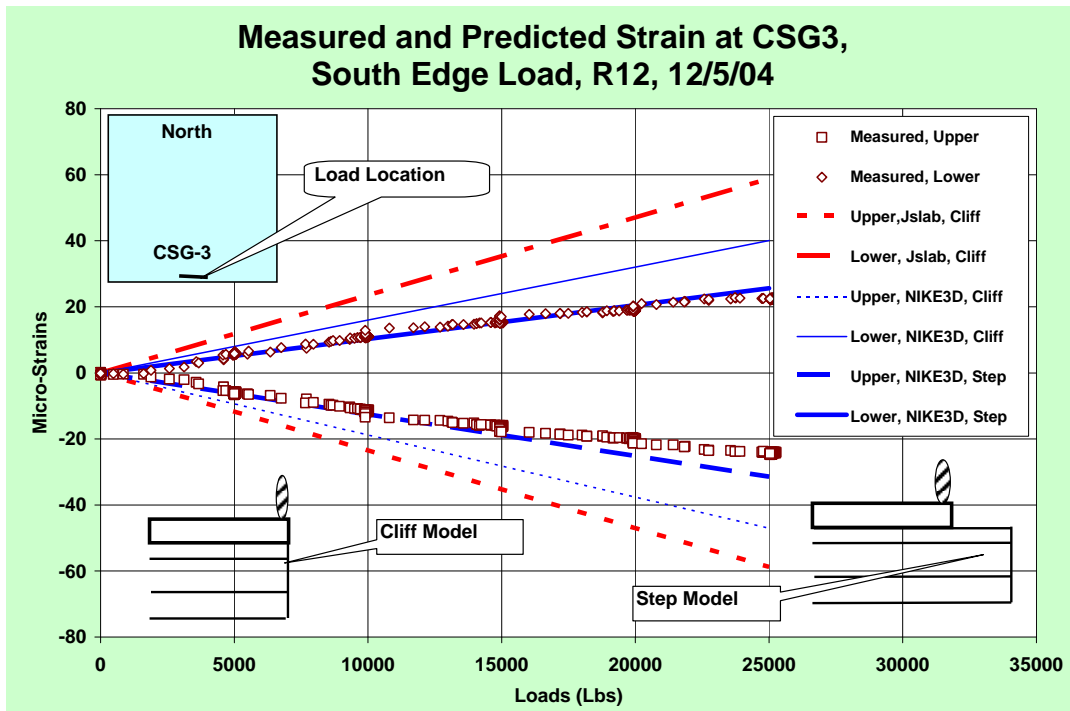
Figure 49. Measured and Predicted Edge Strain Under an Edge Load

60

The analysis of the test slab data supports two general conclusions with implications for the FAA airport pavement design procedures:

- Although the cliff model has a greater affinity to the Westergaard model [Westergaard, 1926 and 1948], the step model is a more accurate representation of the slab response under edge loading.

- The interior stress is lower than what would be predicted by the 3D-FEM model due to bonding between the PCC slab and subbase. Thus, for pavement thickness design, the edge stress reduced by 25% should always be considered the critical stress.

7. IMPLEMENTATION OF 3D-FEM INTO FEDFAA.

This section describes the process of implementing 3D-FEM into FEDFAA. It describes programming changes to LEDFAA that are needed to run the 3D-FEM modules. It gives an overview of the main 3D-FEM program components—AMClassLib, NIKE3D.dll, and INGRID.dll—and shows how they fit into the overall FEDFAA program organization. Finally, it provides the minimum system requirements for FEDFAA to run on a PC with the Windows operating system.

7.1 ADAPTING THE 3D-FEM PROGRAM NIKE3D.

As discussed in section 1, the 3D-FEM analysis of the rigid pavement structure uses a modified version of two computer programs, INGRID and NIKE3D, that were originally developed by LLNL. Both programs were originally written in FORTRAN 77 and were intended for use on a variety of specialized platforms, including vectorizing supercomputers and UNIX workstations. The versions of these programs used by the FAA in FEDFAA retain the FORTRAN language, but have been recompiled to run on Windows-based PCs.

INGRID is a preprocessing program; i.e., it is used to generate a 3D-FE mesh. In its original version, meshes could be created using combinations of beam, shell, and hexahedral elements. A complex set of commands controls the mesh generation [Christon, et al., 1992]. As discussed earlier, NIKE3D as originally developed by LLNL is a fully implicit 3D-FEM program for analyzing static and dynamic responses of elastic and inelastic solids, shells, and beams. Since both INGRID and NIKE3D are general-purpose programs in their original versions, they include many procedures that are not needed for the problem of interest, which is the static, linear elastic analysis of pavement structures. To determine which subroutines in INGRID and NIKE3D are needed and which are redundant, all subroutines in both programs were modified so that when any subroutine is called during INGRID or NIKE3D execution, its name is written to an output file. Originally, the NIKE3D source code consisted of 1,045 files, and the INGRID source code consisted of 792 files. After identifying the unused subroutines, the NIKE3D source code was reduced to 350 files and the INGRID source code was reduced to 256 files.

Using the Compaq Visual FORTRAN programming environment, both programs were recompiled as FORTRAN dynamic link libraries (DLL) and fully integrated with the main FEDFAA program. The main FEDFAA program is written in Visual Basic .NET. Thus, the design program involves mixed-language programming. The interactions between Visual Basic

.NET and FORTRAN may result in unexpected behavior. For example, to determine the final concrete design thickness, the main program calls the INGRID/NIKE3D DLL sequence multiple times as part of an iterative loop. However, it was found that when the Visual Basic main program calls a FORTRAN DLL, the global DLL variables retain their values after the first run. These variables may be the source of run-time errors when the FORTRAN DLL is called the second and subsequent times. To correct this condition, code was added to both INGRID and NIKE3D so that all global variables are reinitialized at the end of each DLL call. Thus, multiple calls to the 3D-FEM response module can be made without causing run-time errors. Extensive testing and debugging was required to identify and correct sources of error by the interaction between the programming languages.

7.2 CALCULATION OF DESIGN STRESS.

This section presents procedure for calculating the maximum tensile stress for design based on the output from the 3D-FEM model.

As discussed in section 2, the 3D-FEM model returns displacements at the element nodes and stresses at the Gauss IP within each element. These stresses are generally not the maximum stresses and need to be extrapolated to the critical location on the element surface. Layered elastic analysis models have the ability to return computed stresses at any specified point within the layered elastic domain. By contrast, with 3D-FEM, it may be necessary to extrapolate from or interpolate between the discrete stresses locations to obtain the stress vector at a given point.

The calculation of design stress is done in two steps:

1. For each element along the edge of the slab, stresses are extrapolated from Gauss points to the bottom of the slab.

2. A polynomial interpolation procedure is used to find the maximum stress along the slab edge using stress values obtained in step 1.

7.2.1 Description of the Extrapolation From Gauss Points to the Bottom of the Slab.

The Gauss IPs for the eight-node brick element used in NIKE3D FAA 1.0 are distributed as shown in figure 50. The distance from any IP to the central plane of the element is always equal to 0.57735 * H/2 (see figure 50), where H is the element thickness. This is also true for the distance to the other two middle planes in the x and y directions. In the FEDFAA 3D-FEM model, the thickness of the PCC slab is the element thickness.
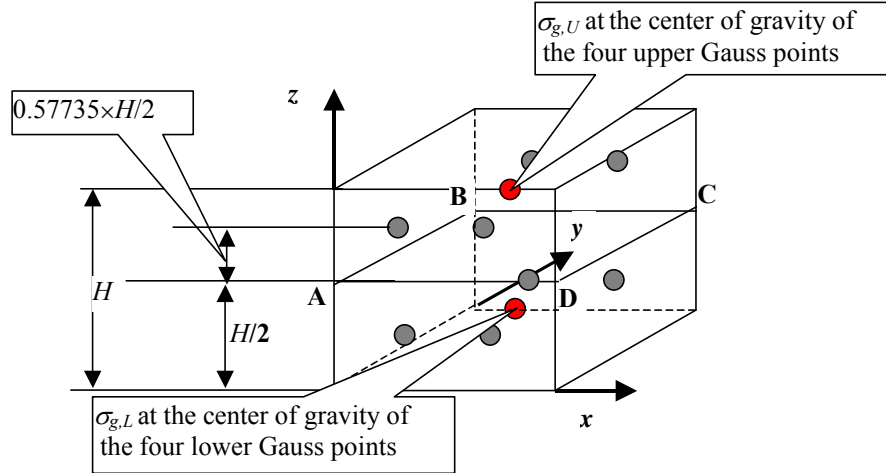
Figure 50. Solid Brick Element Showing Locations of Gauss Integration Points

The extrapolation procedure is done in two steps. First, calculate the average stress $\sigma_{g,L}$ of the lower four IPs shown in figure 50 using the following equation:

$$\sigma_{g,L} = \left(\sigma_{L,1} + \sigma_{L,2} + \sigma_{L,3} + \sigma_{L,4}\right) x 0.25$$
$$\sigma_{g,U} = \left(\sigma_{L,5} + \sigma_{L,6} + \sigma_{L,7} + \sigma_{L,8}\right) x 0.25$$

(33)

where $\sigma_{L,1}$, $\sigma_{L,2}$, $\sigma_{L,3}$, and $\sigma_{L,4}$ are stresses at the lower four IPs, and $\sigma_{L,5}$, $\sigma_{L,6}$, $\sigma_{L,7}$, and $\sigma_{L,8}$ are stresses at the upper four IPs (see figure 50).

Second, calculate the average element bottom stress (σ_{BM}) and top stress (σ_{TP}) by the following linear extrapolation equation:

$$\sigma_{BM} = \frac{\sigma_{g,L} - \sigma_{g,U}}{2x0.57735} + \frac{\sigma_{g,L} + \sigma_{g,U}}{2}$$
$$\sigma_{TP} = \frac{\sigma_{g,U} - \sigma_{g,L}}{2x0.57735} + \frac{\sigma_{g,L} + \sigma_{g,U}}{2}$$

(34)

Stresses σ_{BM} are calculated for all elements along the edge of the PCC layer and later used in the interpolation calculations described in the following sections.

7.2.2 Description of the Stress Interpolation Along the Slab Edge.

There are two cases requiring interpolation of stresses along the slab edge. The first case is for either a single wheel or a dual wheel, when the wheel is located at the axis of symmetry. The location of the maximum stress in this case is known, and it is at the axis of symmetry. The interpolation subroutine POLINT [Press, et al., 1986] was implemented to obtain the maximum stress by polynomial interpolation. POLINT employs an *n*-level polynomial algorithm. As implemented in FEDFAA, the subroutine uses ten points, five points on each of the axis of

symmetry, to find the interpolated stress at the axis of symmetry. This calculated stress is then used later in the failure model in FEDFAA.

The second case of interpolation involves gear configurations other than single wheel or dual wheel, where the location of the maximum edge stress is unknown. In this case, the subroutine LOCATE [Press, et al., 1986] is used to find the maximum value from among the extrapolated stresses (equations 33 and 34).

Next, a bisection procedure is used to search for the maximum interpolated stress (calculated with subroutine POLINT) along the slab edge between the maximum extrapolated stress and the second largest stress in the adjacent element. The subroutine POLINT is used with ten points ($n = 10$) to evaluate the stress value in any location along the edge. The maximum interpolated stress found using the bisection method becomes the input to the failure model in FEDFAA.

7.2.3 Case 1: Example of Interpolation Procedure for SWL.

Rigid pavement structure A (table 7) was analyzed, as shown in figure 51. Due to symmetry, figure 51 shows only one-half of the 3D-FEM model and one-half of the 50,000-lb SWL. Table 16 presents the results for Case 1 calculated according to equation 34. Stresses for five points ranging along the positive y axis from 3 to 27 inches were extrapolated from the IPs to the bottom of the slab. Since both the pavement structure and loading are symmetric on the x-z plane, stresses for coordinates on the negative y axis were obtained from the corresponding stresses at positive y coordinates.
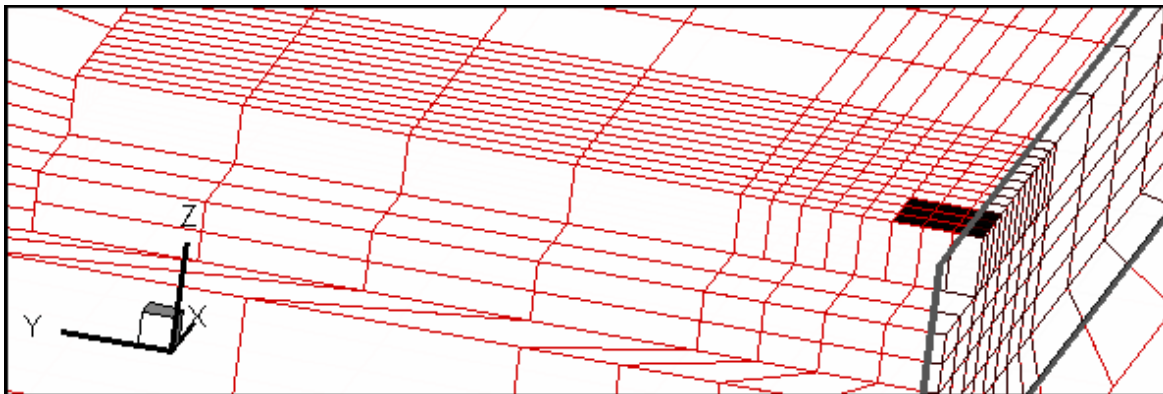
Figure 51. The 3D-FEM Mesh for Case 1

Table 16. Results for Case 1

Interpolated Stress (psi)	y Coordinate (inch)	Extrapolated Stress (psi)
	27	22.71
	21	89.95
	15	199.45
	9	355.47
	3	472.63
	0	489.51
	-3	472.63
	-9	355.47
	-15	199.45
	-21	89.95
	-27	22.71

Since the center of the single load coincides with the axis of symmetry of the pavement structure ($y = 0$), the location of the maximum stress is also on the axis of symmetry below the center of the single wheel. Following the procedure in section 6.2.2, ten points were used with the POLINT subroutine to obtain the maximum interpolated stress (489.51 psi). A graphical representation of the results for case 1 is shown in figure 52. The interpolated stress of 489.51 psi was greater by 16.88 psi, or 3.57%, than the maximum extrapolated stress of 472.63 psi. In general, it is found that without the extrapolation procedure, the 3D-FEM analysis will underestimate the maximum design stress for a SWL by 3%-4%.
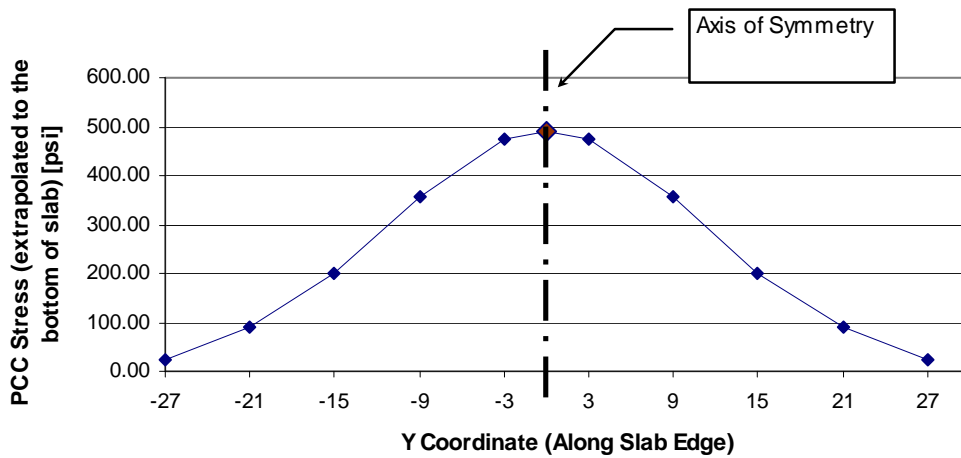
Figure 52. Stresses Extrapolated for Case 1

7.2.4 Case 2: Example of Interpolation Procedure for Two Dual Wheels in Tandem.

Rigid pavement structure A (table 7) was loaded by a dual-tandem gear, as shown in figure 53. The load on each wheel was 47,500 lb, at 200-psi tire pressure.

65
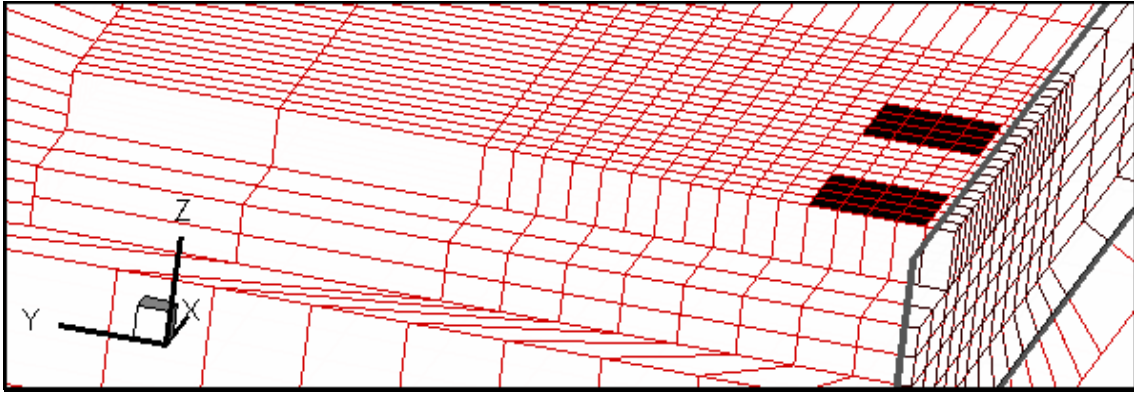
Figure 53. The 3D-FEM Mesh for Case 2

Figure 53 shows only one-half of the 3D-FEM model and one-half of the two dual-tandem configuration due to symmetry. Table 17 presents results for case 2 following the procedure in section 6.2.1. Stresses for 16 points along the positive y axis (y = 3 to 93 inches) were obtained by linear extrapolation from the IPs to the bottom of the slab. Since both the pavement structure and load are symmetric with respect to the x-z plane, stresses for an additional 16 points along the negative y axis (y = -3 to -93 inches) were identical to the corresponding stresses on the positive y axis. Ten points out of these 32 points were used as input data for the polynomial interpolation.

Table 17. Results for Case 2

	y Coordinate (inch)	Extrapolated Stress (psi)
	-15	598.98
	-9	557.46
	-3	465.08
	3	465.08
	9	557.46
	13.64	604.76
Interpolated Stress (psi)	15	598.98
	21	452.12
	27	253.24
	33	111.55
	39	15.40
	45	-54.14
	51	-101.88
	57	-134.44
	63	-155.05
	69	-166.64
	75	-171.90

66

Table 17. Results for Case 2 (Continued)

Interpolated Stress (psi)	y Coordinate (inch)	Extrapolated Stress (psi)
	81	-170.96
	87	-166.84
	93	-159.65

The maximum stress for a dual-tandem gear is located in one of the elements along the slab edge. The subroutine LOCATE was used to find the maximum extrapolated stress of 598.98 psi at $y = 15$ inches. Next, it was determined that the second highest value of extrapolated stress is 557.46 psi at coordinate $y = 9$ inches. An additional four points with coordinate y larger than 15 inches and four points with coordinate smaller than 9 inches were selected. Altogether, ten points with y coordinates from -15 to 33 inches were used in subroutine POLINT to interpolate between the points. A bisection method was used to search for the solution of the maximum interpolated stress, which was found to be 604.76 psi at coordinate $y = 13.64$ inches. A graphical representation of the results for Case 2 is shown in figure 54. The interpolated stress of 604.76 psi was greater by 5.78 psi, or 0.97%, than the maximum extrapolated stress of 598.98 psi.
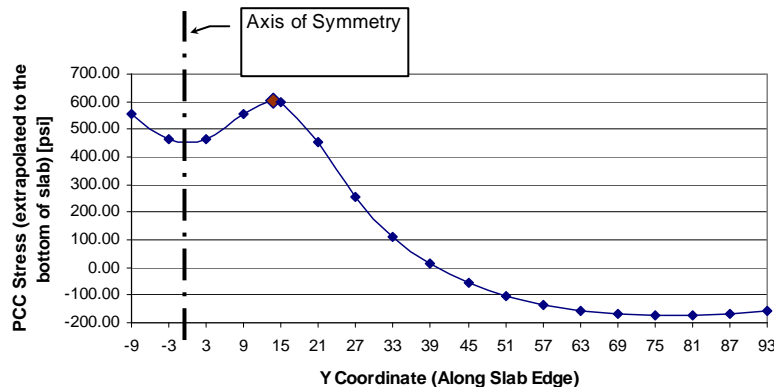
Figure 54. Stresses Extrapolated for Case 2

7.3 INCORPORATION OF NIKE3D CALCULATED STRESS INTO FEDFAA.

Figure 55 shows the current FEDFAA program organization. FEDFAA is similar in organization to LEDFAA 1.3, except that in FEDFAA, the final stresses in PCC slabs and rigid overlays are calculated using 3D-FEM (NIKE3D), not LEAF. However, when designing a new rigid pavement structure or rigid overlay, FEDFAA uses LEAF to arrive at an initial, approximate thickness for the PCC layer, as shown in figure 55. A FEDFAA user can select an initial thickness for the PCC layer, which may be far away from the final designed one. The initial LEAF computations save time by bringing the starting point for 3D-FEM computation much closer to the final design thickness, thus eliminating unnecessary, time-consuming 3D-FEM iterations. A second method of saving time in NIKE3D computations is also illustrated in figure 55. This involves eliminating from the final mix all aircraft whose individual contribution to the cumulative damage factor, as determined by the initial LEAF computation, is less than

some small value taken as 0.05. Elimination of such aircraft does not affect the final design thickness computed using 3D-FEM, but does significantly reduce design calculation time.
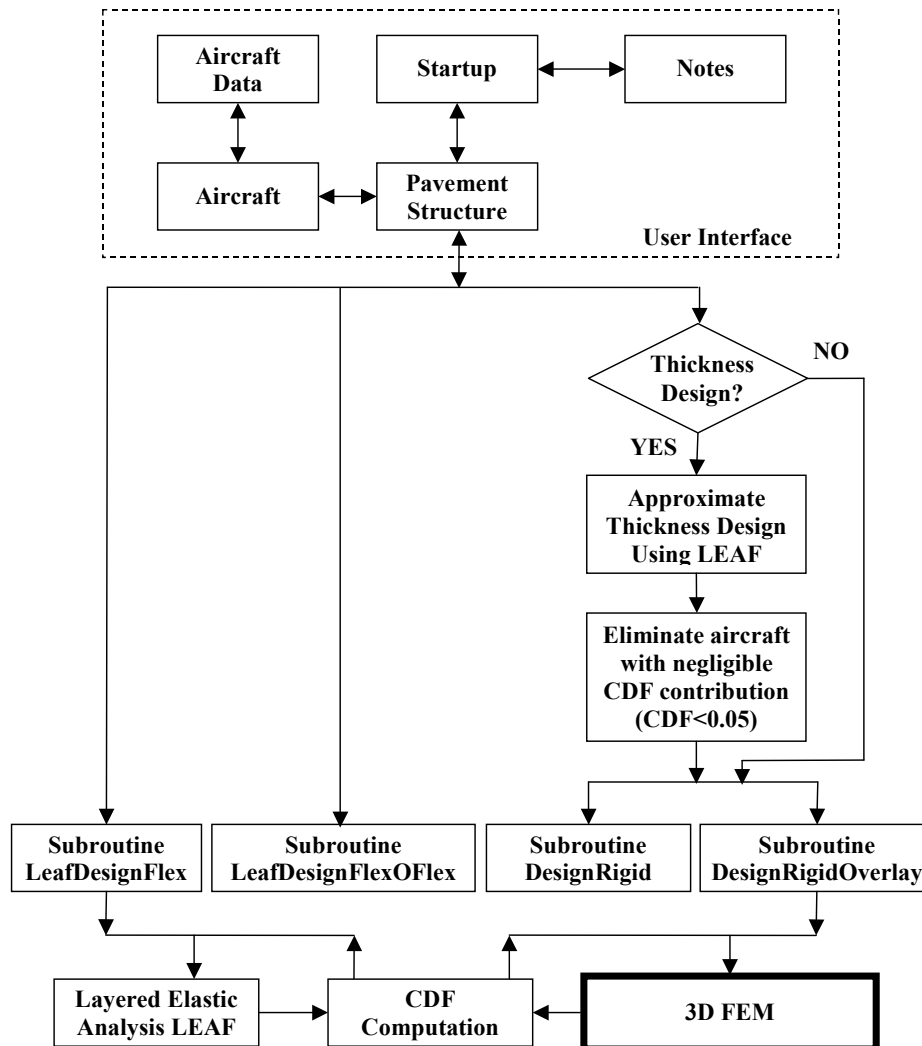
Figure 55. FEDFAA Program Organization

The process followed by FEDFAA in computing the 3D-FEM stress is shown schematically in figure 56. The main program links to one of two DLLs, depending on whether responses will be computed using 3D-FEM or layered elastic analysis. For 3D-FEM, the program links to a DLL called AMClassLib.dll, which in turn drives the three main processes that produce the 3D-FEM solution:

- Subroutine AMMain. This Visual Basic subroutine generates the commands that drive the preprocessor program, INGRID. These commands are contained in two text files (nikein.ing and nikein.rgd).

- INGRID.dll. This DLL contains the modified preprocessor program INGRID. The generated 3D-FEM mesh data, including nodal coordinates, element incidences, and load and boundary data, are written to a third text file (nikein), which becomes the input for NIKE3D.

- NIKE3D.dll. This DLL contains the modified FE processor program NIKE3D_FAA 1.0. The output from this DLL is a text file (n3dhsp) containing detailed output of the 3D-FEM analysis. Only the critical data for design are extracted automatically from file n3dhsp, but the file is retained for the last 3D-FEM operation performed.
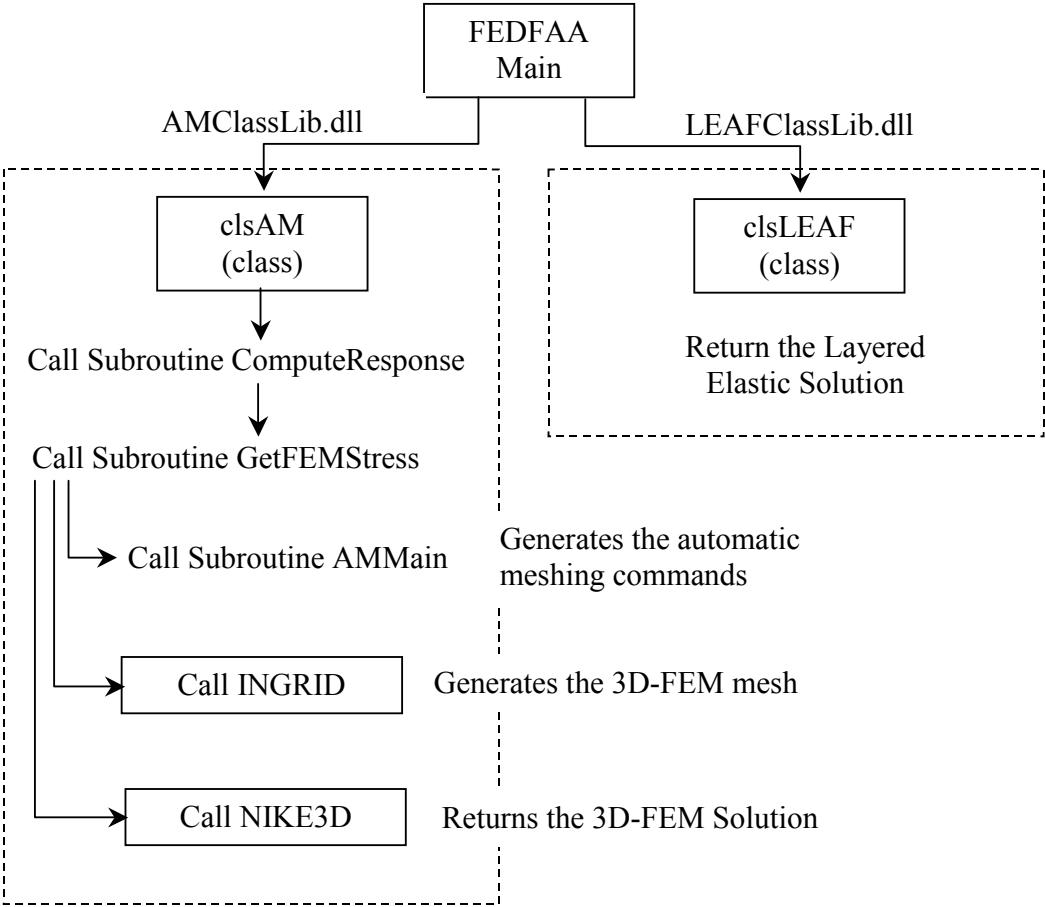
Figure 56. The 3D-FEM Stress Calculation in FEDFAA

All the intermediate files (nikein, nikein.ing, nikein.rgd, n3dhsp) are overwritten each time the 3D-FEM procedure is called.

In Visual Basic.NET, a programming class is defined as a user-defined aggregate type that supports inheritance [Kimmel, 2002]. As shown in figure 56, the subroutines ComputeResponse and GetFEMStress (which in turn calls the three processes listed above) are defined as members (methods) of a Visual Basic.NET class called clsAM, which is compiled to the DLL AMClassLib.dll. In the FEDFAA organization, the class clsAM is parallel to the class clsLEAF,

which implements the LEAF layered elastic program and is compiled to the DLL
LEAFClassLib.dll.

Pavement structural data are passed between the main program and the dependent DLLs as a
Visual Basic.NET data structure called LEAFStrParms. This is a special data type defined
within the program as follows:

```
Public Structure LEAFStrParms
    Dim NLayers As Integer
    Dim Thick( ) As Double ' 1 To NLayers
    Dim Modulus( ) As Double ' 1 To NLayers
    Dim Poisson( ) As Double ' 1 To NLayers
    Dim InterfaceParm( ) As Double ' 1 To NLayers
    Dim EvalDepth As Double
    Dim EvalLayer As Double
    Dim lngDummy( ) As Integer ' Expansion
    Dim dblDummy( ) As Double ' Expansion
    Dim strDummy( ) As String ' Expansion
```

The variables are described in table 18 (the last three are not used). A similar data structure is
defined in FEDFAA to efficiently pass aircraft load data between the main program and
dependent DLLs. Structure LEAFACParms is defined in table 19 and shown in table 20.

Table 18. Definition of Data Structure LEAFStrParms for Pavement Structure

	Variable Name	Variable Type	Description
1	NLayers	Integer	Number of layers
2	Thick()	Double	Layer thickness, 1 to NLayers
3	Modulus()	Double	E modulus, 1 to NLayers
4	Poisson()	Double	Poisson ratio, 1 to NLayers
5	InterfaceParm()	Double	Interface condition, 1 to NLayers
6	EvalDepth	Double	Depth below surface at which response is evaluated
7	EvalLayer	Double	Evaluation layer

Table 19. Definition of Data Structure LEAFACParms for Aircraft

	Variable Name	Variable Type	Description
1	ACname	String	Aircraft name
2	GearLoad	Double	Gear load
3	Ntires	Integer	Number of tires
4	TirePress()	Double	Tire pressure, 1 to Ntires
5	TireX()	Double	Coordinate x of wheel location, 1 to Ntires
6	TireY()	Double	Coordinate y of wheel location, 1 to Ntires
7	LibGear	String	Gear symbol

Table 20. Example of Data Structure LEAFACParms (Instance for B777-200)

Variable Name	Variable Value	Description
AcName	B777-200	Number of layers
GearLoad	255074.9	Gear load (lbs)
Ntires	6.0	Number of tires
TirePress(1)	185.0	Tire pressure for tire 1 (psi)
TirePress(2)	185.0	Tire pressure for tire 2 (psi)
TirePress(3)	185.0	Tire pressure for tire 3 (psi)
TirePress(4)	185.0	Tire pressure for tire 4 (psi)
TirePress(5)	185.0	Tire pressure for tire 5 (psi)
TirePress(6)	185.0	Tire pressure for tire 6 (psi)
TireX(1)	-27.5	Coordinate x for tire 1 (inch)
TireX(2)	27.5	Coordinate x for tire 2 (inch)
TireX(3)	-27.5	Coordinate x for tire 3 (inch)
TireX(4)	27.5	Coordinate x for tire 4 (inch)
TireX(5)	-27.5	Coordinate x for tire 5 (inch)
TireX(6)	27.5	Coordinate x for tire 6 (inch)
TireY(1)	-57.0	Coordinate y for tire 1 (inch)
TireY(2)	-57.0	Coordinate y for tire 2 (inch)
TireY(3)	0.0	Coordinate y for tire 3 (inch)
TireY(4)	0	Coordinate y for tire 4 (inch)
TireY(5)	57	Coordinate y for tire 5 (inch)
TireY(6)	57	Coordinate y for tire 6 (inch)
libGear	N	Library gear designation

7.4 HANDLING OF AIRCRAFT TRAFFIC MIXES WITH FEDFAA.

FEDFAA can compute the thickness design or life of a pavement structure with up to 20 aircraft in the traffic mix. In general, this computation may involve up to 40 separate load analyses, since certain aircraft (such as the Airbus A380) require both wing gears and body gears to be analyzed. When analyzing a pavement section, aircraft are divided into a maximum of four categories according to table 21. Aircraft in the same category have an identical 3D-FEM mesh and are analyzed with one call to NIKE3D.dll. Therefore, a maximum of four calls to NIKE3D.dll is needed to obtain all required PCC slab and overlay edge stresses for all aircraft in the mix. Depending on the input traffic mix, the actual number of calls may be fewer than four. Figure 57 shows the four types of meshes implemented in FEDFAA, corresponding to the aircraft categories I-IV in table 21. In the first three categories, 3D-FEM meshes are generated for one-half of the pavement structure, since both the gear loads and the pavement structure are symmetric in the x-z plane. Gear loads for aircraft in category IV (e.g., C-5 and C-17) are not symmetric on a major axis, and therefore, the complete pavement structure must be analyzed by

NIKE3D, which is more time-consuming. The orientation of the aircraft gear in FEDFAA is also a function of the aircraft category in table 21. The aircraft is oriented parallel to the slab edge for aircraft categories I and IV. The orientation is perpendicular to the slab edge for aircraft categories II and III. Extensive testing was performed to verify that these orientations produce the maximum edge stress response for their respective categories.
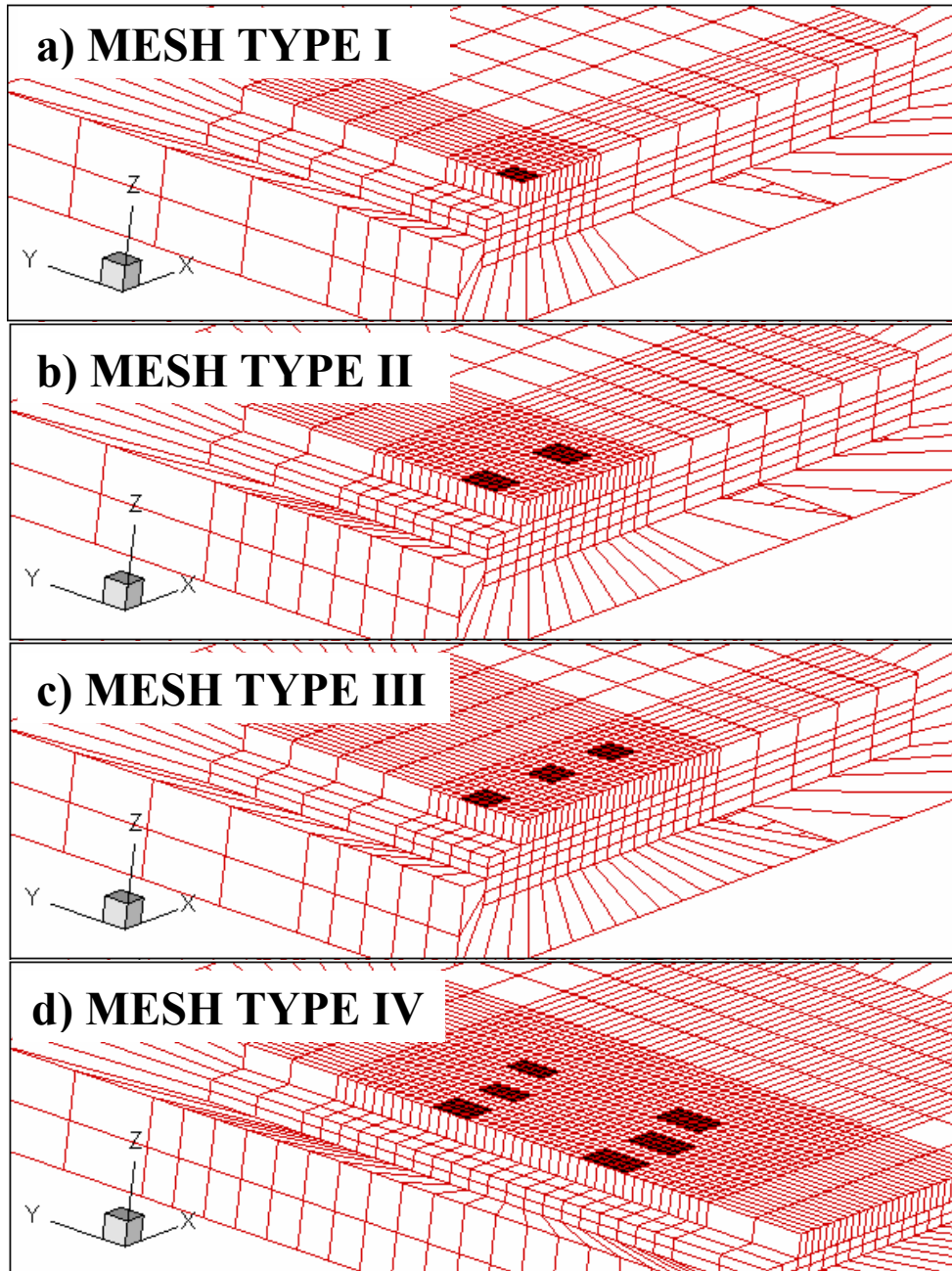
Figure 57. Types of 3D-FEM Meshes in FEDFAA

Table 21. Aircraft Categories

Aircraft Category	Example Aircraft	Fine Mesh Region Dimensions		Comments
		x (inch)	y (inch)	
I. Single Wheel and Dual Wheel	B737	72	48	Symmetry implemented
II. Dual Tandem	B747	120	96	Symmetry implemented
III. Triple Tandem	B777	180	60	Symmetry implemented
IV. Complex Gear Configurations	C-5, C-17A	168	240	No symmetry

Analyzing all aircraft in the same category with a single call to NIKE3D is a far more efficient approach than performing a separate 3D-FEM computation for each aircraft. In NIKE3D, the greatest part of the computational effort is taken up by the formation and factorization of the global stiffness matrix. For each call to NIKE3D, the factorization needs to be performed only once. Within each aircraft category, the individual aircraft are treated as variations of the loading function with a time variable in a pseudo-dynamic analysis. The concept is illustrated in figure 57. For *n* aircraft in the same category, FEDFAA defines *n* load functions. Figure 58 shows load functions defined for three aircraft in the same category. Each load function takes on the value 1 at some time step, and 0 at all other time steps. The time step in this case refers to discrete changes in the load function and each time step is associated with exactly one aircraft load. Therefore, the number of time steps equals the number of loads needed for analysis. Practically, this means that the full set of linear equations needs to be assembled and factorized only for the first aircraft in the category. Responses for the subsequent aircraft loads are then obtained by back-substitution in the stored factorized matrix.
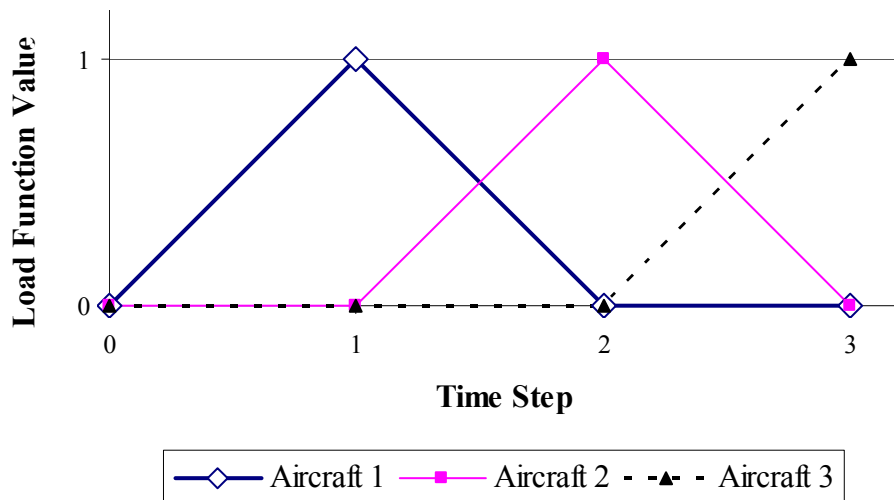
Figure 58. Load Functions for Analyzing a Three-Aircraft Mix

The time-step approach was implemented in FEDFAA and appears to provide a reasonable solution to the excessive run times normally associated with analyzing mixed aircraft traffic in 3D-FEM. One problem was encountered (and corrected) during testing. In theory, the sequence of the aircraft in the traffic mix is not important (for a Miner's Law-based design). Originally,

the order in which NIKE3D processed the aircraft was simply the order in which they were entered by the user. It was then observed that for certain traffic mixes, where two aircraft gears in sequence were of roughly similar geometry and load, that the time step associated with the second aircraft failed to converge causing a run-time error. Although the cause of this problem has not yet been identified, a work-around solution was implemented that prevents the occurrence of run-time errors. First, all aircraft in the same category are sorted by increasing gear load. Again, this reordering is possible since the sequence does not affect the design. Next, for each time step, the gear load of the associated aircraft is scaled, either increased or decreased as appropriate, to ensure that the solution converges. Finally, the stresses obtained for gear loads that were scaled, are scaled by a reciprocal factor to obtain the correct solution for the original gear loads. For example, if a gear load is scaled by a factor of 1.1, the stress returned by NIKE3D must then be scaled by a reciprocal factor of $1/1.1 = 0.909$ to obtain the stress for the original gear load. It was possible to implement this solution because NIKE3D analyzes a linear elastic system, and stresses therefore increase in linear proportion to gear loads.

7.5 MINIMUM SYSTEM REQUIREMENTS FOR FEDFAA.

Table 22 lists the minimum system requirements for FEDFAA installation. The Microsoft .NET™ Framework needs to be installed before FEDFAA will run. If the .NET Framework is not already installed, then the current version of the .NET Framework Redistributable Package file dotnetfx.exe should be located on the Microsoft website http://www.microsoft.com/downloads/, downloaded, and installed on the computer.

Table 22. Minimum System Requirements for FEDFAA Installation

Processor	450-MHz Pentium II-class processor, 600-MHz Pentium III-class processor recommended
Operating System	Windows Server 2003 Windows XP Professional Windows XP Home Edition Windows 2000 (Service Pack 4 or higher recommended)
Memory	Windows Server 2003: 360 MB of RAM Windows XP Professional: 360 MB of RAM Windows XP Home Edition: 296 MB of RAM Windows 2000 Professional: 296 MB of RAM Windows 2000 Server: 392 MB of RAM
Hard Disk	10 MB of available space required for program installation, 100 MB of available space required for temporary NIKE3D files
Drive	CD-ROM or DVD-ROM drive
Display	Super VGA (1024 x 768) or higher-resolution display with 256 colors
Mouse	Microsoft mouse or compatible pointing device

RAM = Random-access memory

8. BIBLIOGRAPHY.

Boussinesq, J., "Application des Potentiels a l'etude de l'equilibre et du Mouvement des Solids Elastiques," Cauthier-Villars, Paris, 1885.

Brill, D.R., "Development of Advanced Computational Models for Airport Pavement Design," FAA report DOT/FAA/AR-97/47, August 1998.

Brill, D.R. and Parsons, I.D., "Three Dimensional Finite Element Analysis in Airport Pavement Design," *Proceedings of the Second International Symposium on 3D Finite Element for Pavement Analysis, Design, and Research*, October 11-13, 2000.

Brill, D.R., "Field Verification of a 3D Finite Element Rigid Airport Pavement Model," FAA report DOT/FAA/AR-00/33, July 2000.

Christon, M.A. and Dovey, D., "INGRID – A 3D Mesh Generator for Modeling Nonlinear Systems," Report No. UCRL-MA-109790 (Draft), Lawrence Livermore National Laboratory, Livermore, California, September 1992.

Cook, R.D., Malkus, D.S., Plesha, M.E., and Witt, R.J., *Concepts and Applications of Finite Element Analysis, Fourth Edition*, Published by John Wiley & Sons Inc., 2002.

FAA (1) Advisory Circular No. 150.5320-6D, "Airport Pavement Design and Evaluation," Federal Aviation Administration, July 1995.

FAA (2) Advisory Circular No. 150.5320-6D, Change 3 "LEDFAA 1.3 User's Manual for Aircraft with Triple-Dual Tandem Landing Gear," Federal Aviation Administration, April 2004.

Guo, E.H., Hayhoe, G.F., and Brill, D.R., "Analysis of NAPTF Traffic Test Data for the First-Year Rigid Pavement Test Items," Federal Aviation Administration Technology Transfer Conference, 2002.

Hayhoe, G.F., "LEAF – A New Layered Elastic Computational Program for FAA Pavement Design and Evaluation Procedures," FAA Technical Transfer Conference, May 2002.

Huang, Y.H., *Pavement Analysis and Design*, Prentice Hall, 1993.

Kimmel, P., "Visual Basic .NET Unleashed," Indianapolis, Indiana, SAMS, 2002.

Koninklijke/Shell, "BISAR: Bitumen Structures Analysis in Roads, User's Manual," Laboratorium, Shell Research N.V., Amsterdam, 1978.

Kreger, W.C., "Computerized Aircraft Ground Flotation Analysis – Edge-Loaded Rigid Pavement," Research Report ERR-FW-572, Research and Engineering Departments, General Dynamics, supported by General Dynamics Research Program, Task RDP 414-61-506, January 1967.

Mackerle, J., "Some Remarks on Program with Finite Elements," *Computer & Structures*, Vol. 55, No. 6, pp. 1101-1106, 1995.

Maker, B.M., "NIKE3D—A Nonlinear, Implicit, Three-Dimensional Finite Element Code for Solid and Structural Mechanics—User's Manual Report," UCRL-MA-105268, Rev. 1, Lawrence Livermore National Laboratory, Livermore, CA, 1995.

Press, W.H., Flannery, B.P., Teukolsky, S.A., and Vetterling, W.T., *Numerical Recipes, The Art of Scientific Computing*, Published by Cambridge, 1986.

Rollings, R.S., "Design of Overlays for Rigid Airport Pavements," Report No. DOT/FAA/PM-87/19, April 1988.

Taylor, R.L, Beresford, P.J., and Wilson, E.L., "An Non-conforming Element for Stress Analysis," *International Journal for Numerical Methods in Engineering*, Vol. 10, No. 6, 1976, pp. 1211-1219.

USACE (1), "Lockbourne No. 1 Test Track, Final Report," U.S. Army Corps of Engineers, Ohio River Division Laboratories, 1946, Mariemont, OH.

USACE (2), "Final Report, Lockbourne No. 2 – Experimental Mat," U.S. Army Corps of Engineers, Rigid Pavement Laboratory, 1950, Mariemont, OH.

USACE (3), "Final Report, Lockbourne No. 2 – Modification, Multiple-Wheel Study," U.S. Army Corps of Engineers, Rigid Pavement Laboratory, 1950, Mariemont, OH.

Westergaard, H.M., "New Formulas for Stresses in Concrete Pavements of Airfields," Transactions, American Society of Civil Engineers, Vol. 113, 1948, pp. 425-439.

Westergaard, J.M., "Stresses in Concrete Pavements Computed by Theoretical Analysis," Public Roads, Vol. 7, 1926.

Wilson, E.L., "The Static Condensation Algorithm," International Journal for Numerical Methods in Engineering, Vol. 8, No. 1, 1974, pp. 198-203.

Wilson, E.L., Taylor, R.L., Doherty, W.P., and Ghaboussi, T., "Incompatible Displacement Models," Numerical and Computer Methods in Structural Mechanics, ed. by S. Fenves et al., Academic Press, New York, 1973, pp. 43-57.

Zienkiewicz, O. C. and Chen, Y.K., *The Finite Element Methods in Structural and Continuum Mechanics*, McGraw-Hill Publishing Co. Ltd., London, 1967.

Zienkiewicz, O.C. and Taylor, R.L., *The Finite Element Method, Fifth Edition, Volume 1—The Basis*, Butterworth-Heinemann, 2000.

APPENDIX A—RESULTS AS CALCULATED BY DIFFERENT PAVEMENT DESIGN METHODS

Existing layer elastic design methods (BISAR, LEAF) were used to verify the FEDFAA pavement design thickness calculation. Additionally, a series of tests were run to validate the correctness of the 3-dimensional finite element pavement model, specially the NIKE3D brick incompatible mode element used to build the pavement model. Also, the cliff versus step pavement model was evaluated using the H51 software (Winkler Foundation), where the calculated edge stress by H51 was compared to the NIKE3D computation. The detailed numerical results from these calculations have been included in this appendix.

Table A-1. NIKE3D Calculated Nodal Displacements for Center Points A and B

Nodes	Center at A (inch)			Center at B (inch)		
	dx	dy	dz	dx	dy	dz
1	0.000E+00	0.000E+00	0.0000E+00	0.000E+00	0.000E+00	0.0000E+00
2	0.000E+00	0.000E+00	0.0000E+00	0.000E+00	0.000E+00	0.0000E+00
3	0.000E+00	0.000E+00	0.0000E+00	0.000E+00	0.000E+00	0.0000E+00
4	0.000E+00	0.000E+00	0.0000E+00	0.000E+00	0.000E+00	0.0000E+00
5	0.000E+00	0.000E+00	0.0000E+00	0.000E+00	0.000E+00	0.0000E+00
6	0.000E+00	0.000E+00	0.0000E+00	0.000E+00	0.000E+00	0.0000E+00
7	0.000E+00	0.000E+00	0.0000E+00	0.000E+00	0.000E+00	0.0000E+00
8	0.000E+00	0.000E+00	0.0000E+00	0.000E+00	0.000E+00	0.0000E+00
9	0.000E+00	0.000E+00	0.0000E+00	0.000E+00	0.000E+00	0.0000E+00
10	-6.368E-17	5.344E-18	-1.5000E-01	-7.367E-17	1.962E-17	-1.5000E-01
11	-6.621E-17	9.593E-18	-1.5000E-01	-7.834E-17	2.158E-17	-1.5000E-01
12	-6.805E-17	1.237E-17	-1.5000E-01	-7.834E-17	2.447E-17	-1.5000E-01
13	-6.843E-17	4.497E-18	-1.5000E-01	-8.245E-17	1.761E-17	-1.5000E-01
14	-6.919E-17	8.846E-18	-1.5000E-01	-6.048E-17	1.999E-17	-1.3000E-01
15	-6.931E-17	1.358E-17	-1.5000E-01	-8.157E-17	2.748E-17	-1.5000E-01
16	-7.381E-17	3.166E-18	-1.5000E-01	-8.207E-17	2.045E-17	-1.5000E-01
17	-7.324E-17	1.025E-17	-1.5000E-01	-8.584E-17	2.147E-17	-1.5000E-01
18	-7.422E-17	1.292E-17	-1.5000E-01	-8.671E-17	2.982E-17	-1.5000E-01
19	-1.911E-16	5.689E-18	-3.0000E-01	-2.902E-16	-8.204E-17	-3.0000E-01
20	-1.867E-16	8.773E-18	-3.0000E-01	-2.802E-16	-4.588E-17	-3.0000E-01
21	-1.849E-16	1.284E-17	-3.0000E-01	-2.806E-16	-1.364E-17	-3.0000E-01
22	-1.924E-16	6.890E-18	-3.0000E-01	-3.123E-16	-7.366E-17	-3.0000E-01
23	-1.929E-16	8.418E-18	-3.0000E-01	-3.071E-16	-3.943E-17	-3.0000E-01
24	-1.911E-16	1.289E-17	-3.0000E-01	-3.111E-16	-1.640E-17	-3.0000E-01
25	-1.943E-16	8.598E-18	-3.0000E-01	-3.459E-16	-7.629E-17	-3.0000E-01
26	-1.950E-16	7.417E-18	-3.0000E-01	-3.407E-16	-4.631E-17	-3.0000E-01
27	-1.961E-16	1.260E-17	-3.0000E-01	-3.437E-16	-1.964E-17	-3.0000E-01

Table A-2. NIKE3D Calculated Element Stresses for Center Points A and B

Gauss Point	Center at A (psi)			Center at B (psi)		
	σx	σy	σz	σx	σy	σz
Element 1						
1	1.167E-30	1.467E-30	-1.000E+02	-1.421E-14	1.421E-14	-1.000E+02
2	9.454E-31	1.803E-30	-1.000E+02	-2.842E-14	2.132E-14	-1.000E+02
3	9.689E-31	1.498E-30	-1.000E+02	-2.842E-14	1.421E-14	-1.000E+02
4	9.719E-31	1.465E-30	-1.000E+02	-1.421E-14	1.421E-14	-1.000E+02
5	-7.105E-15	2.577E-29	-1.000E+02	1.421E-14	-2.132E-14	-1.000E+02
6	1.120E-30	1.190E-29	-1.000E+02	1.421E-14	-1.421E-14	-1.000E+02
7	9.952E-31	1.230E-29	-1.000E+02	3.553E-14	-2.842E-14	-1.000E+02
8	9.923E-31	-7.105E-15	-1.000E+02	3.553E-14	-2.132E-14	-1.000E+02
Average	-8.882E-16	-8.882E-16	-1.000E+02	1.776E-15	-2.665E-15	-1.000E+02
Element 2						
1	-7.105E-15	1.237E-30	-1.000E+02	6.277E-30	1.421E-14	-1.000E+02
2	-1.520E-30	1.497E-30	-1.000E+02	7.105E-15	7.105E-15	-1.000E+02
3	1.641E-30	1.406E-30	-1.000E+02	7.105E-15	7.105E-15	-1.000E+02
4	6.684E-30	1.332E-30	-1.000E+02	-2.030E-30	1.421E-14	-1.000E+02
5	-7.105E-15	2.328E-29	-1.000E+02	-1.421E-14	-7.105E-15	-1.000E+02
6	4.765E-30	9.487E-30	-1.000E+02	-7.105E-15	-7.105E-15	-1.000E+02
7	1.354E-30	9.888E-30	-1.000E+02	-1.421E-14	-7.105E-15	-1.000E+02
8	-7.105E-15	2.335E-29	-1.000E+02	-2.842E-14	-1.421E-14	-1.000E+02
Average	-2.665E-15	8.934E-30	-1.000E+02	-6.217E-15	8.882E-16	-1.000E+02
Element 3						
1	1.174E-30	-7.905E-31	-1.000E+02	-7.105E-15	-7.105E-15	-1.000E+02
2	9.496E-31	-4.537E-32	-1.000E+02	-1.421E-14	-7.105E-15	-1.000E+02
3	8.537E-31	1.442E-29	-1.000E+02	-2.132E-14	-2.132E-14	-1.000E+02
4	8.561E-31	1.454E-29	-1.000E+02	-1.421E-14	-1.421E-14	-1.000E+02
5	-7.105E-15	2.404E-29	-1.000E+02	3.553E-14	2.132E-14	-1.000E+02
6	9.121E-31	1.362E-29	-1.000E+02	2.132E-14	1.421E-14	-1.000E+02
7	7.105E-15	1.753E-30	-1.000E+02	1.421E-14	7.105E-15	-1.000E+02
8	9.893E-31	1.125E-29	-1.000E+02	2.132E-14	1.421E-14	-1.000E+02
Average	9.125E-31	9.849E-30	-1.000E+02	4.441E-15	8.882E-16	-1.000E+02

Table A-2. NIKE3D Calculated Element Stresses for Center Points A and B (Continued)

Gauss Point	Center at A (psi)			Center at B (psi)		
	σx	σy	σz	σx	σy	σz
Element 4						
1	-3.070E-31	-9.291E-31	-1.000E+02	7.105E-15	-7.105E-15	-1.000E+02
2	-1.450E-30	-3.504E-31	-1.000E+02	7.105E-15	-1.421E-14	-1.000E+02
3	1.124E-30	1.185E-29	-1.000E+02	1.421E-14	-7.105E-15	-1.000E+02
4	4.930E-30	1.194E-29	-1.000E+02	7.105E-15	-7.105E-15	-1.000E+02
5	2.330E-30	2.858E-29	-1.000E+02	-2.842E-14	7.105E-15	-1.000E+02
6	3.483E-30	1.277E-29	-1.000E+02	-2.132E-14	7.105E-15	-1.000E+02
7	9.336E-31	1.395E-30	-1.000E+02	-1.421E-14	7.105E-15	-1.000E+02
8	-2.050E-30	1.327E-29	-1.000E+02	-2.132E-14	1.522E-31	-1.000E+02
Average	1.124E-30	9.815E-30	-1.000E+02	-6.217E-15	-1.776E-15	-1.000E+02

Table A-3. Interior Stresses Calculated by BISAR and LEAF for PCC Overlay and Base PCC

| Center line offset (inch) | PCC Overlay | | | | | | Base PCC | | | | | |
| | BISAR | | | LEAF | | | BISAR | | | LEAF | | |
	Pav A	Pav B	Pav C	Pav A	Pav B	Pav C	Pav A	Pav B	Pav C	Pav A	Pav B	Pav C
0.9	181.0	168.0	145.0	180.3	167.3	145.1	272.0	212.0	165.0	271.6	212.5	165.7
5.2	162.0	148.0	125.0	163.7	147.7	124.4	264.0	200.0	153.0	263.8	201.1	153.1
9.5	116.0	98.1	73.4	116.1	97.8	73.4	248.0	178.0	128.0	247.9	178.8	128.5
13.8	88.2	66.4	40.3	88.8	66.1	40.0	230.0	154.0	102.0	230.0	154.5	102.2
18.0	85.5	60.1	32.8	85.7	59.7	32.8	215.0	134.0	81.2	214.5	134.7	81.5
22.3	86.6	58.8	30.9	87.3	58.5	30.8	203.0	121.0	68.0	203.2	121.5	68.3
26.6	86.6	57.8	30.0	86.9	57.5	29.9	196.0	114.0	61.8	196.2	114.5	62.0
30.9	84.9	56.9	29.9	85.2	56.5	29.7	193.0	112.0	61.8	193.2	113.1	62.0
35.2	81.6	55.8	30.4	82.4	55.6	30.3	195.0	117.0	67.9	194.3	117.3	68.1
39.5	77.3	55.3	32.0	77.5	54.9	32.0	200.0	127.0	81.0	199.6	127.7	81.2
43.8	78.4	61.1	40.4	79.1	60.6	40.2	209.0	144.0	101.0	208.8	144.4	101.5
48.1	107.0	94.9	77.1	107.3	94.6	77.0	220.0	164.0	126.0	219.8	164.7	126.4
52.3	148.0	140.0	125.0	149.9	139.7	124.8	228.0	181.0	148.0	227.8	181.5	147.9
56.6	160.0	153.0	140.0	158.9	152.5	139.7	227.0	185.0	156.0	226.9	185.9	155.7
60.9	146.0	139.0	126.0	147.2	138.8	126.3	215.0	173.0	145.0	214.3	173.4	144.7
65.2	102.0	92.0	79.5	101.6	91.5	79.3	192.0	146.0	118.0	192.0	146.9	118.4
69.5	59.0	45.6	32.7	59.4	45.1	32.5	166.0	114.0	86.1	165.3	115.0	86.3
73.8	47.5	30.0	16.6	48.0	29.8	16.5	139.0	84.3	56.7	139.2	85.0	56.9
78.1	43.9	22.9	9.4	44.2	22.4	9.3	117.0	59.5	33.4	116.4	60.2	33.6
82.3	39.9	16.3	3.0	40.4	15.9	2.9	97.0	39.6	15.4	96.8	40.3	15.6
86.6	34.7	9.4	-3.2	34.8	9.0	-3.3	80.2	23.4	1.5	80.0	24.2	1.7
90.9	28.9	2.8	-8.9	29.7	2.4	-9.0	65.5	10.1	-9.4	65.3	10.8	-9.2
95.2	23.3	-3.2	-13.8	23.4	-3.6	-13.8	52.5	-1.2	-18.2	52.2	-0.5	-17.9
99.5	17.9	-8.5	-17.8	18.4	-8.8	-18.0	40.8	-10.8	-25.2	40.6	-10.0	-24.9
103.8	12.9	-13.0	-21.1	13.3	-13.5	-21.1	30.2	-18.9	-30.7	30.0	-18.1	-30.5
108.1	8.4	-16.9	-23.6	8.8	-17.2	-23.7	20.7	-25.7	-35.1	20.5	-25.0	-34.8
112.3	4.3	-20.1	-25.5	4.8	-20.5	-25.7	12.1	-31.4	-38.4	11.9	-30.7	-38.1
116.6	0.6	-22.7	-26.9	1.0	-23.1	-27.0	4.4	-36.2	-40.8	4.1	-35.4	-40.6
133.8	-6.4	-27.0	-28.5	-6.0	-27.4	-28.5	-10.5	-43.9	-43.7	-10.7	-43.2	-43.4
163.8	-19.6	-30.1	-25.2	-19.0	-30.5	-25.3	-38.0	-50.0	-39.2	-38.3	-49.2	-39.0

Table A-4. NIKE3D Stress Distribution for the PCC Overlay and Existing PCC Slab at the
BOTOM IP

Center line offset, y-axis (inch)	PCC Overlay						Base PCC					
	Pav A		Pav B		Pav C		Pav A		Pav B		Pav C	
	BISAR	NIKE3D	BISAR	NIKE3D	BISAR	NIKE3D	BISAR	NIKE3D	BISAR	NIKE3D	NIKE3D	BISAR
0.9	181	204	168	182	145	159	272	262	212	193	165	149
5.2	162	169	148	147	125	123	264	251	200	177	153	132
9.5	116	109	98	84	73	60	248	237	178	158	128	111
13.8	88	79	66	51	40	26	230	221	154	138	102	90
18.0	86	75	60	45	33	20	215	207	134	121	81	72
22.3	87	75	59	45	31	20	203	198	121	110	68	61
26.6	87	74	58	45	30	20	196	193	114	104	62	56
30.9	85	71	57	43	30	19	193	191	112	105	62	58
35.2	82	67	56	40	30	17	195	194	117	112	68	68
39.5	77	63	55	38	32	17	200	201	127	126	81	84
43.8	78	73	61	51	40	32	209	210	144	143	101	104
48.1	107	133	95	112	77	95	220	218	164	156	126	121
52.3	148	192	140	172	125	155	228	221	181	160	148	127
56.6	160	198	153	178	140	162	227	216	185	156	156	124
60.9	146	164	139	144	126	129	215	203	173	144	145	113
65.2	102	97	92	76	80	62	192	184	146	126	118	96
69.5	59	48	46	27	33	13	166	162	114	103	86	75
73.8	48	38	30	14	17	1	139	138	84	78	57	52
78.1	44	37	23	11	9	-1	117	116	60	54	33	31
82.3	40	35	16	9	3	-4	97	99	40	35	15	11
86.6	35	31	9	5	-3	-7	80	84	23	18	2	-6
90.9	29	27	3	1	-9	-11	66	71	10	4	-9	-18
95.2	23	23	-3	-3	-14	-15	53	60	-1	-4	-18	-22
99.5	18	20	-8	-7	-18	-18	41	49	-11	-9	-25	-23
103.8	13	17	-13	-9	-21	-18	30	39	-19	-14	-31	-26
108.1	8	14	-17	-11	-24	-19	21	28	-26	-19	-35	-26
112.3	4	10	-20	-12	-26	-19	12	23	-31	-20	-38	-29
116.6	1	6	-23	-13	-27	-18	4	18	-36	-21	-41	-29
126.3	-6	4	-27	-14	-29	-18	-11	13	-44	-22	-44	-29
134.0	-13	3	-29	-15	-27	-18	-25	8	-47	-24	-42	-29
156.3	-20	2	-30	-16	-25	-18	-38	4	-50	-24	-39	-29

Table A-5. NIKE3D and JULEA Stress Comparison Through Pavement Thickness

Location	Slab Depth (inch)	Unbonded		Partially Bonded		Fully Bonded	
		NIKE3D	JULEA	NIKE3D	JULEA	NIKE3D	JULEA
PCC Overlay Top	0.00	-567.340	-595.335	-560.270	-585.831	-499.520	-473.212
PCC Overlay Upper IP	2.11	-331.400	-349.000	-356.975	-375.000	-364.300	-360.000
PCC Overlay Lower IP	7.89	313.200	324.000	198.450	201.000	5.126	-50.700
PCC Overlay Bottom	10.00	549.160	570.335	401.750	411.831	140.340	62.512
Base PCC Top	10.00	-366.880	-342.482	-249.130	-230.592	-18.730	11.615
Base PCC Upper IP	12.96	-213.150	-199.000	-123.950	-112.000	39.748	63.700
Base PCC Lower IP	21.04	206.850	193.000	218.050	212.000	199.500	206.000
Base PCC Bottom	24.00	360.588	336.482	343.238	330.592	257.966	258.086

Table A-6. Responses by NIKE3D for Horizontal Mesh Size

Single Wheel Load

Element Size (in.)	Equations Number	Elements Number	Nodal Loads Number	Very Low-Strength Subgrade			High-Strength Subgrade		
				Iterations	Time (sec)	Critical Stress at Slab Bottom (psi)	Iterations	Time (sec)	Critical Stress at Slab Bottom (psi)
2	18226	4599	48	7	724	281	12	812	234
4	5494	1356	16	7	88	277	12	109	230
6	3362	816	9	11	74	270	11	71	224
8	2414	568	6	5	19	261	11	27	215
12	1500	348	4	3	9	233	12	15	188

B777-200ER

Element Size (in.)	Equations Number	Elements Number	Nodal Loads Number	Very Low-Strength Subgrade			High-Strength Subgrade		
				Iterations	Time (sec)	Critical Stress at Slab Bottom (psi)	Iterations	Time (sec)	Critical Stress at Slab Bottom (psi)
2	34388	6598	217	5	6741	408	8	4569	292
4	15880	3656	72	7	684	407	11	688	285
6	7966	1824	39	3	122	405	11	246	282
8	5276	1196	20	3	62	395	21	185	276
12	2542	588	8	8	29	363	6	20	245

Table A-7. Responses by NIKE3D for Different Element Sizes Used in Horizontal Mesh

8″	Stress (psi)	6″	Stress (psi)	4″	Stress (psi)	3″	Stress (psi)	2″	Stress (psi)	1.5″	Stress (psi)
4.00	411.07	3.00	436.13	2.00	446.24	1.50	442.68	1.00	439.53	0.75	437.92
12.00	278.86	9.00	343.96	6.00	410.00	4.50	423.47	3.00	431.96	2.25	434.04
20.00	145.29	15.00	218.58	10.00	324.90	7.50	379.39	5.00	413.88	3.75	424.38
28.00	62.22	21.00	127.67	14.00	229.94	10.50	309.68	7.00	385.10	5.25	409.12
36.00	8.29	27.00	66.63	18.00	163.16	13.50	238.25	9.00	343.19	6.75	387.79
44.00	-29.34	33.00	22.36	22.00	112.03	16.50	184.07	11.00	292.46	8.25	359.73
		39.00	-10.37	26.00	71.95	19.50	140.54	13.00	245.34	9.75	322.60
		45.00	-35.14	30.00	39.67	22.50	104.82	15.00	206.62	11.25	282.55
				34.00	13.33	25.50	74.92	17.00	173.48	12.75	247.85
				38.00	-8.33	28.50	49.59	19.00	144.83	14.25	217.85
				42.00	-26.04	31.50	27.90	21.00	119.68	15.75	191.37
				46.00	-40.00	34.50	9.26	23.00	97.47	17.25	167.70
						37.50	-6.89	25.00	77.68	18.75	146.38
						40.50	-20.76	27.00	59.99	20.25	127.08
						43.50	-32.39	29.00	44.06	21.75	109.49
						46.50	-40.98	31.00	29.72	23.25	93.42
								33.00	16.73	24.75	78.67
								35.00	4.99	26.25	65.12
								37.00	-5.69	27.75	52.60
								39.00	-15.34	29.25	41.04
								41.00	-24.07	30.75	30.33
								43.00	-31.80	32.25	20.41
								45.00	-38.35	33.75	11.19
								47.00	-43.49	35.25	2.62
										36.75	-5.35
										38.25	-12.76
										39.75	-19.65
										41.25	-26.00
										42.75	-31.79
										44.25	-36.86
										45.75	-40.89
										47.25	-43.60

Table A-8. Maximum Stresses by FEDFAA Step Pavement Model vs H51 for Different Slab Sizes

Design Method	Edge Stress (psi)					
	15 ft	20 ft	25 ft	30 ft	40 ft	50 ft
Very Low-Strength Subgrade						
FEDFAA (6-in.)	466.90	535.87	587.14	622.02	653.26	659.51
H51	655.41	655.41	655.41	655.41	655.41	655.41
FEDFAA/H51	0.71	0.82	0.90	0.95	1.00	1.01
Low-Strength Subgrade						
FEDFAA (6-in.)	450.49	511.40	551.68	575.63	591.89	592.91
H51	621.13	621.13	621.13	621.13	621.13	621.13
FEDFAA/H51	0.73	0.82	0.89	0.93	0.95	0.95
Medium-Strength Subgrade						
FEDFAA (6-in.)	420.55	466.23	491.02	502.65	506.95	505.01
H51	594.73	594.73	594.73	594.73	594.73	594.73
FEDFAA/H51	0.71	0.78	0.83	0.85	0.85	0.85
High-Strength Subgrade						
FEDFAA (6-in.)	391.35	425.07	440.48	446.13	446.90	443.78
H51	577.18	577.18	577.18	577.18	577.18	577.18
FEDFAA/H51	0.68	0.74	0.76	0.77	0.77	0.77

Table A-9. Coordinates Used in NIKE3D FAA 1.0 Analysis

r (inch)	σ_r (psi)	
	Boussinesq	BISAR
0.000	-162.000	-162.000
2.350	-162.000	-162.000
4.700	-162.000	-162.000
7.050	-162.000	-162.000
9.400	-162.000	-162.000
9.410	17.974	18.000
12.500	10.186	10.200
15.625	6.519	6.520
18.750	4.527	4.530
25.000	2.546	2.550
36.000	1.228	1.230
54.000	0.546	0.550
72.000	0.307	0.310
108.000	0.136	0.140
144.000	0.077	0.077